TDMA DIGITAL MOBILE RADIO TRANSMISSION SYSTEM

By

Li Wang

Thesis submitted in accordance with the requirement of The University of Liverpool for the degree of Doctor in Philosophy.

October 1990

Department of Electrical Engineering and Electronics

ABSTRACT

This thesis presents the design, construction and results from field experiments of a versatile experimental TDMA digital transmission system operating at 1.8 GHz. GMSK modulation with $BT = 0.3$ was used and the data rate was 500 kb/s. The field experiments were conducted in a typical urban area with a maximum 1 km separation between the transmitter and the receiver. Real time channel impulse response and baseband quadrature waveforms were recorded and analysed later in the laboratory. Representative channel impulse responses were selected and related to the bit error statistics. Adaptive Decision Feedback Equalisers utilising the fast Kalman algorithm and Maximum likelihood Equalisers using the Viterbi algorithm, both implemented in computer software, were used to process the recorded data. It was concluded that the DFE with 3 forward and 3 backward delay taps is the most cost effective technique. Future research work is suggested.

ACKNOWLEDGEMENT

I wish to thank professor J. D. Parsons for his supervision, guidance and encouragement during the course of this research project. I am grateful to Dr. A. Turkmani for his enthusiastic support, guidance and many valuable discussions during the preparation of the experiment and presentation of this thesis. I would like to thank Dr. A. S. Bajwa, formerly of Telecom Securicor Cellular Radio Limited for his keen interest, support, encouragement and many stimulating discussions during the development of several projects in my career, from which I gained invaluable experiences and all of which, directly or indirectly, contribute to this thesis.

I wish to thank Mr. M. Khorami and Mr. P. Carter for encouragement, discussions and for their generous help. They both spent their spare time driving the experimental vehicle.

I wish to thank Mr. D. G. Lewis and Mr. R. Smith for providing their expertise in preparation of the experiment.

I also wish to thank Dr. M. T. Feeney for suggesting the experimental areas and offering advice on the presentation of this thesis. I wish to thank Dr. A. Demery for providing the channel profiles for the computer simulation.

The research support from Telecom Securicor Cellular Radio Limited is gratefully acknowledged.

I would like to express my deep appreciation to my parents and to my wife for their continued love, support, understanding and encouragement.

TO MY BELOVED WIFE YI MIEN

TABLE OF CONTENTS

LIST OF ABBREVIATIONS

ADC	Analogue to Digital Converter.
ASK	Amplitude Shift Keying.
BER	Bit Error Rate.
CDF	Cumulative distribution function.
CPM	Continuous Phase Modulation.
DAC	Digital to Analogue Converter.
DFE	Decision Feedback Equaliser.
DPM	Digital Phase Modulation.
DSSS	Direct Sequence Spread Spectrum System.
ECL	Emitter Coupled Logic.
EPROM	Erasable Programmable Read Only Memory.
FDMA	Frequency Division Multiple Access.
FSK	Frequency Shift Keying.
GSM	Groupe Spécial Mobile.
GSMK	Gaussian Minimum Shift Keying.
IF	Intermediate Frequency.
MLSE	Maximum Likelihood Sequence Estimation.
MSE	Mean Square Error.
MSK	Minimum Shift Keying.
PDF	Probability Density Function.
PRBS	Pseudo Random Binary Sequence.
QPSK	Quadrature Phase Shift Keying.
SCPC	Single Channel Per Carrier.
SIPO	Serial Input Parallel Output.

SNR	Signal to Noise Ratio.
TTL	Transistor Transistor Logic.
VCO	Voltage Controlled Oscillator.
VE	Viterbi Equaliser.

CHAPTER 1 INTRODUCTION

The recent release of radio spectrum around 1.8 GHz for the Personal Communication Network (PCN) has signified another major step forward, after the standardisation of the Pan-European GSM (Groupe Spécial Mobile) digital cellular radio system, in meeting the fast growing demand for mobile radio communications [1, 2]. The PCN is a system concept developed to ease the telecommunication traffic within a large GSM cell by providing extra channels, which are dedicated to local communications, through micro-cellular structures [3]. As a result of this double coverage concept, the PCN system is likely to adopt the Time Division Multiple Access (TDMA) technique used by the GSM system to enable users to access both systems with compatible radio telephones.

In addition to TDMA, there are other multiple access techniques existing in the present mobile radio services, such as the Single Channel Per Carrier (SCPC) Frequency Division Multiple Access (FDMA) techniques used in radio paging systems and in the analogue cellular radio telephone system TACS (Total Access Communication System). Advancements in technology have made the spread spectrum multiple access technique, which was previously exclusive to the military applications, a practical contender in the design of a future civilian mobile radio system. Frequency Hopped Spread Spectrum (FHSS) and Direct Sequence Spread Spectrum (DSSS) multiple access techniques can be adopted in order to combat the multipath propagation exhibited in the mobile radio channel [4,5]. Looking beyond the PCN, most of the different techniques and approaches are set to merge into a single infrastructure, such as the Universal Mobile Telecommunication System (UMTS) under development by the European Commission's RACE (Research into Advanced Communications for Europe) project, which will pro-

vide a common air interface to support various types of mobile radio communications [6,7].

A more fundamental question about the compatibility between the GSM and PCN systems however, is whether the quality of data transmissions at 1.8 GHz will be comparable to that at 960 MHz, due to the possible differences between the propagation characteristics at the two frequencies. This is because, at higher frequencies, the basic attenuation will be greater and the scattering and diffraction from obstacles along the propagation path will be different. The fading of the received signal envelope which is caused by the arrival of multiple delayed waves at the receiver antenna is likely to be characterised by a Rayleigh distribution, as at lower frequencies, but the fading rate and signal spectrum will be different.

Experimental investigations [8,9] have been reported recently, where the radio wave propagation characteristics inside buildings at carrier frequency of 1.7 GHz were studied. However, they were not extended to include investigations of the quality of digital transmissions, e.g. Bit Error Rate (BER). Furthermore, the propagation characteristics inside buildings may be different from those outside, because the larger physical distances between the obstacles outside will increase the time delays in the reflected waves. If such delays become comparable to the data transmission bit period, they will cause InterSymbol Interference (ISI), which will increase the BER in a digital transmission. Although computer simulations based upon various statistical models can provide a general assessment of the quality of the data transmission, there may be specific situations in real time digital transmission where the models could not be sufficiently accurate.

Such a concern provides the motivation for an experimental investigation at 1.8 GHz, in order to assess the performance of a digital communication system in terms of the statistics of the bit errors. Such an investigation should be extended to include a comparison of various channel equalisation techniques to determine how the channel distortions arising from multipath propagation can be mitigated.

This thesis presents the results of work on the design and implementation of an experimental system which consists of both hardware and software, together with the results of analysing data obtained from field trials made in the University of Liverpool precinct. The thesis is organised as follows.

Chapter 2 reviews spectrally efficient digital modulation techniques and the demodulation of such signals in the presence of interference which is modelled as Additive White Gaussian Noise (AWGN). Two aspects of the multiple signal delays are discussed. Firstly, the effect of signal fading caused by the constructive and destructive combination of the delayed signals is outlined, and secondly, the ISI introduced by the delayed signals is included. The discussion is specifically orientated toward TDMA systems where the data transmission rate is high (e.g. 500 kb/s) and the transmission duration is short (e.g. 0.5 ms). The purpose of Chapter 2 is to identify the sources which cause degradation to a system utilising a specific modulation and demodulation technique, as some of these sources can be controlled by the system designers (e.g. modulation index) whereas others depend upon the radio channel (e.g. channel impulse response). The characteristics of the latter must be estimated and modelled statistically, so that signal processing techniques can be developed to minimise their effects. This chapter discusses, in particular, why the channel impulse response should be measured and related to the average BER.

Chapter 3 describes the design, construction and laboratory calibration of a versatile coherent TDMA experimental system. As the exact specifications of PCN were still under review, the experimental system designed for the investigation is flexible, in order to accommodate various data transmission parameters (i.e. modulation technique, transmission rate, transmission format etc.), as well as the carrier frequency. The system records the demodulated quadrature waveforms, which are sampled simultaneously at a bit transmission period T, together with the measured signal strength and the estimated channel impulse response at the start of data transmission period. The investigations of the effectiveness of the equalisation techniques are carried

out by implementing equalisers in computer software and processing the recorded data in the laboratory.

Chapter 4 presents the results from field measurements made in areas around the University of Liverpool precinct at a carrier frequency of 1.8 GHz using Gaussian Minimum Shift Keying (GMSK) modulation with the normalised bandwidth BT of the baseband shaping filter equal to 0.3. These results include the statistics on real time mobile channel impulse responses, signal strengths and bit error distributions.

Chapter 5 discusses various channel equalisation techniques in order to determine which is the more efficient in reducing the bit error rate caused by the channel distortions. The effects of these equalisers on the bit error distributions are determined. The adaptive Decision Feedback Equalisers (DFE) using Fast Kalman Algorithm (FKA) with variable length of forward and backward delay lines , and Viterbi Equalisers (VE) with various state lengths are implemented in software to process the experimental data. The parameters of each type of equalisers are varied to investigate their effects on the improvement of the bit error distribution. Comparisons between the two types of equalisers are made on the basis of performance with the different types of channels encountered during the measurement.

Chapter 6 draws conclusions from the results presented in the thesis and suggests topics for future study.

REFERENCE

[1] Moralee, D. "Companies line up for PCN battle", IEE Review, pp.364-365, Nov 1989.

[2] Balston, D. M. "Pan-European Cellular Radio : or 1991 and all that", Electronics and Communication Engineering J., Jan/Feb 1989.

[3] Green, J. "Design a mobile future", Communication International, pp.3, Nov 1989.

[4] "Second Nordic Seminar on Digital Land Mobile Radio Communication", Oct 1986.

[5] Jakes, W. C. "Microwave Mobile Communications", John Wiley & sons, New York, 1974.

[6] "Cordless, the way forward for Europe", Mobile and Cellular Magazine, pp.12, Oct 1989.

[7] Green, J. "The mobile explosion", Communication International, pp.17, Aug 1989.

[8] Motely, A. J. "Personal Communication Coverage in Building at 900 and 1700 MHz", Electronics Letters, Vol. 24, No. 12, pp.763-764, June 1988.

[9] Bultitude, R. J. C. et al. "A Comparison of Indoor Radio Propagation Characteristics at 910 MHz and 1.75 GHz", IEEE Journal on Selected Areas in Communications, Vol. 7, No. 1, pp.20-30, Jan 1989.

CHAPTER 2 DIGITAL SIGNALLING IN A TDMA MOBILE RADIO SYSTEM

2.1 INTRODUCTION

Digital signalling in a cellular radio system involves a compromise between spectrally efficient modulation techniques, which reduce adjacent channel interference, and the average BER in the presence of signal fading and multipath signal delays.

The radio spectrum is a natural resource which, as far as industrial services are concerned, has become increasingly scarce. It is therefore important, both in technical and commercial terms, to utilise this spectrum efficiently. Although the spectrum allocated to the cellular radio system is very limited, it can be efficiently utilised by a combination of the following methods. The first method is to select an efficient multiple access technique to maximise the number of users who are sharing the total available spectrum. There are many such techniques available, for example, the FDMA technique, where each user is assigned a given bandwidth or channel for communication; the TDMA technique, where a user accesses a single channel intermittently in order to share it with other users in the time domain; the DSSS technique which assigns unique code sequences to individual users so that simultaneous communications can take place over the same channel. The second method is to adopt spectrally efficient modulation techniques. The spectral efficiency of a digital modulation technique is determined by the ratio of the spectral power of the modulated carrier inside the main lobe (in which the majority of the spectral power is contained) to that in the side lobes. As an example, Figure 2.1 shows the power spectrum of Binary Phase Shift Keying modu-

lation. Increasing this ratio will improve the spectral efficiency, because very low power level in the spectral side lobes enables the main lobes occupied by individual users to be brought very close to each other in order to attain a higher overall spectral efficiency. The third method is to pre-process the information data from each user in order to reduce the width of its main lobe, so that more users can be included in the original bandwidth.

This chapter concerns digital transmissions in a TDMA mobile radio system. It starts by generally reviewing spectrally efficient modulation techniques in section 2.2 and discusses why Continuous Phase Modulation (CPM) is particularly favourable. Section 2.3 discusses the theoretically calculated average BER in the detection of CPM signals subject to Additive White Gaussian Noise (AWGN), which is used to model the total interference in a cellular radio system. The degradation in BER caused by the carrier phase offset and sampling time offset are considered. In section 2.4, the effects of multiple signal delays in a mobile radio channel, in terms of both selective and non-selective signal fading, are then included in the calculation of the average BER, with the assumption that the radio transmitter is stationary while the receiver is mobile. Section 2.5 discusses special concerns related to a TDMA system in the mobile radio environment and an experimental investigation is suggested.

2.2 SPECTRALLY EFFICIENT DIGITAL MODULATION TECHNIQUES

Digital modulation is a process which maps the binary information symbols {-1,1} onto the amplitude, phase and frequency of a radio wave carrier. This process has been studied extensively in the literature and there are four major categories of digital modulation techniques available [1-4], They are listed as follows.

ASK Amplitude Shift Keying, where the amplitude of the carrier varies according to the information symbols.

FSK Frequency Shift Keying, where the instantaneous frequency of the carrier is shifted by a predetermined amount from the nominal carrier frequency according to the information symbols while the amplitude of the carrier is kept constant.

PSK Phase Shift Keying, where the instantaneous phase of the carrier is proportional to the information symbol while the amplitude and frequency of the carrier are kept constant.

OTHERS The combination of both amplitude and phase modulation (eg. Quadrature Amplitude Modulation.)

The bandwidth occupied by the main lobe of the spectrum of the modulated carrier is directly proportional to the information symbol rate $1/T$. In order to reduce the occupied bandwidth, N of the binary information symbols are grouped together and one of their M ($M = 2^N$) combinations is used to shift the amplitude, frequency or the phase of the carrier. This is referred to as M-ary modulation. The width of the main lobe of this type of modulated carrier is reduced by a factor $1/N$.

One of the advantages of constant amplitude modulation techniques is that they do not require a linear power amplifier at the transmitter, which requires a constant direct current bias in its operation [5]. The non-linear power amplifiers used for constant amplitude modulation systems are generally much more efficient in power consumption. This feature makes constant amplitude modulation a favoured technique for adoption in the new digital cellular radio systems. Constant amplitude modulation techniques are now briefly reviewed.

The general form of the constant amplitude modulated signal can be expressed as

$$s(t) = A\cos(\omega t + \rho(t)) \tag{2.1}$$

where ω is the angular carrier frequency and $\rho(t)$ is the instantaneous phase of the modulated signal corresponding to the information symbol(s) . A is the amplitude.

In a real communication system where the data transmission starts at time reference zero, a sequence of binary information symbols can be represented as:

$$d(t) = \sum_{n=0}^{\infty} a_n \; U(t - nT) \tag{2.2}$$

where $a_n = \pm 1$, and $U(t)$ is the unit pulse function, which is defined as

$$U(t) = \begin{cases} 1, & \text{for } 0 \le t \le T \\ 0, & \text{otherwise} \end{cases}$$

The binary information symbol duration is equal to T.

For Binary Phase Shift Keying (BPSK) modulation, the phase of the carrier is defined as

$$\rho(t) = \frac{\pi}{2} \; d(t) \tag{2.3}$$

When $N(N \ge 2)$ information digits are grouped together, the $d(t)$ becomes

$$d(t) = \sum_{n=0}^{\infty} \left(\sum_{i=0}^{N-1} 2^i \, a_i \right) U(t - nT) \tag{2.4}$$

where $0 < t < NT$, and $n = 0, N, 2N, \ldots$. The corresponding phase shift in every NT interval is

$$\rho(t) = \frac{\pi}{2^{N-1}} \; d(t) \tag{2.5}$$

This modulation is referred to as M-ary PSK or MPSK, where $M = 2^N$.

As an example, if two information symbols are grouped together, i.e. $N = 2$, then

As an example, in the binary Fast Frequency Shift Keying (FFSK), the carrier is rapidly swiched between two preset frequencies, hence there is no longer a unique main lope in the power spectrum of the modulated signal, and its bandwidth is greater than the data transmission bandwidth $1/T$. Although FFSK is easy to implement in practice, it is not so efficient in terms of spectrum efficiency. More reference can be found in [1-4].

$$d(t) = a_n\, U(t - nT) + 2\, a_{n+1}\, U(t - (n+1)T) \qquad (2.6)$$

Where $n = 0,2,4, \ldots$, the phase of the carrier changes every $2T$ period by

$$\rho(t) = \frac{\pi}{2}\, d(t) \qquad (2.7)$$

This modulation is the commonly used Quadrature Phase Shift Keying (QPSK).

The phase modulated signals described above have considerable spectral power contained in the side lobes because of the abrupt phase shifts in the time domain.

If $\rho(t)$ in equation (2.1) is kept constant and ω is allowed to vary with $d(t)$, i.e.

$$\omega = \omega_o + \Delta\omega\, d(t) \qquad (2.8)$$

where ω_o is the nominal angular frequency of the carrier and $\Delta\omega$ is the angular frequency deviation, this is termed Frequency Shift Keying (FSK) modulation. Once again the spectral power outside the main lobe is large,[1] due to the abrupt frequency shifts.

The spectral power in the side lobes will interfere with the modulated signal in an adjacent channel separated by $\frac{2}{NT}$ in frequency, and therefore a high order spectral shaping filter must be used to attenuate the out of the band energy to an acceptable level.

The spectral power in the side lobes can also be controlled by passing the information symbols through a pre-modulation baseband shaping filter, which has an impulse response of $q(t)$, in order to smooth the abrupt transitions in the time domain. For simplicity, this filter will be referred to as the 'baseband shaping filter' in the following text. The phase change corresponding to the filtered symbols is expressed as

---

[1] Please refer to opposit page.

$$\rho(t) = 2\pi h \int_{-\infty}^{\infty} d(\tau)\ q(t-\tau)\ d\tau \qquad (2.9)$$

where h is the modulation index, which determines the maximum phase shift.

When the impulse response $q(t)$ is represented by k sampled values within a time duration of LT where $k > 2L$, for $L = 1,2,3, \ldots$, and the convolution of equation (2.9) is performed discretely in time, then $\rho(t)$ also becomes discrete, i.e.

$$\rho(\xi) = 2\pi h \sum_{i=-\infty}^{\infty} d(iT)\ q(\xi - iT) \qquad (2.10)$$

Where $\xi = nLT/k$ $(n = 0, \pm 1, \pm 2, \ldots)$. This modulation technique is called Digital Phase Modulation (DPM) [6]. DPM with $L \geq 3$ reduces the spectral energy outside the main lobe substantially compared with QPSK, however the discrete digital filtering process generates spurious spectral elements at multiples of its sampling frequency, which must also be suppressed by a spectrum shaping filter.

If k in the DPM is made to approach infinity and the filtered information symbols are accumulated from $-\infty$ to the present time, the phase transition becomes continuous. This process is expressed as

$$\rho(t) = 2\pi h \int_{-\infty}^{t} \sum_{i=-\infty}^{\infty} d(iT)\ q(\xi - iT)\ d\xi \qquad (2.11)$$

Because of the continuous phase transition, this type of modulation is called Continuous Phase Modulation (CPM) [7, 8]. CPM retains the advantage of DPM in having very low side lobe spectral energy, and in addition it does not generate any spurious spectral components. Therefore CPM is a spectrally efficient modulation technique which is favoured in digital cellular radio systems.

The impulse response $q(t)$ can take many forms in order to occupy a different number of symbol durations T. In order to simplify the theoretical analysis that follows, only the modulation index h is chosen to be a variable, and the time integral of each of the forms of $q(t)$ in the time domain of $-\infty$ to ∞ is defined to be 0.5, i.e.

$$\int_{-\infty}^{\infty} q(t)\ dt = 0.5 \tag{2.12}$$

The lower time limit in the integral allows a convinient time origin to be selected during the analysis.

When the duration of $q(t)$ is longer than T, the smoothness in the phase transitions of the modulated carrier increases. Although these smoother phase transitions can restrict most of the spectral energy to within the main lobe without using any additional spectral shaping filter, the complexity of the demodulator can be substantially increased as the duration of $q(t)$ in the time domain becomes excessive [8].

In practice the modulation index is chosen to be 0.5 and the impulse response $q(t)$ of the shaping filter is finite for a duration less than $4T$. The advantage of having h equal to 0.5 is that the carrier phase will move $\pm\frac{\pi}{2}$ each time an information symbol has passed through the shaping filter and a simple quadrature type of demodulator can be used in the receiver.

Three practical phase modulation techniques are summarised below in order to illustrate their spectral efficiency.

QPSK Quadrature Phase Shift Keying, where there is no baseband shaping filter and two consecutive information symbols are grouped together to define the carrier phase.

MSK Minimum Shift Keying [2, 3], where $q(t)$ is a unit pulse defined as

$$q(t) = \begin{cases} 1, & \text{for } 0 \le t \le T \\ 0, & \text{otherwise} \end{cases} \tag{2.13}$$

GMSK Gaussian Minimum Shift Keying [9], where $q(t)$ is given by

$$q(t) = \frac{1}{2\sqrt{\pi}} \beta \exp(-\beta^2 t^2) \qquad (2.14)$$

$$\text{where } \beta = \pi \sqrt{\frac{2}{\ln 2}} BT$$

where BT is the normalised 3 dB bandwidth of the filter.

A comparison of the phase transitions in QPSK, MSK and GMSK with $BT = 0.3$, according to the same binary information sequence, is shown in Figure 2.2. The corresponding normalised power spectra of the three types of modulation are shown in Figure 2.3. GMSK with $BT = 0.3$ is clearly much more efficient in utilising the frequency spectrum.

Apart from the spectral efficiency, the tolerance of a specific modulation technique to interference in a communication system must also be considered. This subject will be discussed in the following section.

2.3 COHERENT DETECTION OF A CPM SIGNAL

2.3.1 COHERENT DETECTION IN THE PRESENCE OF AWGN

The compact spectral distribution of communication channels and the short physical distances between radio base stations generate two types of interference in a cellular radio system. The first is due to energy in channels adjacent to that occupied by the wanted signal, this being known as adjacent channel interference. The second is energy in the channel occupied by the wanted signal. This energy is generated by transmitters in cells some distance away which use the same set of frequencies, and is termed as co-channel interference.

In order to analyse the effects of the interference on the detection of a CPM signal, the modulated signal is written here in a quadrature form as:

This assumption is not generally true in real cellular systems, where co-channel interferences are stricky controlled by using transmission 'power control' at both base station and mobile, sectorised directional base station antenna with controlled down tilt in order to increase frequency reuse distances, etc. . The adjacent channel interferences are controlled by separating channels with sufficient frequency (eg. 27 channel spacing in TACS and 3 channel separation in GSM). To charaterise the total interference is beyound the scope of this thesis, therefore the more generalised assumption (i.e. AWGN) was used here, and it may not represent the worst case.

$$\begin{aligned} s(t) &= A\cos(\omega t + \rho(t)) \\ &= I(t)\cos\omega t - Q(t)\sin\omega t \end{aligned} \tag{2.15}$$

where

$$I(t) = A\cos\rho(t) \tag{2.16}$$

$$Q(t) = A\sin\rho(t) \tag{2.17}$$

are the baseband inphase and quadrature waveforms which correspond to the mapping of the information symbols onto the carrier. Figures 2.4, 2.5 and 2.6 show such quadrature waveforms and the corresponding phase transitions of QPSK, MSK and GMSK with $BT = 0.3$ modulation respectively, for the same binary information sequence. The demodulation process concerns how to detect correctly the transmitted waveforms in the presence of the interference.

The interference may come from several different directions in a cellular radio system, and in a linear communication channel (i.e. where the superposition principle applies) they all add to the transmitted signal at the input of a receiver to become a resultant vector $r(t)$. The received signal plus the total interference at the receiver is

$$r(t) = s(t) + n(t) \tag{2.18}$$

Where $n(t)$ represents the total interference. By the Central Limit Theorem, when a sufficient number of interferers are added together, the $n(t)$ becomes a zero-mean Gaussian process, with a constant two-sided power spectral density which equals to $N_o/2$. Hence it is referred to as Additive White Gaussian Noise (AWGN).[2] The probability distribution function of such a process is given by

$$p(y) = \frac{1}{\sqrt{\pi N_o}}\exp(-y^2/N_o) \tag{2.19}$$

Where y is the amplitude of the random process, and

---

[2] Please refer to opposit page.

$$< y^2 > = \frac{N_o}{2} \tag{2.20}$$

where $< \bullet >$ denotes the ensemble average.

The coherent detection of the received signal $r(t)$ can be represented by the block diagram shown in Figure 2.7, where $r(t)$ is multiplied individually by the in-phase and quadrature components of a locally re-generated carrier, and integrated over a $2T$ interval. This interval is selected because the baseband quadrature waveforms are orthogonal over such a period. Intervals longer than $2T$ can be selected [8] at the expense of increased complexity in receiver structure, which offers limited improvement in the output signal levels. The detectors in the inphase and quadrature branches take samples from the output of the corresponding integrators at time instants $2nT$ and $(2n-1)T$ respectively (where $n = 0, \pm 1, \pm 2, \ldots .$), and decide which binary symbol has been transmitted. The performance of the coherent detector is assessed by the probability of making incorrect decisions, or errors, in the presence of the AWGN.

The detection of a MSK modulated signal will be discussed first. Figure 2.5 shows that for MSK modulation, the phase transition equals $\pm \pi$ over a $2T$ interval, and taking advantage of the symmetrical property of the trigonometry functions, the phase of the modulated carrier can be written as

$$\rho(t) = \pm \frac{\pi}{2T} t \qquad -T < t < T \tag{2.21}$$

Hence the modulated signal is

$$s(t) = A \cos(\omega t \pm \frac{\pi}{2T} t) \qquad -T < t < T \tag{2.22}$$

In the absence of the AWGN, the sampled value x, from the integrator in the in-phase branch, which is used to remove the 2ω frequency component from the multiplier output, is

$$x_s = \int_{-T}^{T} A \cos(\omega t + \frac{\pi}{2T} t) \cos \omega t \, dt \tag{2.23}$$

which has two possible values, viz

$$x_{s,+1} = + \frac{A}{\pi} 2T \tag{2.24}$$

$$x_{s,-1} = - \frac{A}{\pi} 2T \tag{2.25}$$

where subscript ± 1 denotes the polarities of the sampled values. The noise power at the output of the integrator is calculated as

$$N_s = < \int_{-T}^{T} \int_{-T}^{T} n(\tau) \, n(\zeta) \cos \omega\tau \, \cos \omega\zeta \, d\tau \, d\zeta > \tag{2.26}$$

Since $n(t)$ is a white Gaussian process, it has the property

$$< n(\tau) n(\zeta) > = \frac{N_o}{2} \delta(\tau - \zeta) \tag{2.27}$$

Hence equation (2.26) becomes

$$N_s = \int_{-T}^{T} \frac{N_o}{2} \cos^2 \omega t \, dt = \frac{N_o}{4} 2T \tag{2.28}$$

Since the integration is a linear process, the probability density distribution of the noise at the output of the integrator remains Gaussian. The sample value taken from the output of the integrator contains both signal and noise components. Let this sample be represented by x_i, and let n_s represent the noise sample, then

$$x_i = x_s + n_s \tag{2.29}$$

The detection of $x_{s,+1}$ and $x_{s,-1}$ from x_i can be carried out by calculating their likelihood functions, which are defined as

$$p(x_i|x_{s,+1}) = \frac{p}{\sqrt{2\pi N_s}} \exp(-\frac{(x_i - x_{s,+1})^2}{2N_s}) \qquad (2.30)$$

$$p(x_i|x_{s,-1}) = \frac{q}{\sqrt{2\pi N_s}} \exp(-\frac{(x_i - x_{s,-1})^2}{2N_s}) \qquad (2.31)$$

Where p and q are the probabilities of transmitting $x_{s,+1}$ and $x_{s,-1}$ respectively. The detector makes a decision based on the values of the likelihood functions as

$$d' = \begin{cases} +1, & \text{if } p(x_i|x_{s,+1}) \geq p(x_i|x_{s,-1}) \\ -1, & \text{if } p(x_i|x_{s,+1}) < p(x_i|x_{s,-1}) \end{cases} \qquad (2.32)$$

where d' is the detected binary symbol.

Assuming that the probabilities of transmitting $x_{s,+1}$ and $x_{s,-1}$ are equal, i.e. $p = q = 0.5$, then the probability of making an incorrect decision, or the average Bit Error Rate (BER) P_e, is given by

$$P_e = \frac{1}{2}\int_{l_{opt}}^{\infty} p(x_i|x_{s,-1})\, dx + \frac{1}{2}\int_{-\infty}^{l_{opt}} p(x_i|x_{s,+1})\, dx \qquad (2.33)$$

where

$$l_{opt} = \frac{x_{s,+1} + x_{s,-1}}{2} = 0 \qquad (2.34)$$

is the optimum detection threshold. By evaluating the integral in equation (2.33), the average BER of coherent detection of MSK signal can be expressed as

$$P_{e,\,MSK} = \frac{1}{2}\, erfc\,(\frac{x_{s,+1} - x_{s,-1}}{2\sqrt{2N_s}}) \qquad (2.35)$$

where $erfc\,(x)$ is the complimentary error function, which is defined as

$$erfc\,(x) = \frac{2}{\sqrt{\pi}} \int_x^{\infty} \exp(-y^2)\, dy \qquad (2.36)$$

Substituting equation (2.24), (2.25) and (2.28) into equation (2.35), the average BER is calculated as

$$P_{e,MSK} = \frac{1}{2}\, erfc\,(\sqrt{\frac{4A^2T}{\pi^2 N_o}}) \qquad (2.37)$$

The energy of the transmitted signal $s(t)$ within T interval is calculated as

$$E_b = \int_0^T s^2(t)\, dt = \frac{A^2T}{2} \qquad (2.38)$$

Substituting E_b into equation (2.37), which gives

$$P_{e,MSK} = \frac{1}{2}\, erfc\,(\sqrt{\frac{8E_b}{\pi^2 N_o}}) \simeq \frac{1}{2}\, erfc\,(\sqrt{\frac{0.81\, E_b}{N_o}}) \qquad (2.39)$$

where E_b/N_o is the signal-to-noise ratio (SNR) within the period T. An identical expression can be obtained for the detection in the quadrature branch of the coherent detector at time interval 0 to $2T$. Assuming the probabilities of making a decision error are equal in both branches, then equation (2.39) represents the average BER in coherent detection of the MSK modulated signal in the presence of AWGN.

The average BER in the coherent detection of a QPSK modulated signal can be calculated in a similar way, except that both integrators will now integrate over the same 0 to $2T$ period and the outputs are sampled simultaneously at multiples of $2T$ intervals. The QPSK modulated signal is represented as

$$s(t) = A\cos(\omega t + \frac{m\pi}{4}) \quad , \quad 2nT \le t \le 2(n+1)T \qquad (2.40)$$

Where $n = 0, \pm 1, \pm 2, \ldots$ and $m = \pm 1, \pm 2$. Figure 2.4 shows the phase and baseband quadrature waveforms of such a signal. The two possible sampled values from the output of the in-phase integrator are therefore given by

$$x_{s,+1} = A\cos\frac{\pi}{4}T = +\frac{\sqrt{2}A}{2}T \tag{2.41}$$

$$x_{s,-1} = A\cos\frac{5\pi}{4}T = -\frac{\sqrt{2}A}{2}T \tag{2.42}$$

The noise power after each integrator is the same as in equation (2.28). Substituting equations (2.41), (2.42) and (2.28) into equation (2.35) and using E_b as expressed in equation (2.38), the average BER in the coherent detection of QPSK modulation is obtained as

$$P_{e,QPSK} = \frac{1}{2}\,erfc\,(\sqrt{E_b/N_o}) \tag{2.43}$$

For coherent detection of a CPM signal, when the baseband shaping filter has an impulse response which occupies LT time intervals (where $L \leq 3$), the simple coherent detector shown in Figure 2.7 can still be used. Although the optimum detector with a much more complicated structure exists [8], the improvement in the SNR is limited. As it will be discussed later, the received signal levels in a mobile radio channel may fluctuate over a wide range, hence the adoption of a simple detector with a marginal SNR degradation can be justified. This degradation is caused by the baseband shaping filter in the modulator, which causes the differences between the smoothed carrier phase transitions, over a T interval, to be occasionally less than $\pm\frac{\pi}{2}$. Hence the values of $\rho(t)$ at the sampling instance $t = nT$ will deviate from multiples of $\frac{\pi}{2}$, and the corresponding amplitudes of $x_{s,+1}$ and $x_{s,-1}$ will be less than A. Such amplitude reductions can be observed from Figure 2.6, which shows the phase and baseband quadrature waveforms of GMSK modulation with $BT = 0.3$. The average BER is bounded by the worst case where the maximum phase deviation from multiples of $\frac{\pi}{2}$ occurs at $t = nT$. If $A_{\min}$ denotes the minimum amplitude, the two possible sampled values from the in-phase integrator become

$$x_{s,+1} = +\frac{A_{\min}}{\pi}2T \tag{2.44}$$

$$x_{s,-1} = -\frac{A_{\min}}{\pi} 2T \tag{2.45}$$

The noise power after the integrator is the same as in MSK or QPSK. The worst case BER is calculated by substituting equations (2.44), (2.45) and (2.28) into equation (2.35), which gives

$$P_{e,\,worst-case} = \frac{1}{2}\, erfc(\sqrt{8A_{\min}^2 T/\pi^2 N_o}) \tag{2.46}$$

The average BER is limited by the worst-case BER as

$$P_{eGMSK} \leq P_{e,\,worst-case} \tag{2.47}$$

For a given baseband shaping filter, the maximum phase deviation can be calculated by passing combinations of binary sequences through the filter, and evaluating the phase differences from $\{0, \pm\frac{\pi}{2}, \pi\}$ at $t = nT$.

The maximum phase deviation in GMSK modulation with $BT = 0.3$ was evaluated by a computer program to be approximately $\pm 26°$, which results in a worst-case $A_{\min} \simeq 0.9A$ The average BER is therefore limited by

$$P_{eGMSK} \leq \frac{1}{2}\, erfc(\sqrt{0.66\, E_b/N_o}) \tag{2.48}$$

A more accurate calculation on P_{eGMSK} should be carried out by evaluating the probability p_i of occurrence of amplitude A_i in the baseband waveforms, and then take the average as [23]

$$P_{eGMSK} = \frac{1}{2}\sum_{i}^{M} p_i\, erfc\,(\sqrt{8A_i^2/\pi^2 N_o}) \tag{2.49}$$

where M is the number of different amplitudes. Observing from Figure 2.6, the maximum phase deviation occurs when the adjacent information symbols are different. Therefore between two consecutive symbols, the combination (-1,1) and (1,-1) will result the minimum amplitude $A_{\min}$, whereas the combinations (-1,-1) and (1,1) result the same baseband quadrature waveforms as

in MSK. Assuming the four combinations occur with equal probability 0.25 then the average BER can be calculated from equation (2.49) as

$$P_{eGMSK} = \frac{1}{2}\, erfc\,(\sqrt{0.66E_b/N_o}) + \frac{1}{2}\, erfc\,(\sqrt{0.81E_b/N_o}) \qquad (2.50)$$

Figure 2.8 shows comparisons between the theoretically calculated average BER in coherent detection of QPSK, MSK and GMSK with $BT = 0.3$ against E_b/N_o. This figure shows that for a given BER, GMSK with $BT = 0.3$ will require approximately 1 dB more SNR than MSK, or 2 dB more than QPSK. In a cellular radio system, this degradation can be easily compensated by the much lower adjacent channel interference due to the higher spectral efficiency. Therefore GMSK modulation with $BT = 0.3$ is a good choice for cellular radio systems.

2.3.2 THE EFFECT OF CARRIER PHASE OFFSET ON THE BER

In the previous section the average BER associated with the coherent detection of QPSK, MSK and GMSK signals was discussed. The locally regenerated in-phase and quadrature carrier signals were assumed to have zero phase offset to that in the transmitter. In a practical system this local carrier signal is obtained by processing the received signal which contains noise, and it may therefore have a phase offset compared with the carrier at the transmitter. Let this phase offset be represented by ϕ_o, then equation (2.23) becomes

$$x_s = \int_{-T}^{T} A\cos(\omega t + \frac{\pi}{2T})\cos(\omega t + \phi_o)\, dt \qquad (2.51)$$

The two possible sampled values from the in-phase integrator are

$$x_{s,+1} = +\frac{2AT}{\pi}\cos\phi_o \qquad (2.52)$$

$$x_{s,-1} = -\frac{2AT}{\pi}\cos\phi_o \qquad (2.53)$$

Assuming that $-\frac{\pi}{2} \le \phi_o \le \frac{\pi}{2}$, and substituting equations (2.52), (2.53), (2.28) and (2.38) into equation (2.35), gives

$$P_{eMSK} \simeq \frac{1}{2}\, erfc\,(\sqrt{0.81\, E_b \cos^2\phi_o / N_o}) \qquad (2.54)$$

The same expression applies to the quadrature integrator output in the time interval 0 to $2T$. Therefore, equation (2.54) represents the average BER associated with the coherent detection of an MSK signal when $-\frac{\pi}{2} \le \phi_o \le \frac{\pi}{2}$. The average BER for coherent QPSK and GMSK with $BT = 0.3$ can be derived in a similar way as

For QPSK

$$P_{eQPSK} = \frac{1}{2}\, erfc\,(\sqrt{E_b \cos^2\phi_o / N_o}) \qquad (2.55)$$

For GMSK with $BT = 0.3$

$$P_{eGMSK} \le \frac{1}{2}\, erfc\,(\sqrt{0.66\, E_b \cos^2\phi_o / N_o}) \qquad (2.56)$$

where $-\frac{\pi}{2} \le \phi_o \le \frac{\pi}{2}$. Figure 2.9 shows the average BER against phase offset at two SNRs.

In situations where $\frac{\pi}{2} \le \phi_o \le 3\frac{\pi}{2}$, the polarities of the integrator outputs are reversed. Statistically the detector will make erroneous decisions with the same probability as in $-\frac{\pi}{2} \le \phi_o \le \frac{\pi}{2}$, except the detected binary symbols are inverted (i.e. -1 becomes 1 and vice versa), which causes ambiguity to the digital circuit that follows the detector. Such an ambiguity can be removed by differentiating the two adjacent symbols from the detector, in order to eliminate the absolute polarity(the data stream in the transmitter must therefore be differentiated over a two bits period before being sent to the modulator). Figure 2.10 shows the structure of the differential detector, where the current detected symbol is added in modulo-2 to the previous one. The disadvantage of using the differential detector is that the current detection error will affect the following detected symbol, hence the probability

of errors at the output of the differential detector is twice that of the average BER derived in equations (2.54) to (2.56).

The practical implementation of a system in resolving the phase ambiguity will be discussed in detail in Chapter 3.

2.3.3 THE EFFECT OF SAMPLING TIME OFFSET ON THE BER

The offset in the sampling time intervals during the coherent detection process is another source which contributes to the detection error. Let this time offset be denoted by ΔT, then for coherent MSK detection, equation (2.23) becomes

$$x_s = \int_{-T+\Delta T}^{T+\Delta T} A\cos(\omega t + \frac{\pi}{2T}t)\cos\omega t\, dt \tag{2.57}$$

The two possible sampled values from the integrator are

$$x_{s,+1} = +\frac{2AT}{\pi}\cos(\frac{\pi}{2T}\Delta T) \tag{2.58}$$

$$x_{s,-1} = -\frac{2AT}{\pi}\cos(\frac{\pi}{2T}\Delta T) \tag{2.59}$$

where $0 \le \Delta T \le T$. Substitute equations (2.58), (2.59), (2.28) and (2.38) into (2.35), the average BER in coherent detection of MSK subject to timing offset ΔT is obtained as

$$P_{eMSK} \simeq \frac{1}{2}\, erfc\,(\sqrt{0.81E_b\cos^2(\frac{\pi}{2T}\Delta T)/N_o}) \tag{2.60}$$

The average BER for coherent QPSK and GMSK with $BT = 0.3$ can be obtained in a similar way,

For coherent QPSK

$$P_{eQPSK} = \frac{1}{2}\, erfc\,(\sqrt{E_b\cos^2(\frac{\pi}{2T}\Delta T)/N_o}) \tag{2.61}$$

For coherent GMSK with $BT = 0.3$

$$P_{eGMSK} \leq \frac{1}{2}\ erfc\left(\sqrt{0.66 E_b \cos^2\left(\frac{\pi}{2T}\Delta T\right)/N_o}\right) \qquad (2.62)$$

for $0 \leq \Delta T \leq T$. Figure 2.11 shows the above average BER against timing offset, at two SNRs.

The theoretical analysis of the average BER presented in this section assumes the signal amplitude is constant, therefore E_b is fixed. The sources of errors are AWGN with constant spectral power density $N_o/2$, carrier phase offset ϕ_o and sampling time offset ΔT. In a mobile radio communication environment, the amplitude of the received signal changes with time, therefore the SNR changes accordingly. The average BER in these situations will be analysed in the following section.

2.4 TRANSMISSION OF CPM SIGNALS OVER A MOBILE RADIO CHANNEL

2.4.1 INTRODUCTION TO THE MOBILE RADIO CHANNEL

A radio wave travelling between a transmitter and a receiver is diffracted and reflected by obstacles so that at a particular location in space a number of wave fronts with random phases, time delays and amplitudes arrive to form a resultant signal vector. When they all add in-phase the amplitude of the resultant is large, and when they add in anti-phase the amplitude of the resultant is small. In an area where the environment is stationary, a standing wave pattern is formed. As the receiver moves through this area, it experiences a fluctuation or fading in the received signal amplitude, as well as a random phase shift [10, 11]. If the time delays between the multiple wavefronts are negligible compared with the information symbol period T, then there is no ISI. The fluctuation of the amplitude over a long time duration (e.g. a few seconds) can be statistically modelled and used to calculate

the average BER. This type of signal fading is termed as non-selective or flat fading, because all frequencies are affected in a similar way. If the delay between the multi-wavefronts are comparable to the symbol period T, then the delayed waveforms become echoes to the waveforms that follow and cause ISI. This type of signal fading can be described by the estimated channel impulse response. This impulse response also varies against time as the receiver moves relatively to the transmitter. This is referred to as frequency selective fading.

Both types of signal fading disperse the energy of the transmitted signal, therefore the energy per symbol period E_b will be reduced. If AWGN is present, the average BER will increase. The effects of these two types of signal fading on the average BER in the coherent detection of CPM signals will be discussed in the following sections.

2.4.2 THE EFFECT OF NON-SELECTIVE (FLAT) SIGNAL FADING ON BER

This is the situation where the time delays between the multipath signals are shorter than the data transmission bit period. If there is no dominant received signal (e.g. a line-of-sight signal), the amplitude r of the resultant signal $r(t)$ in the absent of AWGN can be modeled by the Rayleigh distribution, the PDF is

$$p(r) = \frac{2r}{\sigma^2} \exp(-r^2/\sigma^2) \tag{2.63}$$

Where

$$\sigma^2 = < r^2 > \tag{2.64}$$

and $0 < r < \infty$.

In areas where there is a dominant signal component, the amplitude of the received signal r is Rician distributed, i.e.

$$p(r) = \frac{r}{\sigma^2} I_o[\frac{A\,r}{\sigma^2}] \exp(-(r^2 + A^2)/2\sigma^2) \qquad (2.65)$$

Where $I_o[y]$ is the modified Bessel function which is defined by

$$I_o[y] = \frac{1}{2\pi} \int_0^{2\pi} \exp(y \cos \phi)\ d\phi \qquad (2.66)$$

and A is the amplitude of the dominant signal, which is in the form

$$s(t) = A \cos(\omega t + \phi_o) \qquad (2.67)$$

Assuming the coherent receiver tracks the phase of the received signal correctly, then only the fluctuations in amplitude of the received signal affect the average BER. The general expression for coherent detection of QPSK, MSK and GMSK with $BT = 0.3$ modulated signals can be written as

$$P_e = \frac{1}{2}\ erfc\ (\sqrt{\eta\,\gamma}) \qquad (2.68)$$

where $\gamma = E_b/N_o$ and η takes values of 1.0, 0.81 and 0.66 for QPSK, MSK and GMSK with $BT = 0.3$ respectively. $N_o/2$ is the power spectral density of the AWGN, which is independent of signal fading. Therefore

$$\gamma = E_b/N_o = r^2/2N_o \qquad (2.69)$$

and P_e must be averaged over squared amplitudes of the received signal from zero to infinity. This process is carried out firstly by transforming the probability density function of r to that of γ. For the Rayleigh distribution, the transformation yields

$$p(\gamma) = \frac{1}{\gamma_o} \exp(-\gamma/\gamma_o) \qquad (2.70)$$

where $\gamma_o = \sigma^2/2N_o$ is the average received SNR over fading.

The average BER is then calculated by averaging equation (2.68) and (2.70), i.e.

$$P_e = \int_0^{\infty} \frac{1}{2} \, erfc\left(\sqrt{\eta\gamma}\right) \frac{1}{\gamma_o} \exp(-\gamma/\gamma_o) \, d\gamma \qquad (2.71)$$

which gives

$$P_e = \frac{1}{2}\left[1 - \frac{1}{\sqrt{1 + \frac{1}{\eta\gamma_o}}}\right] \qquad (2.72)$$

For the Rician distribution, which is defined by equation (2.65), the transformation of the probability density function from r to γ can only be carried out numerically, because the direct transformation of the Bessel function is not available.

Figure 2.12 shows the average BER for coherent detection of QPSK, MSK and GMSK with $BT = 0.3$ modulated signals before and after the Rayleigh fading.

The average BER in non-selective fading, subject to carrier phase offset and sampling time offset can also be evaluated by averaging equations (2.59) to (2.61) with equation (2.69) in a similar way. The results are shown in Figure 2.13 and 2.14 respectively.

2.4.3 THE EFFECT OF FREQUENCY SELECTIVE SIGNAL FADING ON THE BER

The arrival of multiple signal waveforms with random time delays at the receiver causes ISI to the demodulated quadrature waveforms when the information symbol period T is comparatively shorter than the delays. In this situation, portions of the previous transmitted waveforms are delayed and added, constructively or destructively, to the present waveform. This causes ISI and the levels of the outputs from the integrators in the coherent detector are reduced. The effect of ISI can be illustrated by recursively plotting the received baseband quadrature waveforms over a $2T$ period to form an 'eye

pattern'. Figure 2.15 shows the eye pattern for GMSK with $BT = 0.3$, in the absent of AWGN and ISI. The occasional smaller opening in the eye pattern is due to the phase deviation (caused by the baseband shaping filter in the modulator) from $\pm\frac{\pi}{2}$ at nT intervals, which leads to a reduced amplitude A_{min}, as discussed in section 2.3. The sampled values are taken at time instants where the eye patterns open at the maximum to achieve the minimum BER.

Figure 2.16 shows eye patterns where selective fading occurred in the absence of AWGN. The opening of the eye patterns become smaller occasionally as a result of ISI. Hence in the precence of AWGN, detection errors will be greater on these occasions.

In order to calculate the exact degradation, the channel impulse response $c(t)$ must be estimated so that the channel output $\hat{s}(t)$ corresponding to the modulated signal $s(t)$ can be calculated from

$$\hat{s}(t) = \int_{-\infty}^{\infty} s(t-\tau)\ c(\tau)\ d\tau \tag{2.73}$$

The baseband quadrature waveforms $x_{s,+1}$ and $x_{s,-1}$ can then be evaluated from $\hat{s}(t)$. Such channels can also be modelled in the baseband by finite tapped delay lines with the tap coefficients equal to the estimated channel impulse responses [12, 13].

2.4.3 SUMMARY

The previous discussion has shown that there are four key elements which affect the average BER in coherent detection of a CPM signal over a mobile radio channel, in the present of AWGN.

(1) The normalised bandwidth BT of the baseband shaping filter in the modulator. As the BT becomes smaller, the modulated phase $\rho(t)$ deviates from of $\{0, \pm\frac{\pi}{2}, \pi\}$ at $t = nT$, so that the amplitude of the

quadrature waveforms reduces, hence the average BER increases. The bandwidth of the shaping filter can be controlled by the system designer at the system planning stage in order to compromise between spectral efficiency and the minimum allowable signal amplitude.

(2) The offset caused by the AWGN in the re-generated carrier phase and sampling time. As this offset becomes non-zero, the signal power at the input to the detector decreases, hence the average BER increases. The AWGN can be reduced by adopting the optimum filter in the receiver. This will be discussed in Chapter 3.

(3) The non-selective (flat) fading of the received signal amplitude, which reduces the average signal to noise ratio at the receiver, and increases the average BER.

(4) The imperfect channel impulse response in the form of frequency selective fading, which introduces ISI to the received signal so that the amplitudes of the demodulated baseband quadrature waveforms are further reduced. This leads to a higher BER.

The last two elements are environment-related and hence are not controllable by a radio system designer. However their statistical characteristics can be estimated so that appropriate signal processing techniques can be devised to mitigate their effects.

2.4.4 COMPUTER SIMULATION

A computer simulation was conducted in order to demonstrate the degradation in a digital communication system subject to signal fading and ISI such as exist in the mobile radio channel. Figure 2.17 shows, in terms of functional blocks, how a generalised digital mobile radio transmission system was simulated by using a digital computer. In the simulation the total interference was modelled by AWGN with zero mean and a given power. The digital modulation used in the simulation was GMSK with $BT = 0.3$. The information

was transmitted at 500 kb/s. The radio channel is represented by a tapped delay line, which has tap coefficients equal to the sampled values of an estimated channel impulse response [13]. Each coefficient represents the average energy of multiple radio waves arriving at the receiver antenna with a fixed time delay. The amplitude of the resultant signal at each fixed time delay is assumed to be Rayleigh distributed. This assumption is not strickly accurate for the situations where a receiver travels over a large distance (eg. 1km), and the average power of the received signal becomes log-normal distributed [13]. If the receiver only travels over a short distance(eg. 50m), then the average signal power and the channel impulse response can be regarded as stationary, i.e. it does not change against time, therefore only a small amount of data (eg. 100000 bits) is required in the simulation in order to reduce computing time. The estimated channel impulse response used in the simulation was obtained from [13], which was measured at 837MHz and 0.1 μs resolution in Liverpool University precinct. Figure 2.18 shows the sampled values of this impulse response. The Rayleigh distributed amplitude was generated by using the method described in [10], where 8 sinusoidal signals, each with its own independent amplitude and phase, are combined together in order to simulate the arrival of multiple wave fronts. The maximum frequency of these sinusoidal signals was set to 40 Hz in order to simulate the Doppler frequency shift. The receiver was assumed to be in complete phase and clock synchronisation with the transmitter. This assumption is made because the simulation was intended to serve as a demonstration of degradation (which is caused by the Rayleigh fading and the ISI introduced by the mobile radio channel) in the performance of a digital mobile radio system. Simulations on carrier and clock recovery techniques are beyond the scope of this thesis.

The average BER obtained from the computer simulation are presented in Figure 2.19, which shows that the average BER remains high as the average SNR increases. This is because the eye pattern has already been closed by the ISI in the absence of AWGN, and if the received signal is faded a slight amount of AWGN can cause a large number of errors. Because the BER is

high the bits errors may occur in a group (or an error burst). IEEE defines [1] an error burst as a group of bits in which two consecutive erroneous bits are always separated by less than a given error free gap length. An error free gap length (or gap length for simplicity) is defined as the number of correct bits between two errors. For example, let 'c' and 'e' represent a correct and erroneous bit respectively, then a bit stream '...ecccccccc...' will have a gap length of 7. An investigation on the error free gap length distribution will help the system designer to determine the realistic error burst length, and if this length is long, a more complicated, hence more expensive, signal processor (e.g. an error-correction coder-decoder or an equaliser) should be used in order to reduce the BER. Figure 2.20 shows the gap length distribution from the computer simulation. From this graph it was found that 70 percent of the gap length are under 10, and 90 percent of the gap length are under 20 etc..

It should be emphasised again that this simulation only serves as a demonstration,

2.4.5 METHODS FOR REDUCING BER

The average BER may be reduced by the following methods.

(1) Selecting an optimised modulation-demodulation technique which compromises between the maximum SNR and high power spectral efficiency.

(2) Using diversity techniques either in space, time or frequency to reduce the effects of non-selective signal fading [10].

(3) Using channel equalisation to cancel the ISI in the received baseband signals [1, 4].

---

[1] IEEE Dictionary of Technical Terms

(4) Introducing error control codes after channel equalisation to further reduce the BER [15].

Specific knowledge of the channel for a given transmission frequency and data rate are essential and must be available before an optimum communication system can be designed. Estimation of the statistical distributions of the signals amplitudes will aid the selection of suitable diversity techniques whereas from the estimated channel impulse responses the most effective channel equalisation strategy can be planned. Finally, the bit error statistics can be obtained from equalised data so that an appropriate error correcting code can be devised. These important parameters should be estimated through an experimental investigation.

2.5 SPECIFIC REQUIREMENTS FOR A TDMA SYSTEM

2.5.1 BASIC TDMA STRUCTURE

In a TDMA system, a single radio channel is shared sequentially by a certain number of users in short time durations, or time bursts. As a consequence, each user will transmit and receive high speed data intermittently via a buffer memory. Figure 2.21 shows the timing relationship in a 7-user TDMA system, where bursts from each user with equal time duration are organised in a TDMA frame. The frame begins with a reference burst RB0, which is sent out by a radio base station in order to establish the synchronisation of the TDMA frame. User 1 will then access the channel at time t_1 with a burst UB1, user 2 at t_2, with UB2 and so on.

Due to the delays in propagation of radio waves, a user who is nearer to the radio base station will respond to the reference burst quicker than those who are further away. In order to prevent the bursts from overlapping, a 'guard period' is attached at the end of each burst, where no signal is sent. For example, the GSM system uses a guard period which is equivalent to 8.5 bits

[16]. Also in a practical TDMA system such as GSM, frames carrying control data are multiplexed with the frames that carry information [16], in order to perform supervisory tasks such as 'power control', 'handover' etc. The signal conditions in a TDMA system will be discussed in the following section.

2.5.2 SWITCHING NOISE IN A TDMA SYSTEM

The switched mode transmissions in a TDMA system cause sudden transitions in the time domain, hence it will generate spurious spectral energies over a wide bandwidth. When these energies spread to the adjacent TDMA channels, they appear to be noise power so that the average BER in that channel will increase.

This switching noise can be reduced by adopting a time domain window on the transmission burst to restrict the on-off transitions [17], and by using bandpass filters in the receiver to reduce the admitted noise. The selection of such a filter in the receiver will be discussed in Chapter 3. The disadvantage of using the window and filter is that the first few information symbols in a transmission burst will be distorted. Therefore extra protection symbols which do not carry information are put in front of the data sequence. These protection symbols are referred to as 'tail bits'. For example, the GSM system uses 3 tail bits [16].

2.5.3 THE CHANNEL IMPULSE RESPONSES

The data transmission rate in a TDMA system is generally high (e.g. 270 kb/s in GSM), therefore the transmission is more vulnerable to the multiple signal delays exhibited by the channel. The channel impulse response can be regarded as the same within a transmission burst because of the short time duration, but it may vary from one transmission burst to another, depending upon the relative movement between the transmitter and the receiver.

2.5.4 DISTRIBUTION OF THE AMPLITUDES OF THE RECEIVED SIGNAL

In a practical TDMA system, the burst length is very short (e.g. 0.5 ms in GSM). The relative movement between a transmitter and a receiver during this interval is negligible, hence the received signal amplitude can be regarded as unchanged. As the receiver moves across an area where a standing wave pattern exists, the amplitudes measured at each burst interval can be regarded as sampled values of the standing wave. Within a certain observation space, these samples form a stationary random process with constant mean and variance, therefore they are expected to have the same amplitude probability density distribution as a continuous transmission.

2.5.5 AN EXPERIMENTAL INVESTIGATION

The signal fading and channel impulse responses discussed in the previous sections are related to the carrier frequency and environment. The statistical models adopted in the theoretical analysis represent a general situation, where a large number of samples were collected for lengthy periods of time in order to form a random process.

Although a computer simulation of the performance of digital transmissions over a mobile radio channel can be conducted based upon the result from propagation measurements, it only provides a general assessment of the system performance, or a boundary of performance, because of the generalised statistical models used in such simulations. In reality, there may be exceptional circumstances during a high bit rate TDMA digital transmission over a real time communication channel (e.g. at 1.8 GHz carrier frequency), where the general statistical models would require modifications in order to maitain a certain degree of accuracy. These modifications are normally made

based upon results from experimental investigations over a real time mobile radio channel.

Experimental investigations of the propagation characteristics at a frequency around 1.7 GHz have been made recently [18, 19], but they were not extended to include the quality (e.g. in terms of BER) of data transmissions. It would be useful to systematically investigate the performance, in terms of the average BER and bit error distribution, of a TDMA system operating in the real time mobile radio channel at 1.8 GHz. Such an investigation can be extended to include estimation of the real time channel impulse response and the amplitude of the received signal in order to relate such parameters to the measured BER. Furthermore, channel equalisation techniques can be applied in order to investigate their effects on the bit error distributions. The bit error distributions after the channel equaliser will provide valuable information in the selection of cost-effective error-correcting codes.

In order to carry out such investigations, it is necessary to develope a dedicated experimental system. The design of this system can be divided into two parts.

The first part of the system should be able to estimate and record parameters in the real time communication channel, such as signal level, demodulated waveforms and channel impulse response from the field trials. As it was mentioned in Chapter 1, there are many contenders for the future digital mobile radio system (eg.PCN is likely to adopt the GSM standard of using GMSK modulation and TDMA transmission). In order to assess their performances in a real time communication channel, the experimental system should be versatile so that it can accept different modulation techniques, with variable data transmission bit rates and at different carrier frequencies, and it should not be limited to using the TDMA format alone. For example, the SCPC FDMA technique ought to be accepted as an alternative.

The recorded data can then be transferred to the second part of the system, which is a computer, where data analysis can be carried out to extract statistical information, such as distributions of the received signal level, delays in

the estimated channel impulse response, average BER and error-free gap distribution etc., from the measurements. In addition to the statistical data analysis, more sophisticated signal processing techniques can be tested. For example, channel equalisers with different structures and various parameters can be implemented in computer software. Their performance in terms of BER and error free gap distribution after the equalisation can be compared in order to determine which is more efficient.

The development of such an experimental system will be presented in Chapter 3.

2.6 REFERENCE

[1] Proakis, J. G. "Digital Communications", McGraw-Hill, New York, 1985.

[2] Feher, K. "Digital Communications, Satellite/Earth Station engineering", Prentice-Hall Inc., New Jersey, 1981.

[3] Stremler, F. G. "Introduction to Communication Systems", Addison-Wesley Publishing Company, Massachusetts, 1982.

[4] Stein, S. Jones, J. J. "Modern Communication Principles With Application to Digital Signaling", McGraw-Hill, 1967.

[5] Carson, R. S. "High-Frequency Amplifiers", 2nd edition, John Wiley & Sons, New York, 1982.

[6] Maseng, T. "Digitally Phase Modulated (DPM) Signals", IEEE Trans. Commun., vol. COM-33, NO.9, pp. 911-918, Sept 1985.

[7] Aulin, T. "Continuous Phase Modulation-Part I: Full Response Signaling", IEEE Trans. Commun., vol. COM-29, NO.3, pp. 196-209, Mar 1981.

[8] Aulin, T. "Continuous Phase Modulation-Part II: Partial Response Signaling", IEEE Trans. Commun., vol. COM-29, NO.3, pp. 210-225, Mar 1981.

[9] Murota, K. Hirade, K. "GMSK modulation for Digital Radio Technology", IEEE Trans. Commun., vol. COM-29, NO.7, pp.1044-1050, July 1981.

[10] Jakes, W. C. "Microwave Mobile Communications", John Wiley & Sons, New York, 1974.

[11] Lee, W. C. Y. "Mobile Communications Engineering", McGraw-Hill, New York, 1982.

[12] Cox, D. C. "Delay Doppler Characteristics of Multipath Propagation at 910 MHzin a Suburban Mobile Radio Environment", IEEE Trans. Antennas and Propagation, vol. AP-20, NO.5, Sept 1972.

[13] Demery, A. "Wideband Characterisation of the UHF Mobile Radio Channel", Ph.D. Thesis, Department of Electrical Engineering and Electronics, University of Liverpool, Mar 1989

[14] Lucky, R. W. Salz, J. Weldon, E. J. "Principles of Data Communication", McGraw-Hill, New York, 1968.

[15] Lin, S. Costello, Jr. D. J. "Error Control Coding: Fundamentals and Applications", Prentice-Hall, New Jersey, 1983.

[16] Balston, D. M. "Pan-Europen cellular radio: or 1991 and all that", Electronics and Communication J., pp.7-13, Jan 1989.

[17] Oppenheim, A. V. Schafer, R. W. "Digital Signal Processing", Prentice-Hall, New Jersey, 1975.

[18] Motley, A. J. "Personal Communication Coverage in Buildings at 900 and 1700 MHz", Electronic Letters, Vol. 24, No. 12, pp.763-764, June 1988.

[19] Bultitude, R. J. C. et al. "A comparison of Indoor Radio Propagation Characteristics at 910 MHz and 1.75 GHz", IEEE Journal on Selected Areas in Communications, Vol. 7, No. 1, Jan 1989.

[20] Simon, M. K. Wang, C. C. "Differential Detection of Gaussian MSK in a Mobile Radio Environment", IEEE Trans. on Vehiclar Technology, Vol. VT-33, No. 4, Nov 1984.

[21] Wozencraft, J. M. Jacobs, I. M. "Principles of Communication Engineering", John Wiley & Sons, New York, 1967.

[22] Sundberg, C. E. "Continuous Phase Modulation", IEEE Communication Magazine, Vol. 24, No. 4, pp.25-38, April 1986.

[23] Papoulis, A. "Probability, Random Variables, and Stochastic Processes", McGraw-Hill, New York, 1985.

[24] Cooper, G. R. McGillen, C. D. "Probabilistic Methods of Signal and System Analysis", Holt, Rinehart and Winston, New York, 1971.

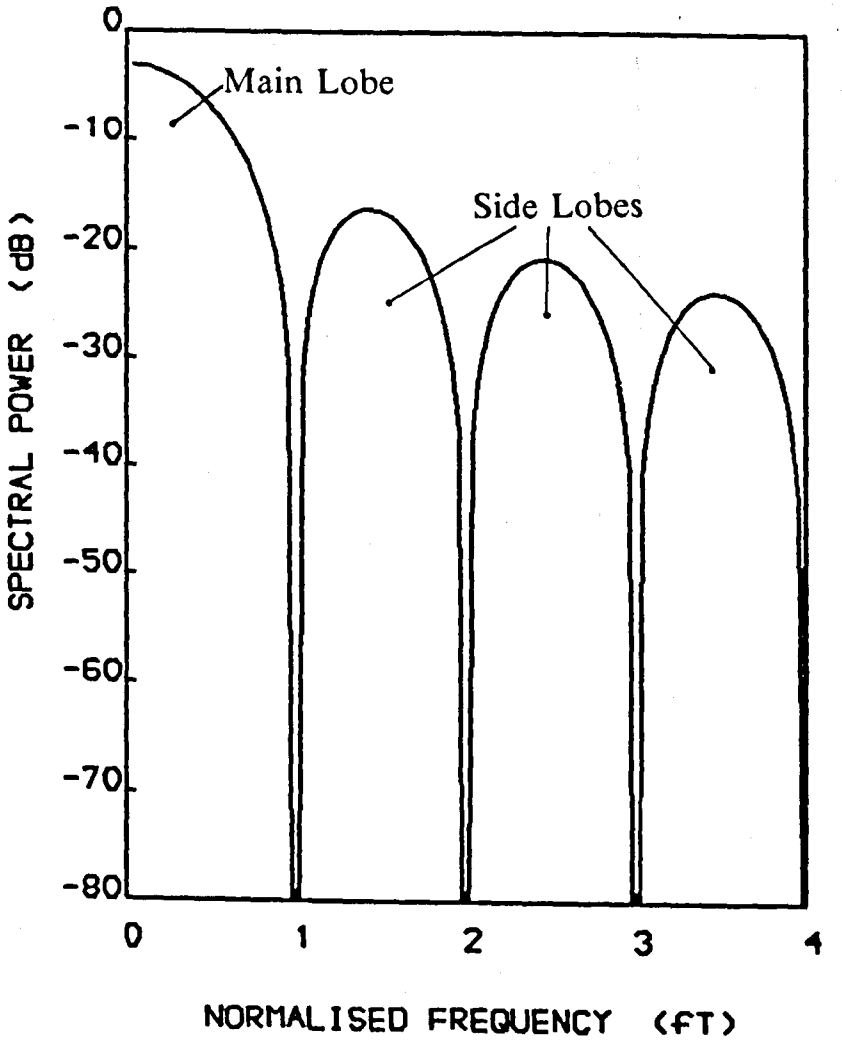

Figure 2.1 Power spectrum of a Binary Phase Shift Keying modulated signal.

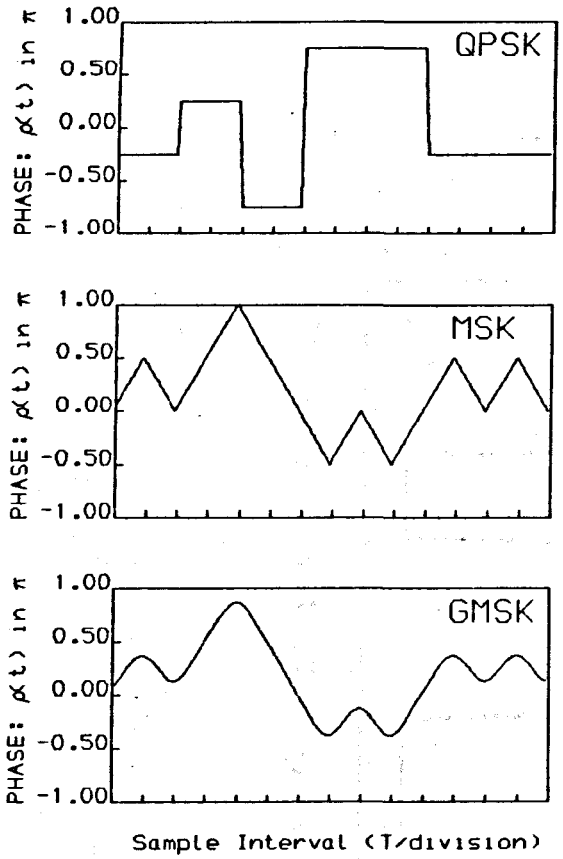

Figure 2.2 Modulated phase in QPSK, MSK, GMSK with $BT = 0.3$ modulations.

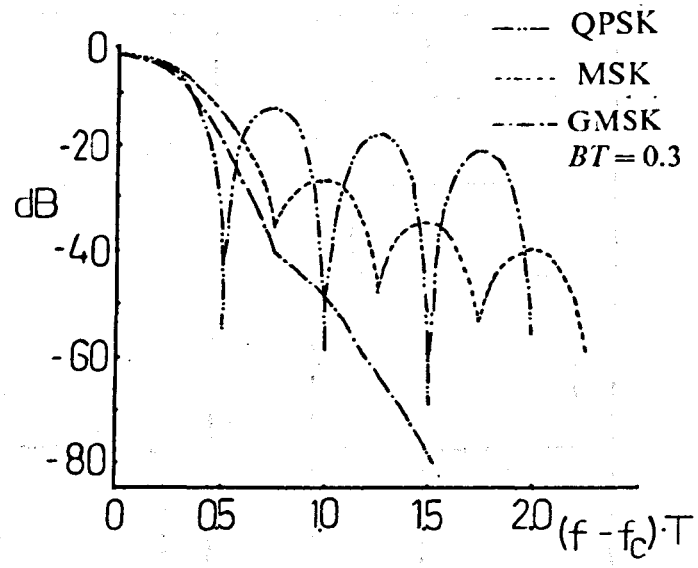

Figure 2.3 Power spectra of QPSK, MSK and GMSK with $BT = 0.3$.

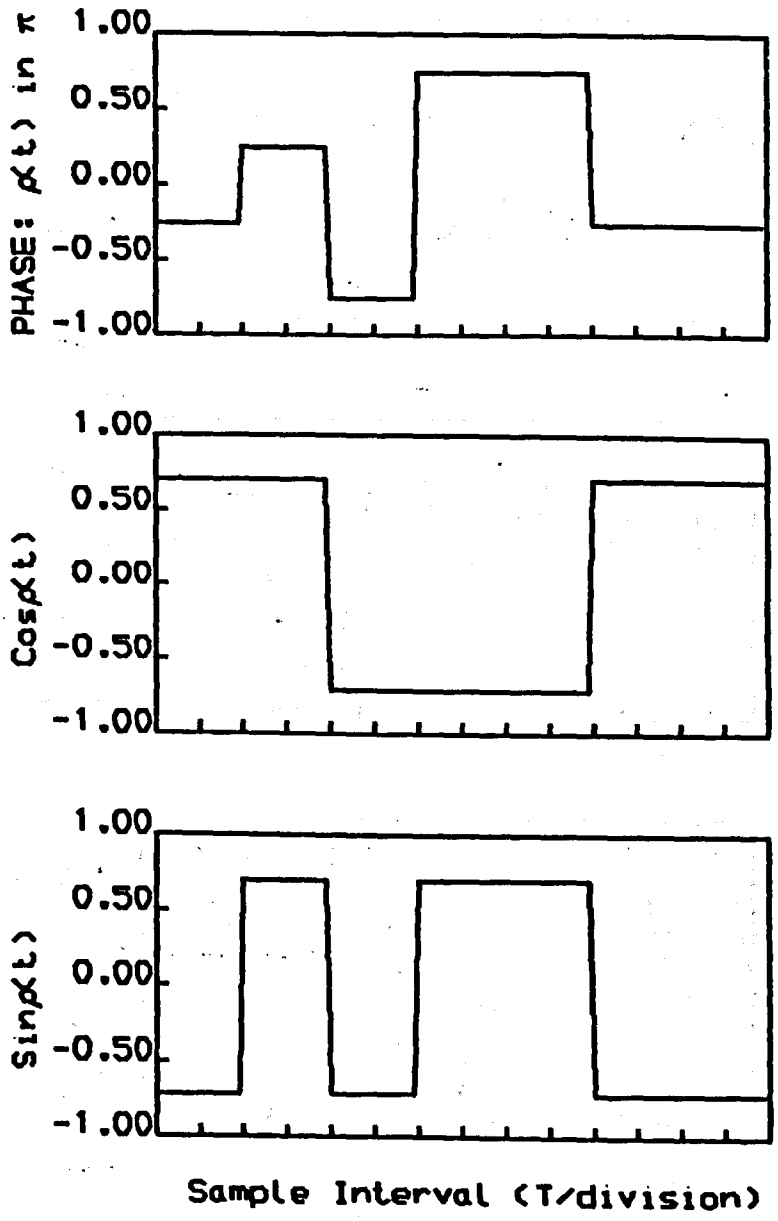

Figure 2.4 Phase and baseband quadrature waveforms in QPSK modulation.

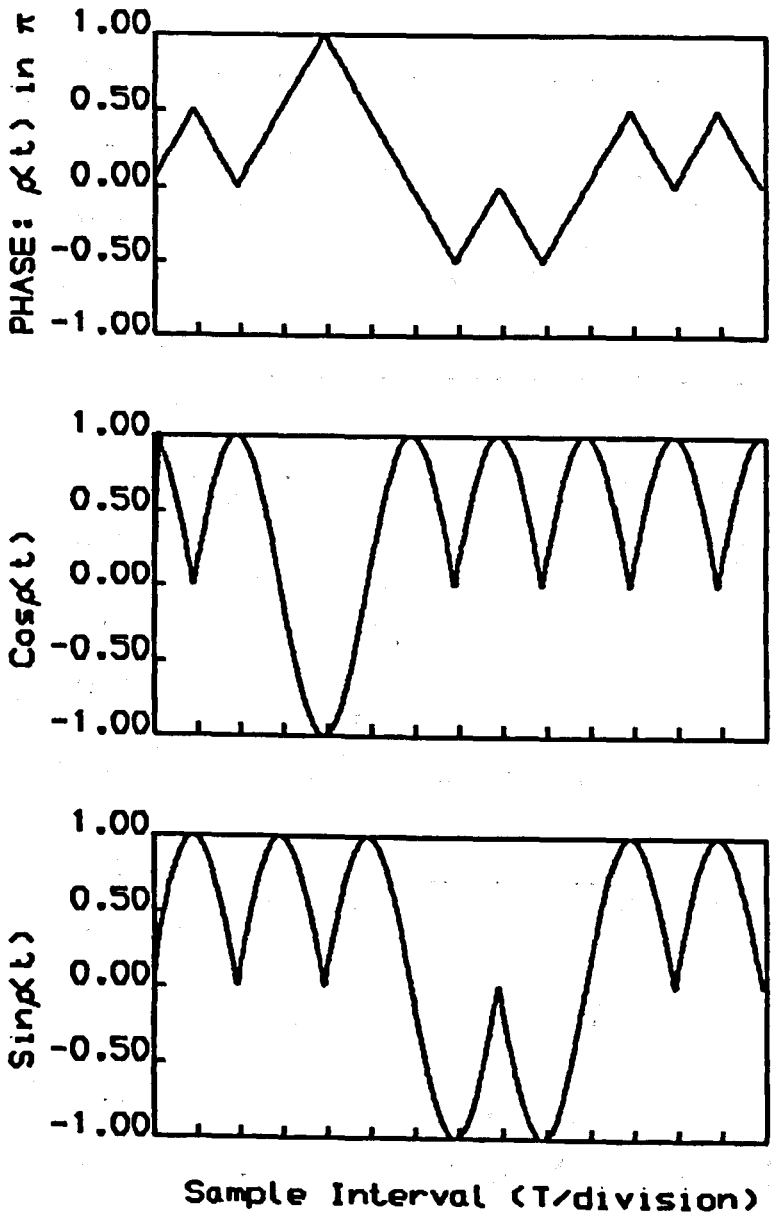

Figure 2.5 Phase and baseband quadrature waveforms in MSK modulation.

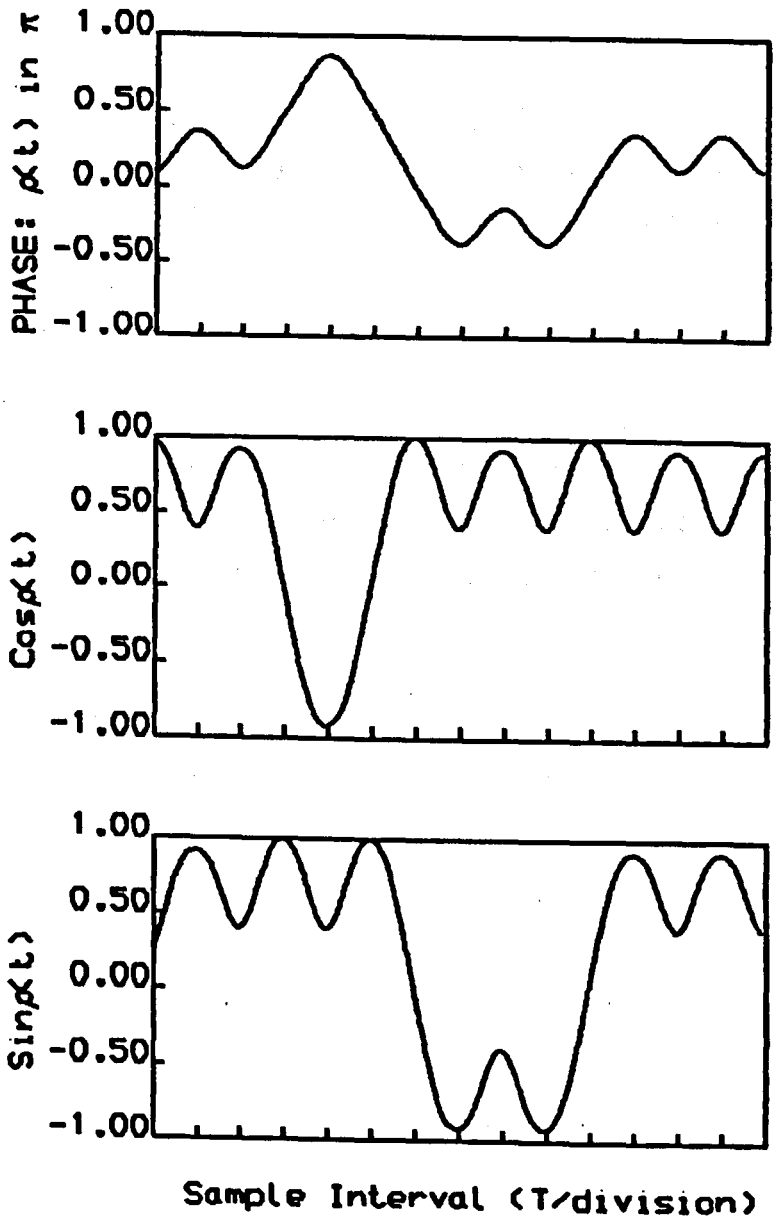

Figure 2.6 Phase and baseband quadrature waveforms in GMSK with $BT = 0.3$ modulation.

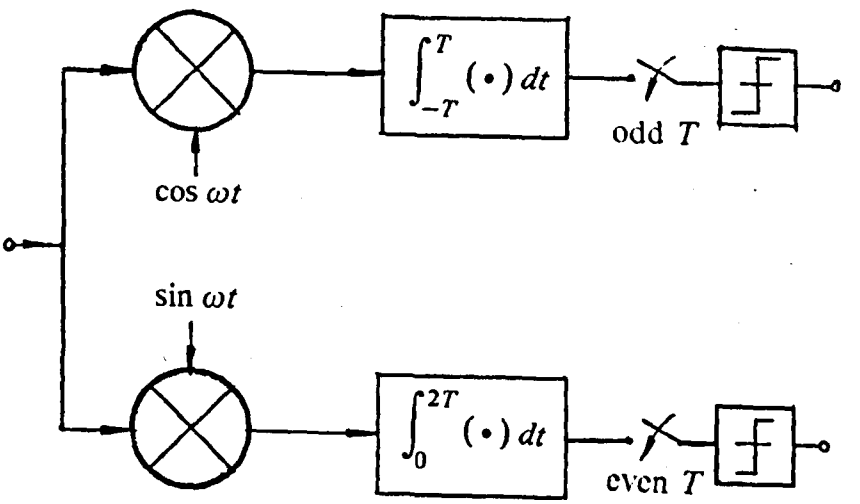

Figure 2.7 Block diagram of the coherent detector.

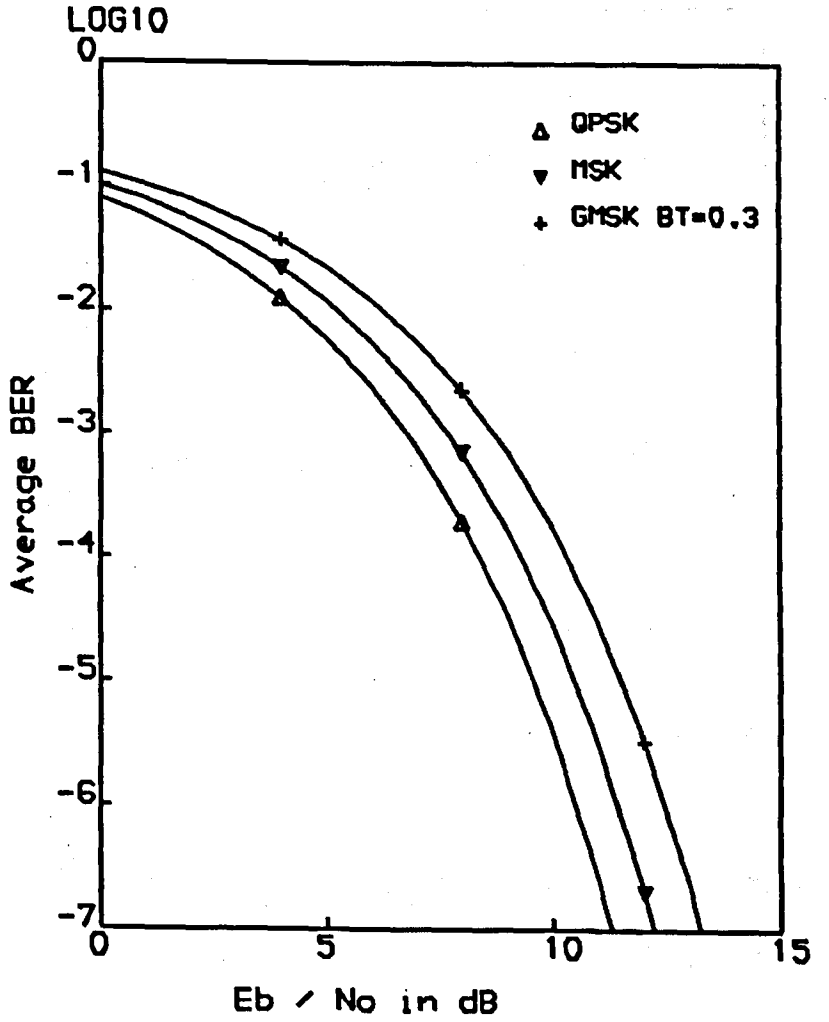

Figure 2.8 Average BER in coherent detection of QPSK, MSK and GMSK with $BT = 0.3$ signals in the presence of AWGN.

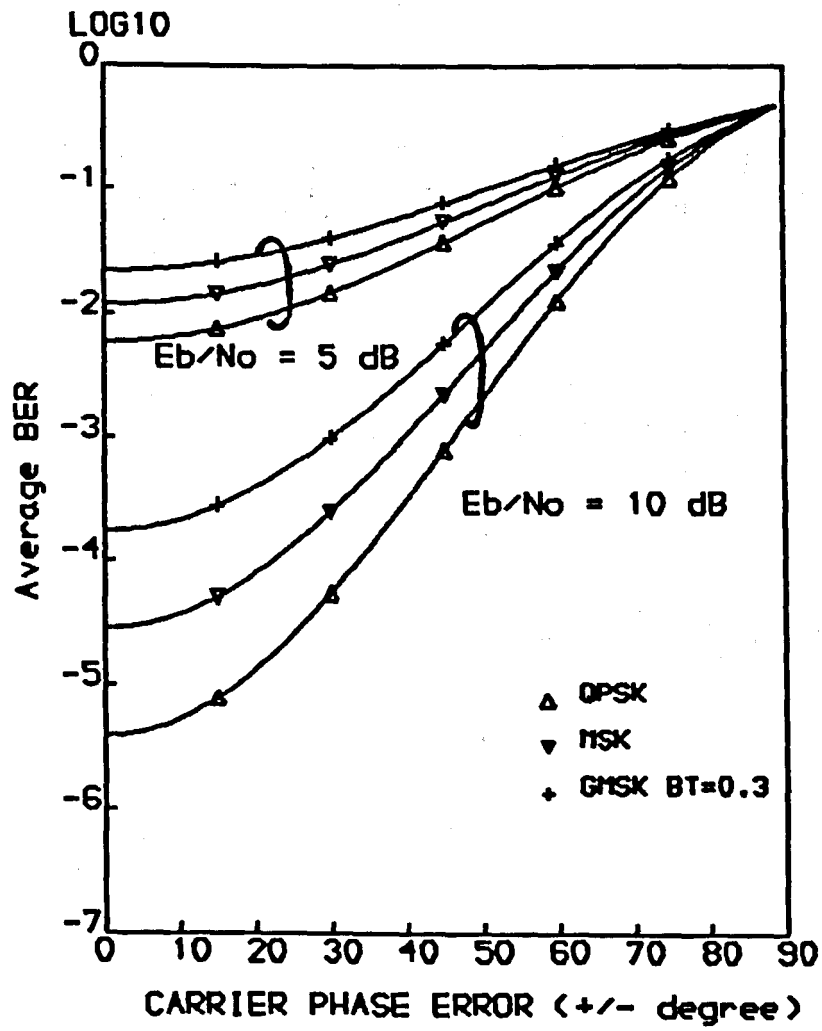

Figure 2.9 Average BER in coherent detection of QPSK, MSK and GMSK with $BT = 0.3$ signals in the presence of AWGN, subject to carrier phase error.

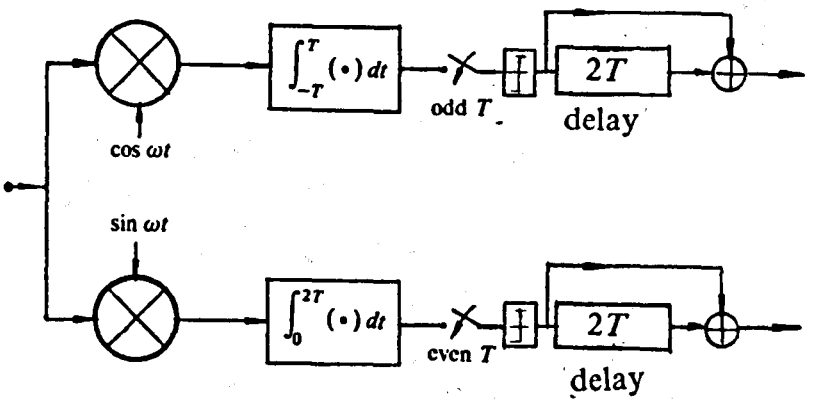

Figure 2.10 Block diagram of the coherent differential detector.

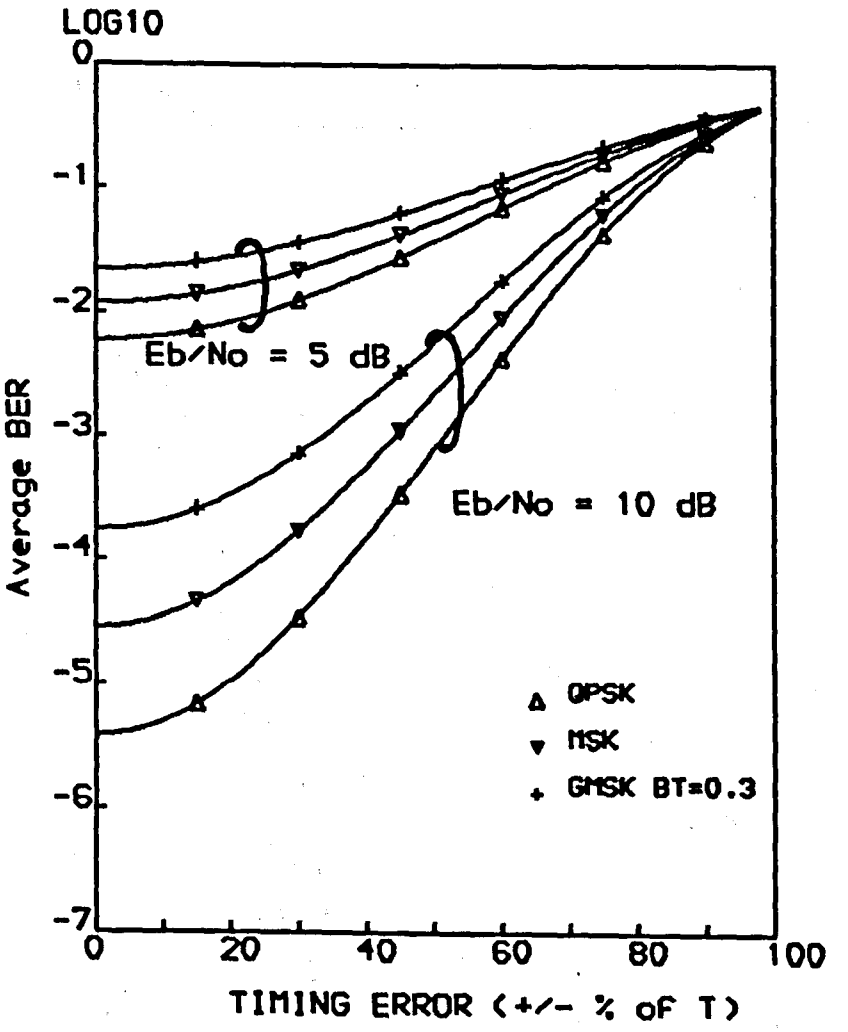

Figure 2.11 Average BER in coherent detection of QPSK, MSK and GMSK with $BT = 0.3$ signals in the presence of AWGN, subject to sampling time error.

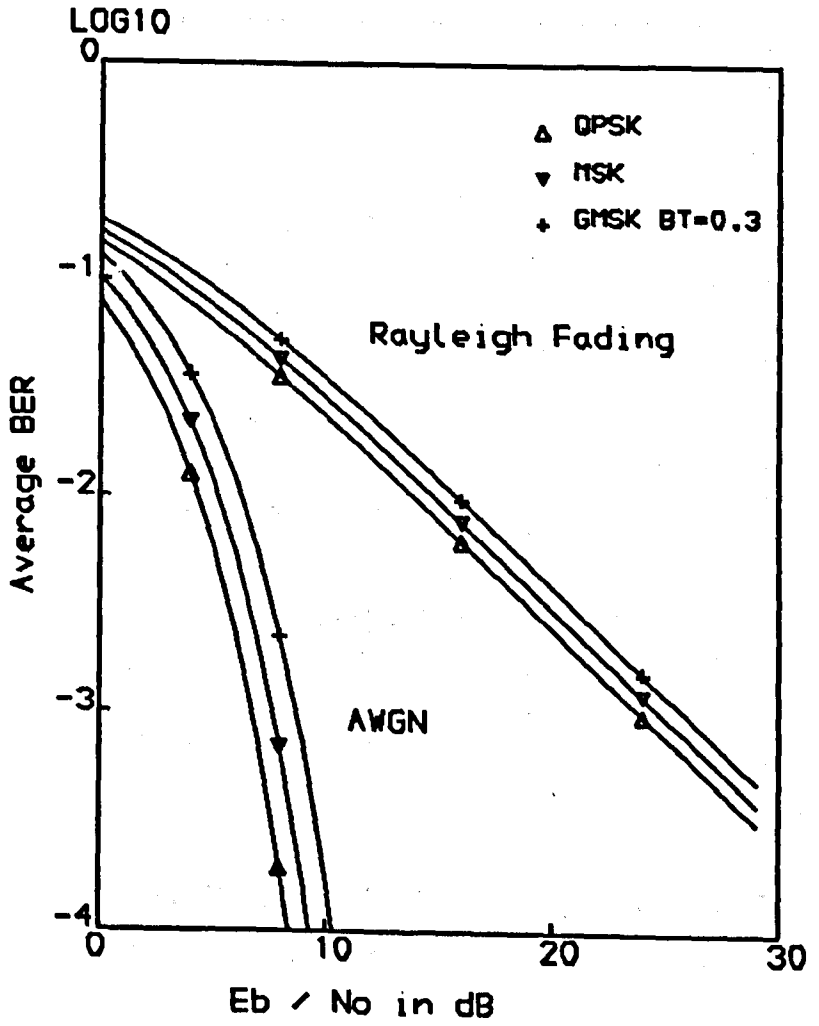

Figure 2.12 Average BER in coherent detection of QPSK, MSK and GMSK with $BT = 0.3$ signals in the presence of AWGN, before and after Rayleigh fading.

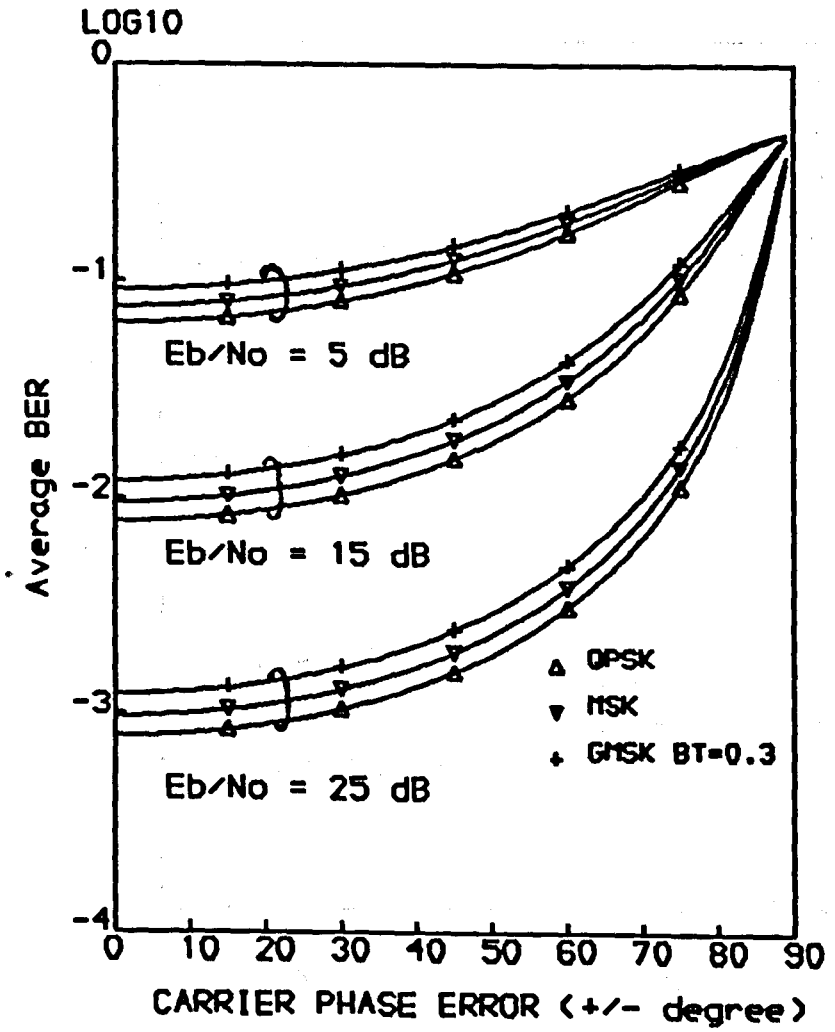

Figure 2.13 Average BER in coherent detection of QPSK, MSK and GMSK with $BT = 0.3$ signals in the presence of AWGN, Rayleigh fading and carrier phase error.

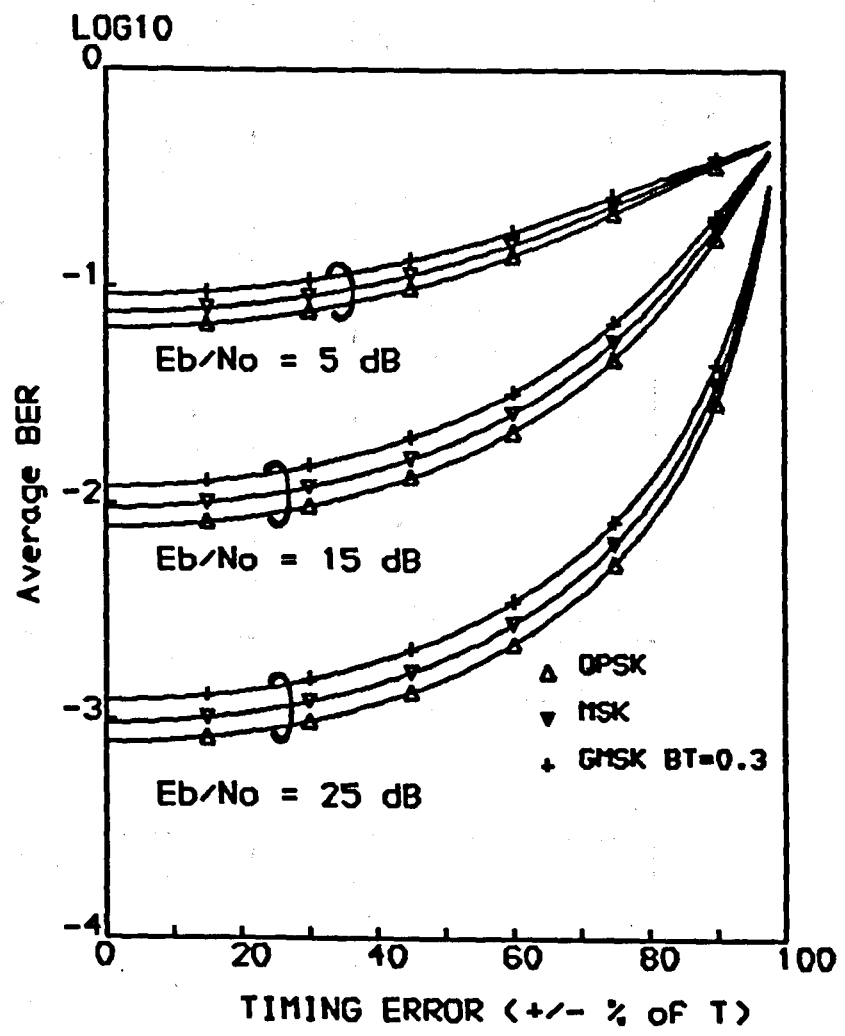

Figure 2.14 Average BER in coherent detection of QPSK, MSK and GMSK with $BT = 0.3$ signals in the presence of AWGN, Rayleigh fading and sampling time error.

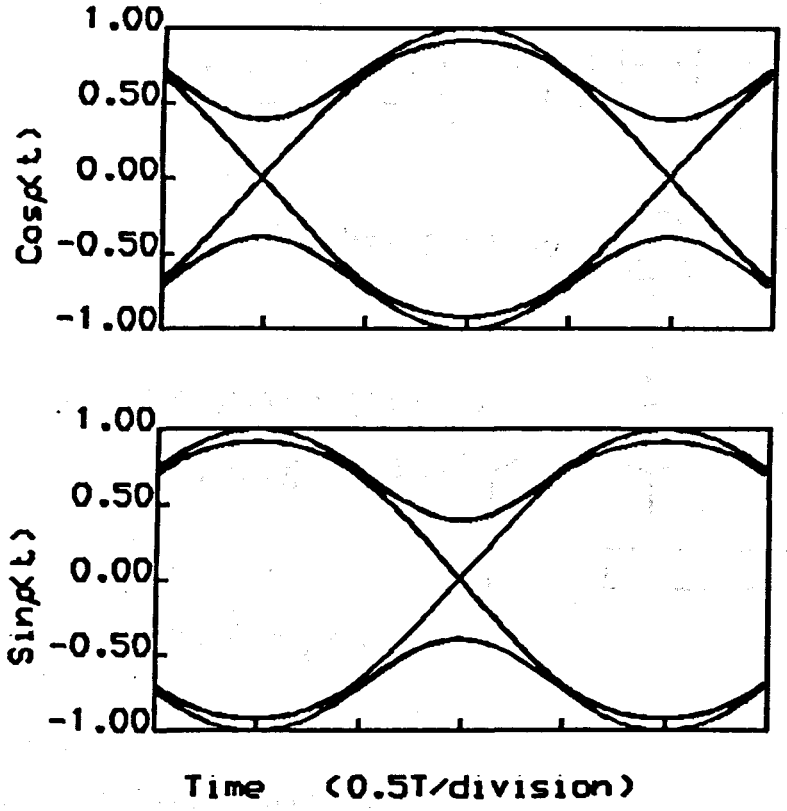

Figure 2.15 Eye pattern of the GMSK with $BT = 0.3$ modulated signal in the absence of ISI.

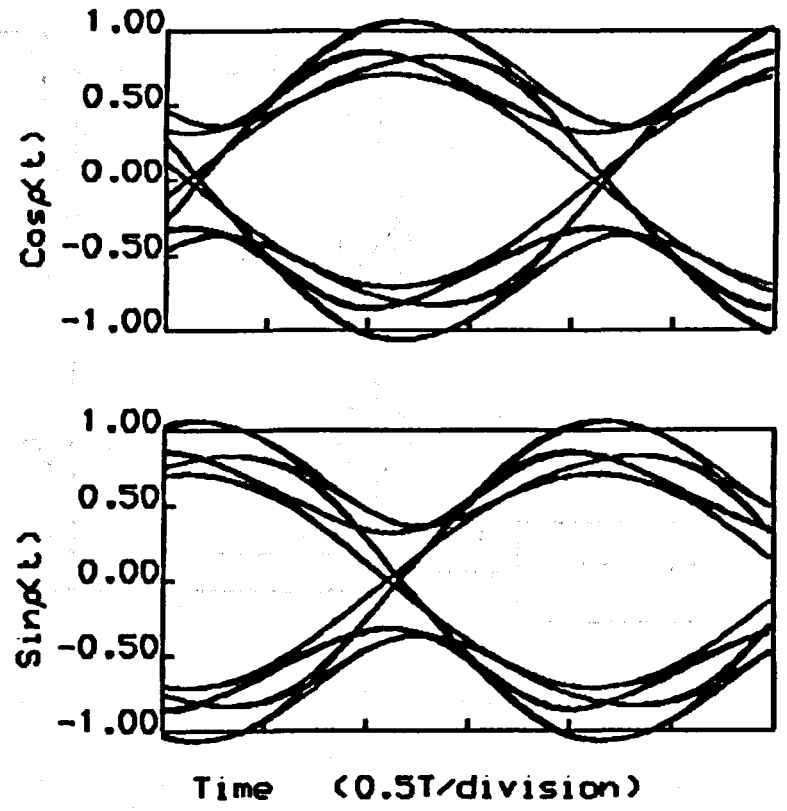

Figure 2.16 Eye pattern of the GMSK with $BT = 0.3$ modulated signal in the presence of ISI.

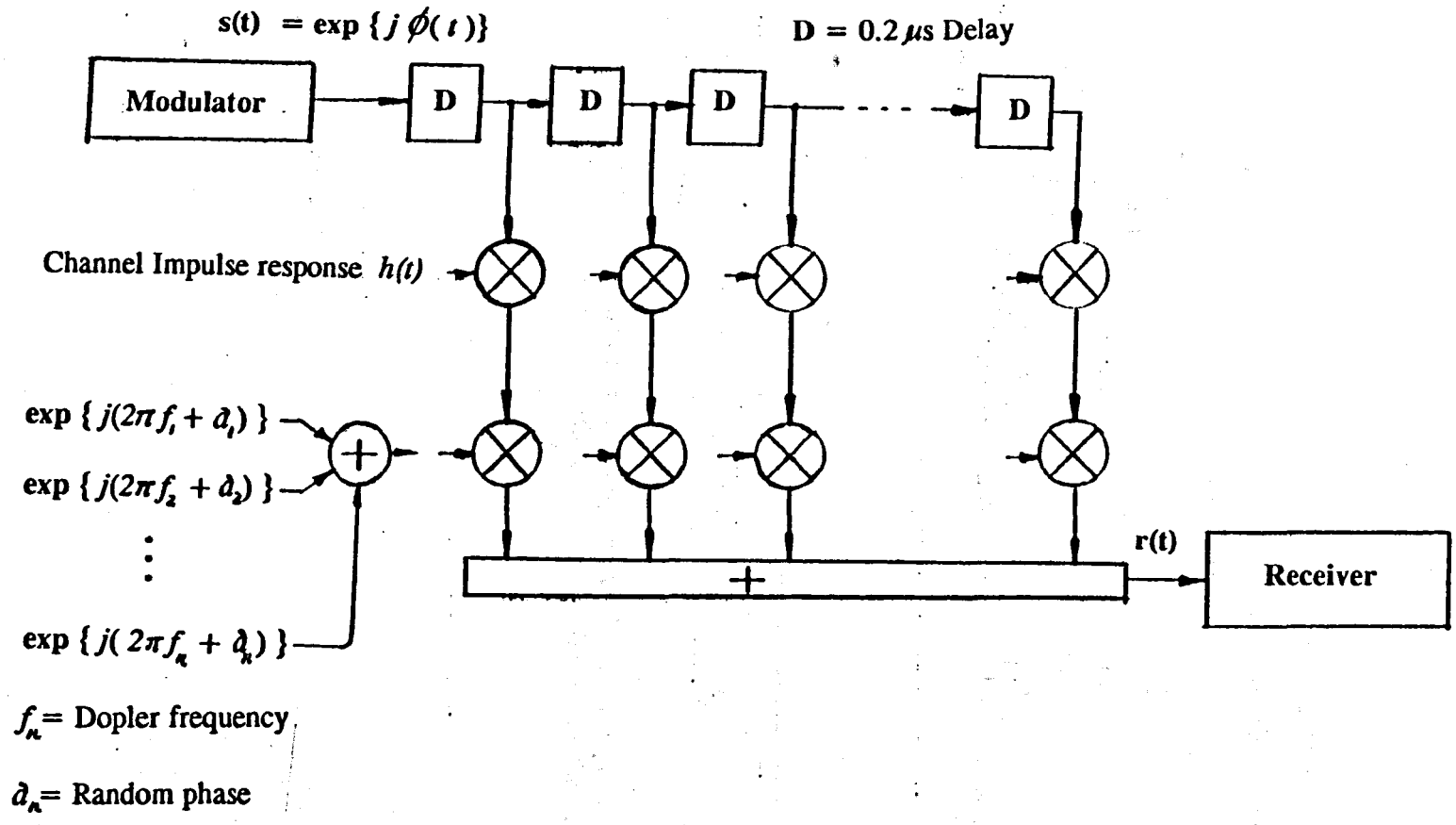

Figure 2.17 The block diagram of the computer simulated system.

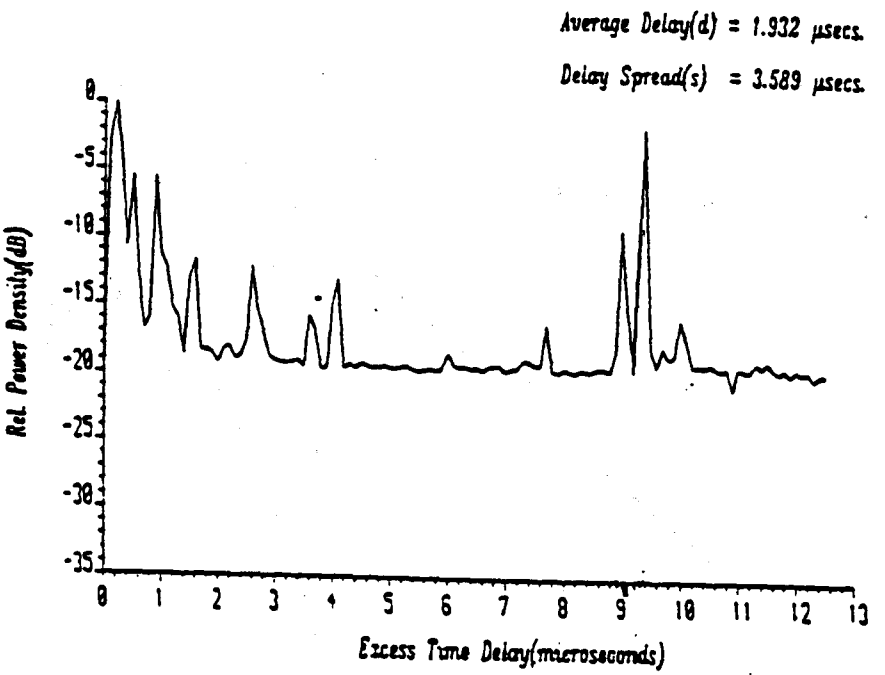

Figure 2.18 Channel impulse response used in the computer simulation. (Courtesy of Dr. A. Demery, reference [13])

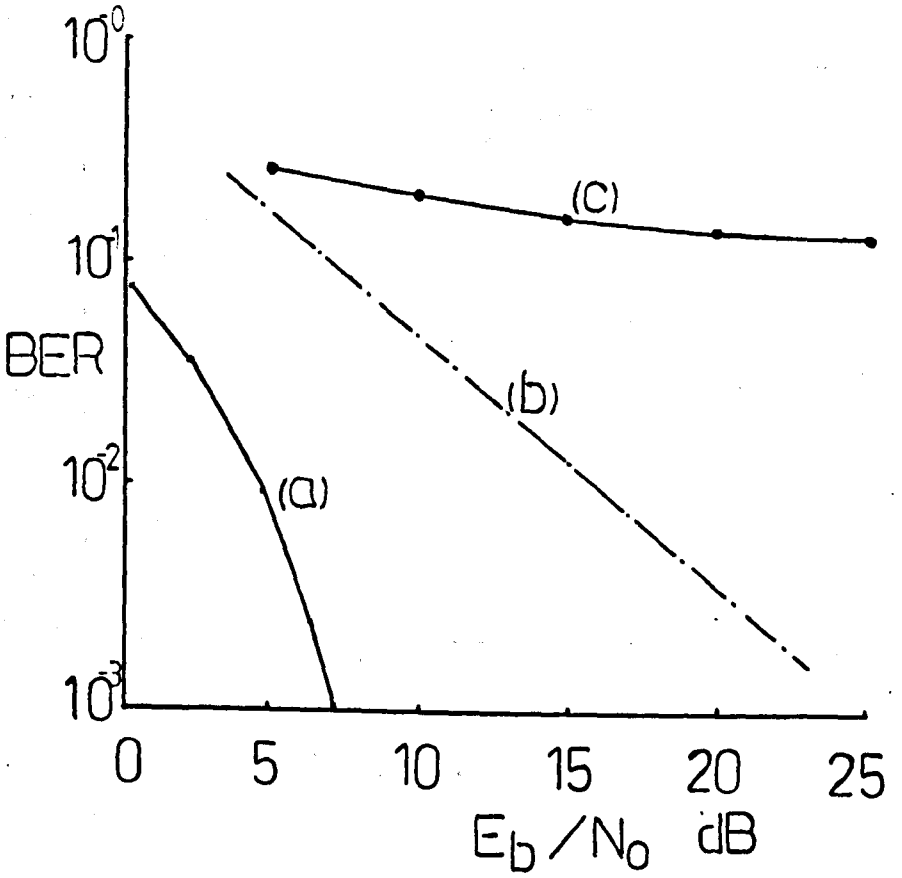

Figure 2.19 Simulated BER in (a) AWGN, no fading and no ISI, (b) AWGN, Rayleigh fading and no ISI, (c) AWGN, Rayleigh fading and using the channel impulse response in Figure 2.18.

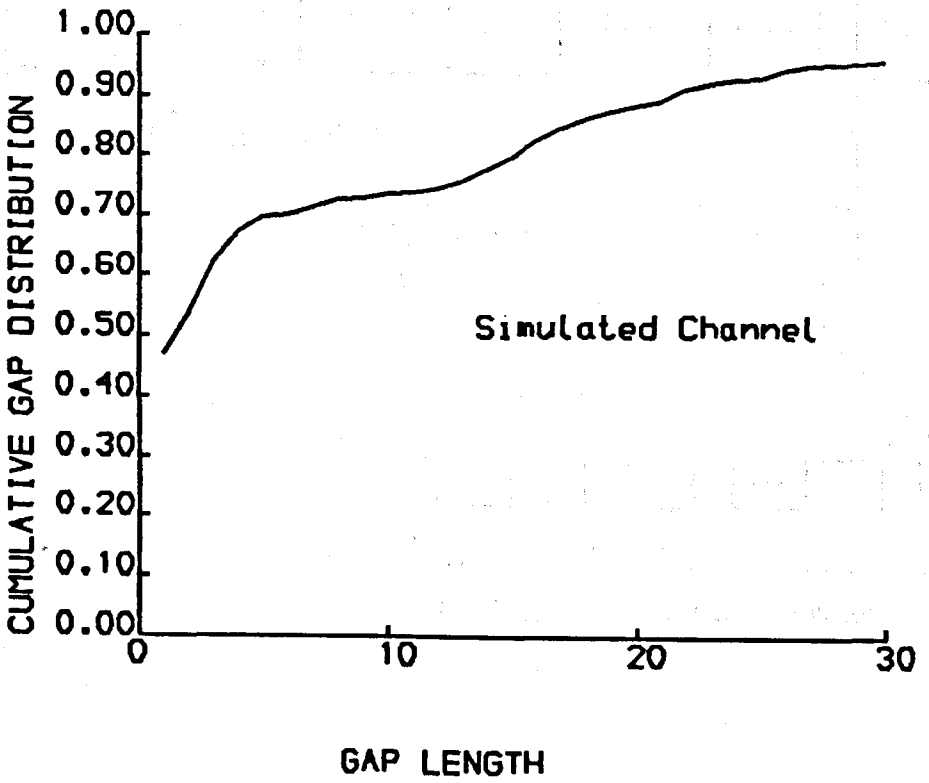

Figure 2.20 Simulated error free gap length distribution at $E_b/N_o = 20$ dB .

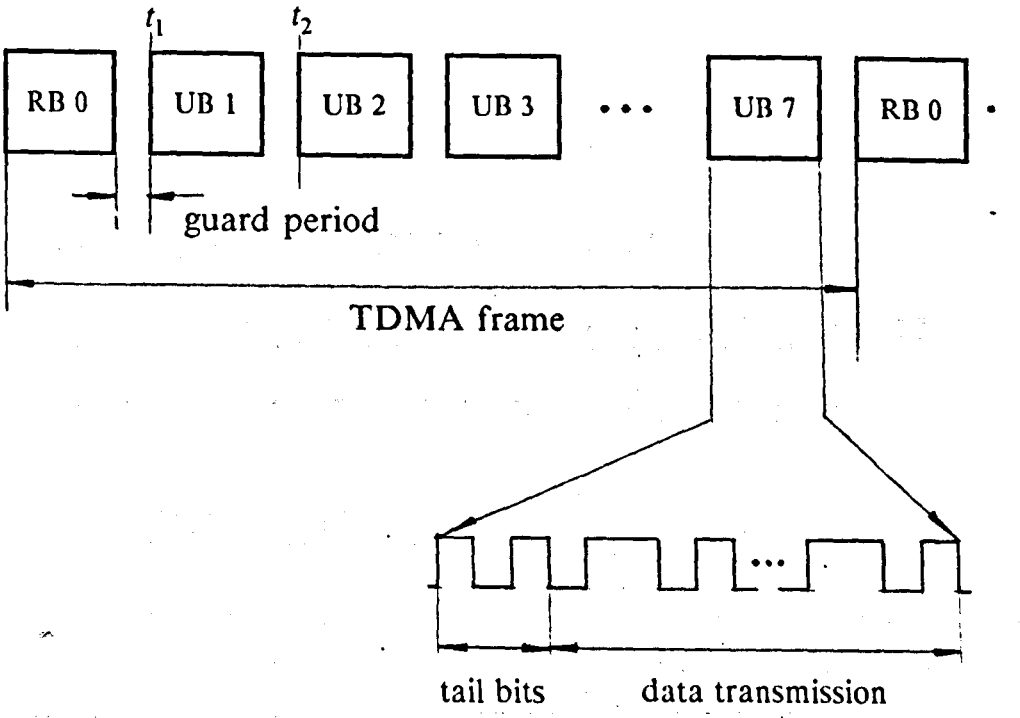

Figure 2.21 Timing relationship in a 7 user TDMA system.

CHAPTER 3 DESIGN AND IMPLEMENTATION OF A VERSATILE TDMA EXPERIMENTAL SYSTEM

3.1 INTRODUCTION

The effects of various parameters on the average BER in the coherent detection of digital transmission over a mobile radio channel have been reviewed in Chapter 2. Special attention was directed toward the TDMA system, where information symbols are transmitted in short bursts with a high bit rate. The two environmental and frequency dependent parameters were identified as the imperfect channel impulse response, which introduces ISI, and the fading of the received signal amplitude, which reduces the SNR (E_b/N_o) in the presence of AWGN. It was emphasised that these parameters and their effects on the average BER should be estimated and analysed before a cost effective communication system can be designed. The design and implementation of a versatile experimental system to carry out such estimations will be presented in this chapter. The results from a laboratory calibration of the system are also included.

3.2 OVERVIEW OF THE SYSTEM

Digital transmission over a mobile radio channel may take place within a wide range of the radio spectrum, with various bit rates, and utilise different modulation techniques. An experimental system, therefore, should be adaptable to a specific requirement with minimum modifications. The exper-

imental system presented in this chapter consists of two major parts, i.e. a transmitter and a coherent receiver, which is interfaced to a digital tape recorder via a computer controlled buffer. The block diagrams which represent the transmitter and receiver are shown in Figure 3.1 and Figure 3.11 respectively, and their functions will be discussed in detail in the following sections. In general, the transmitter is able to accept various digital modulation techniques and to transmit binary data at a variable bit rate, either continuously or in short time bursts, within a wide range of radio frequency spectrum. The coherent receiver includes a radio frequency down converter, an IF carrier recovery circuit, a clock recovery circuit and a digital complex channel impulse response estimator. This system can estimate, in real time, the received signal power (which is also referred to as the received signal level) and the channel impulse response. The in-phase and quadrature demodulated waveforms are sampled by the recovered clock. The estimated signal level and the demodulated samples are digitised and recorded with the estimated impulse response for off-line signal processing (using computer software), at a later stage of the experiment. The arrangement of the hardware and the software combination provide a cost effective solution to testing a vast number of digital signal processing algorithms in real time mobile radio channels.

The experimental system is versatile in two aspects. The first is that it can adopt various digital modulation techniques by simply re-programming the Erasable Programmable Read Only Memory (EPROM) in the modulator, through a dedicated computer program. The second is that coherent detection is performed at a variable Intermediate Frequency (IF), where the carrier re-generating circuit is able automatically to track the slow phase variations, which are either due to the Doppler shift associated with relative movement between the transmitter and receiver, or the relative phase drift between various frequency sources used in the experimental system. Since various types of radio signal generators with very low phase-noise, general purpose radio frequency amplifiers and balanced mixers are commercially available, which can operate over a wide range of frequencies, the modulated IF signal can be up-converted, by utilising the above equipment, to any required experimental frequency. The experimental system can also provide a

wide range of timing sequences (e.g. frame period, burst duration, etc. as defined in Chapter 2) for the TDMA specification, or it can be switched to continuous transmission.

In the following sections the operational principle, design, implementation, and test results of each part of the system, represented in the functional blocks, will be presented.

3.3 THE TRANSMITTER

3.3.1 GENERAL DESCRIPTION OF THE TRANSMITTER

The transmitter consists of three fundamental building blocks which are, a timing control circuit, a versatile digital modulator and a frequency up conversion section, as shown in Figure 3.1. The timing control circuit generates timing sequences to set the transmission format of the modulator so that the transmitter can either continuously or intermittently transmit information with variable bit rates. The versatile modulator modulates the information symbols onto an IF carrier with the specific digital modulation technique required for the experiment. The frequency up conversion section converts the modulated IF carrier to the experimental frequency band.

3.3.2 THE TIMING CONTROL CIRCUIT

The timing control circuit derives three timing sequences (clocks) from a temperature compensated 10 MHz crystal oscillator by using cascaded Transistor Transistor Logic (TTL) programmable dividers. These timing sequences determine whether the system will operate in burst (TDMA) or continuous (FDMA) mode. These sequences are illustrated in Figure 3.2 and their functions are described as follows.

As mentioned in section 2.5, the TDMA bursts are organised in frames. The first timing sequence (sequence A in Figure 3.2(b)) generates the frame period, and it is referred to as 'frame'. Since the experimental system only has one user, the frame sequence is also used to set the burst duration. When the frame period is set to zero, a continuous transmission is achieved.

The second sequence (sequence B in Figure 3.2(b)) decides the transmission bit rate, $1/T$.

The third timing sequence (sequence C in Figure 3.2(b)) sets the over-sampling rate. In the experimental system, the baseband quadrature waveforms, which were described in section 2.3, are pre-calculated and sampled N (where $N = 2, 3, 4, \ldots$) times within a T bit interval. These samples are stored sequentially in two EPROM's. During the data transmission, they will be retrieved at a rate of N/T in order to restore the modulation waveform. This rate is referred to as the over-sampling rate and it was set to 10 times the bit rate $1/T$ during the experiment. Figure 3.3 shows how the over-sampling clock is used to read the data from the EPROM's.

These sequences can be changed by pre-loading the programmable dividers. As an example, the experimental results presented in this thesis used a burst transmission mode, with a burst duration of 512 μs, and the frame was 40 ms. The data transmission bit rate was set to 500 kb/s with an over sampling rate of 10. The reason for selecting the parameters listed above is as follows. The 40 ms frame period is the due to the limitation on the recording speed of the digital tape recorder used in the experiment. The 500 kb/s bit rate was selected (which is nearly twice the bit rate of the GSM system) in order to test the effectiveness of different equalisers. One of the objectives of this experimental study is to find which equaliser is most effective to combat the ISI. Since at a higher bit rate the effect of ISI on the system performance becomes more severe, the improvement of each equaliser at 500 kb/s is expected to be more noticable, hence easier to be compared. When the recorded data are processed by various channel equalisers at a later stage the most effective equaliser structure can be determined. A burst duration of 512 μs is selected because 256 information bits are transmitted in a burst in order to

estimate the channel impulse response, which will be discussed in detail in section 3.4.7.

3.3.3 THE QUADRATURE MODULATOR

This modulator, as shown in the block diagram in Figure 3.3, modulates the phase of a synthesised IF carrier by addressing the contents of two look-up tables, which contain the pre-calculated baseband quadrature waveforms corresponding to the information symbols. This modulator has three main sections, which are baseband quadrature waveform look-up tables, quadrature IF balanced mixers and a 45 to 90 MHz frequency synthesiser.

The operational principle of this quadrature modulator in generating a CPM signal is as follows. The CPM signal at a carrier angular frequency ω can be expressed as

$$\begin{aligned} s(t) &= A\cos(\omega t + \rho(t)) \\ &= A\cos\rho(t)\cos\omega t - A\sin\rho(t)\sin\omega t \end{aligned} \tag{3.1}$$

where A and $\rho(t)$ are the amplitude and phase of the carrier respectively. In order to generate this waveform, the $\cos\omega t$ term is derived from the IF frequency synthesiser, and its 90 degree phase-shifted version is the required $\sin\omega t$. In a linear system with a finite impulse response, the baseband quadrature waveforms $A\cos\rho(t)$ and $A\sin\rho(t)$ are defined within the information symbol duration T, and they can be pre-calculated as appropriate, according to each binary information symbol or a finite number of combinations of binary information symbols. The pre-calculated values can then be sampled and stored in a memory. When the transmission starts, the information symbols are accumulated to generate the address of the memory location so that the corresponding baseband waveforms can be retrieved and converted to analogue voltages by Digital to Analogue Converters (DAC). Finally the quadrature balanced mixers will combine the quadrature baseband waveforms and the carrier to obtain the modulated waveform $s(t)$.

GMSK modulation with $BT = 0.3$, which was discussed in Chapter 2, is spectrally efficient and does not produce excessive degradation in terms of average BER, compared with coherent QPSK and MSK modulation, in the presence of AWGN. These advantages make this modulation technique a favoured contender for mobile radio systems, and it was therefore selected initially for the experimental investigation. The implementation of this modulation technique, by the versatile modulator, is described below.

For GMSK modulation with $BT = 0.3$, as described in section 2.2, the phase $\rho(t)$ is given by

$$\rho(t) = 2\pi h \int_{-\infty}^{t} \sum_{i=-\infty}^{\infty} a_i \, q(t - iT) \, dt \tag{3.2}$$

where h is the modulation index(equal to 0.5), and $q(t)$ is the impulse response of the Gaussian baseband shaping filter, which is defined as

$$q(t) = \frac{\beta}{2\sqrt{\pi}} \exp(-\beta^2 t^2) \tag{3.3}$$

where β is a constant which is related to the normalised 3 dB bandwidth BT by

$$\beta = \pi \sqrt{\frac{2}{\ln 2}} \, BT \tag{3.4}$$

For $BT = 0.3$ the impulse response of the Gaussian filter is given by

$$q(t) = 0.4516 \exp(-2.5631 \, t^2) \tag{3.5}$$

where a_i takes values from $\{1, -1\}$. By exchanging the order of integration and convolution in equation (3.2), and taking into account that the impulse response of the Gaussian filter in equation (3.4) can be truncated into a finite time duration LT (where $L > 1$ is a positive integer), once its value falls below the quantisation noise level in the digital representation of the quadrature waveforms, the $\rho(t)$ can be approximated as [2]

$$\rho(t) = 2\pi h \sum_{i=n-L+1}^{n} a_i g(t - iT) + \pi h \sum_{i=-\infty}^{n-L} a_i \qquad (3.6)$$

for $nT \leq t \leq (n+1)T$. The $g(t)$ is the integral form of $q(t)$ which is

$$g(t) = \int_{-\infty}^{t} q(t)\ dt \qquad (3.7)$$

The summation in the first term of equation (3.6) only includes L discrete samples, because $g(t) = 1/2$ for $t \geq$ LT . The second term in equation (3.6) takes values from $\{0, \pm\frac{\pi}{2}$ and $\pi\}$, depending upon the summation of all the previous information symbols. Figure 3.4 shows the impulse response $q(t)$ of a Gaussian filter with $BT = 0.3$, which is defined by equation (3.5), and its integral form $g(t)$, which is given by equation (3.7).

If the quadrature waveforms are digitised into 8-bit binary words, the values of $g(t)$ will be masked off by the quantisation noise for $|t| > 2T$, i.e. $L = 4$. Hence in equation (3.6), there are 16 combinations in the first term and 4 initial phases in the second term. 10 sample values of $\rho(t)$ are calculated within an interval T for each of the combinations. The digitised quadrature waveforms are obtained by taking cos(•) and sin(•) of these samples plus one of the four initial phases $\{0, \pm\frac{\pi}{2}, \pi\}$. These waveforms are then digitised into 8-bit binary words. Two EPROMs are used to store the pre-calculated quadrature waveforms as look-up tables. The storage space of each EPROM is divided into four blocks corresponding to each of the four initial phases. Each block contains 160, 8-bit words which are the 10 sample values in the 16 combinations. Two EPROM's are addressed simultaneously in the real time data transmission by passing a stream of information symbols through a Serial Input and Parallel Output (SIPO) shift register, so that the four most recent information symbols are used to locate the memory spaces containing 10 out of the 160 sampled values in both EPROM's. All the previous information symbols are accumulated through a feedback logic circuit, which generates four addresses in order to locate one of the four memory blocks, in each EPROM, which are associated with the four initial phases. The 10 ad-

dressed samples from each EPROM, which represent the quadrature baseband waveforms in a T interval, are clocked out at the over-sampling rate and converted into an analogue voltage by a DAC. The analogue voltages are then low-pass filtered to remove any harmonics above the over sampling frequency. The lowpass filtered waveforms are then multiplied by the in-phase and quadrature components of the IF carrier, and the two products are combined by a power combiner to give the desired modulated carrier $s(t)$, which is then amplified by a linear amplifier to deliver a 3 dBm (dBm denotes dB relative to 1 mW) output power.

A specially-selected 256-bit binary sequence was used to form the information symbols, which are stored in a separate EPROM. This sequence will be discussed in section 3.4.7 with the channel impulse response estimator. The 256 bits are read from the EPROM during the transmission burst. The address of the EPROM is generated by counting the 'symbol' clock from the timing circuit, through two cascaded 4-bit output TTL binary counters, which provide 256 addresses.

A synthesiser covering the frequency range of 45-90 MHz was designed and constructed to allow a suitable IF to be adopted in the experiment, especially in the situation where a bandpass filter for the receiver is commercially available, with the desirable bandwidth but centred at a different IF. The block diagram of the synthesiser is shown at the bottom of Figure 3.3. The synthesiser uses a 0.1 MHz reference frequency which is derived from the temperature-compensated 10 MHz crystal oscillator used in the timing control circuit. The output from the Voltage Controlled Oscillator (VCO) is divided, in frequency, by N (e.g. for 70 MHz, $N = 700$) through cascaded Emitter Coupled Logic (ECL) and TTL dividers. The divided output is fed into a digital phase comparator, which compares the rising edges of the divided VCO waveform to that in the 0.1 MHz reference. A current-pump circuit is switched by the phase comparator in order to either charge or discharge a capacitor. The voltage across the capacitor is filtered by a loop filter and fed back to control the VCO.

Minimisation of the phase noise of the synthesiser is important because any such noise will be added to the modulated phases, and consequently reduce the SNR as discussed in Chapter 2, section 2.3.2. The phase noise of this synthesiser was controlled by reducing the bias current of the transistors in the VCO and careful planning of the circuit layout. Cables carrying radio frequency and control voltage were screened and kept apart. The VCO and digital circuit had separate regulated power supplies to prevent the break through of the pulses from the logic circuits.

The output signal of the synthesiser has a frequency range from 45 MHz to 90 MHz in 0.1 MHz steps, and a maximum output power of 3 dBm. The second harmonic is 35 dB below the main carrier output level. The phase noise was measured on a commercial spectrum analyser as 75 dBc/Hz below the carrier level, at a frequency offset of 200 Hz. Figure 3.5 shows the measured spectrum at 70 MHz.

After accurately balancing the phase as well as the amplitudes of the input and output of the quadrature mixers by using matching networks, a GMSK modulated IF signal was generated. Figure 3.6 shows the power spectrum of a GMSK modulated 70 MHz carrier with $BT = 0.3$, in a continuous transmission mode, from the versatile modulator. The information symbol rate was 500 kb/s and there is no additional IF bandpass filter used at the output. Figure 3.7 (a) shows the baseband quadrature waveforms to illustrate the reduced signal distances in terms of the reduced eye pattern, and Figure 3.7 (b) shows the phase trajectory of the same waveforms to demonstrate the constant envelope feature.

Generally, this versatile modulator can accommodate MSK and QPSK modulation, as well as CPM with its impulse response of the baseband shaping filter extended up to $4T$. The maximum data transmission bit rate, which is limited by the access time of the EPROM's used in the modulator, is 3 Mb/s.

3.3.4 FREQUENCY UP CONVERSION SECTION

The block diagram of this section is shown in Figure 3.8. The modulated 70 MHz IF signal is mixed with a 1720 MHz frequency source, and the upper sideband of the mixed signal is bandpass filtered and amplified before it is sent to the antenna for transmission. The 1720 MHz signal source used in the experiment was a Rohde & Schwartz SMH signal generator, and synchronisation between the generator and the 70 MHz IF synthesiser is not required. This is because the relatively slow (i.e. less than few Hertz at maximum) frequency drifts between the two frequency sources, and later on the third one in the receiver, will be automatically corrected by the IF carrier recovery circuit in the receiver (this will be discussed in section 3.4.5). The mixer was a Mini-Circuits device ZFM-2000, the power amplifier and bandpass filter were from Microwave Modules Ltd. The frequency response of the bandpass filter is shown in Figure 3.9. The power amplifier had a maximum output of 34 dBm (2.5 Watts).

Figure 3.10 shows the power spectrum of the signal that was used in the experiment. The strong carrier component is due to the transmission of a continuous sine wave between the information bursts in order to assist the carrier recovery circuit in the receiver to acquire the carrier phase.

3.4 THE RECEIVER

3.4.1 GENERAL DESCRIPTION OF THE RECEIVER

The receiver has eight major sections as shown in Figure 3.11, they are

(1) Frequency down conversion section.

(2) IF bandpass filter-limiter section.

(3) IF logarithmic signal level monitor.

(4) IF carrier recovery circuit.

(5) Baseband clock recovery circuit.

(6) Coherent quadrature demodulator.

(7) Real time channel impulse response estimator.

(8) Computer-controlled data buffer and digital tape recorder interface.

The received signal is first converted down to an IF (in the experiment it was 70 MHz), which is then bandpass filtered and split into two parts. The first part goes to a logarithmic monitor where the received signal power (in unit of dBm) is converted to a DC voltage. The second part of the signal is bandpass filtered and amplitude limited. It is then divided into two parts again with one going to a carrier recovery circuit and the other to the coherent quadrature demodulator, where the quadrature baseband signalling waveforms are recovered. A clock recovery circuit is used to extract the data transmission clock from these baseband waveforms. The quadrature baseband waveforms are then sampled by the recovered clock at multiple T intervals and then digitised by Analogue to Digital Converters (ADC) into 6-bit binary words, which are buffered and transferred to the digital tape recorder through a buffer control circuit between the transmission bursts. These 6-bit words are also passed to a digital channel impulse response estimator so that real time channel impulse responses can be estimated and recorded at the same time. The details of each receiver section are described below.

3.4.2 THE FREQUENCY DOWN CONVERSION SECTION

The block diagram of this section is shown in Figure 3.12 (a). The received signal from the antenna is amplified by two pre-amplifiers, and bandpass filtered before it is multiplied by a synthesised 1720 MHz unmodulated sine wave. It is not necessary for this sine wave to be in phase synchronisation

with the received carrier, because of the automatic phase tracking provided by the IF carrier recovery circuit, which will be described in section 3.4.5. A ZFM-2000 mixer and two ZHL-1042J amplifiers each with 28 dB gain and 5 dB noise figure, all manufactured by Mini Circuits Ltd, were used as the pre-amplifiers. The 1720 MHz signal was provided by a Farnell SSG-2000 signal generator. The bandpass filter was a Microwave Modules' combline filter. The frequency response of this filter is shown in Figure 3.12 (b).

3.4.3 LOGARITHMIC SIGNAL AMPLITUDE MONITOR

The down-converted IF signal is lowpass filtered and further down converted to 10.7 MHz, as shown in Figure 3.13 (a). Two ceramic bandpass filters with 10.7 MHz centre frequency and 300 kHz 3 dB bandwidth are used to reject any unwanted harmonics before the signal is passed to a logarithmic amplifier, which has a linear output voltage proportional to the power of the input signal measured in dB. A second digital frequency synthesiser (which is similar to the one used in the modulator), with a 59.3 MHz output is used here to convert the 70 MHz IF signal down to 10.7 MHz. Figure 3.13 (b) shows the frequency response of the 10.7 MHz bandpass filter. A logarithmic amplifier manufactured by Pascall Ltd was used in the monitor. The output voltage of the monitor against the input signal amplitude in decibels is shown in Figure 3.13 (c).

3.4.4 IF BANDPASS FILTER-LIMITER

Figure 3.14 shows the block diagram of this circuit. The received IF signal from the frequency down conversion section is bandpass filtered and amplitude limited by this circuit. The bandpass filter plays an important part in optimising the receiver performance. This filter has two functions. The first is to reject any spurious spectral components outside the down converted IF signal bandwidth. The second is to restrict the power of AWGN. The analysis carried out in Chapter 2, section 2.3, assumed the noise source is AWGN,

which has a constant two-sided power spectral density $N_o/2$. The noise power within a given bandwidth B_n is then given by

$$N_r = B_n N_o/2 \tag{3.8}$$

where N_r is the noise power after the filter, and B_n is the equivalent noise bandwidth of the filter. In the analysis discussed in Chapter 2, section 2.3, the B_n was assumed to be infinity. After applying the filter, the noise power admitted by the receiver will be reduced from $N_o/2$ to N_r. Since the bandpass filtering is a linear process, it does not change the probability density function of the noise. Hence the distribution of the noise at the output of the filter remains Gaussian. The bandpass filter can also reduce the switching noise level associated with the TDMA burst transmission. The narrower the equivalent noise bandwidth B_n, the less noise power will be included in the receiver IF. However, this bandwidth can not be made too narrow. This is because the B_n is directly proportional to the 3 dB bandwidth of the filter, and as this bandwidth reduces, the filter will introduce ISI to the quadrature signaling waveforms. Hence the eye pattern (which was discussed in Chapter 2 section 2.4.3,) of the waveforms will be closer. In the present of additive noise, the average BER will increase. Therefore an optimum 3 dB bandwidth exists for a given type of bandpass filter, subject to a specific modulation technique. A method for optimising a Gaussian filter for coherent detection of MSK signal was presented in [4], and it is reviewed here for optimal detection of GMSK signal.

The impulse response of the Gaussian filter is defined as

$$h(t) = \frac{\sqrt{\pi}}{\alpha} \exp\left(-\frac{\pi^2}{\alpha^2} t^2\right) \tag{3.9}$$

and its equivalent baseband frequency response is given by

$$H(f) = \exp(-\alpha^2 f^2) \tag{3.10}$$

where α is a constant. The 3 dB bandwidth B_r and the equivalent noise bandwidth B_n of this filter are calculated from the following two equations respectively,

$$|H(\frac{B_r}{2})|^2 = \frac{1}{2} \tag{3.11}$$

$$B_n = \int_{-\infty}^{\infty} |H(f)|^2 \, df \tag{3.12}$$

and they are expressed as

$$\alpha B_r = \sqrt{2 \ln 2} \simeq 1.1774 \tag{3.13}$$

$$\alpha B_n = \sqrt{\frac{\pi}{2}} \simeq 1.2533 \tag{3.14}$$

Therefore the 3 dB bandwidth of the Gaussian filter is related to the equivalent noise bandwidth through

$$B_r = 2\sqrt{\frac{\ln 2}{\pi}} \, B_n \simeq 0.9386 \, B_n \tag{3.15}$$

Since the optimisation is concerned with minimising both ISI and the equivalent noise bandwidth, the ISI caused by the filter is calculated first. The maximum ISI will occur when the spectral components of the signal have the maximum separation from the filter's centre frequency. Therefore a worst case signal waveform can be selected, and Figure 3.15 shows the quadrature baseband waveforms for GMSK modulation with $BT = 0.3$. Both inphase and quadrature waveforms will be affected by the filter in the same way, but for simplicity only the inphase waveform is used below in the analysis. The inphase waveform from Figure 3.16 can be written as

$$s_i(t) = A \cos(2\pi f_m t) \tag{3.16}$$

where f_m is the frequency of the inphase waveform, which in terms of the bit period T is

$$f_m = \frac{1}{4T} \tag{3.17}$$

Using equation (3.10), the filtered inphase waveform is

$$s_r(t) = A' \cos(2\pi f_m t + \phi_o) \tag{3.18}$$

where ϕ_o is a constant phase delay and

$$A' = A \exp\ (-\alpha^2 f_m^2) \tag{3.19}$$

Assuming the coherent detector has both carrier phase and clock synchronised to the transmitter, then the SNR at the output of the filter is

$$\gamma_f = \frac{A'^2}{2 N_o B_n} = \frac{A^2 T}{2 N_o} \frac{1}{B_n T} \exp(-2\alpha^2 f_m^2) \tag{3.20}$$

Substituting equations (3.15) and (3.16) into equation (3.19), and noting that the SNR per symbol period(which is 2 T) before the filter is

$$\gamma_o = \frac{A^2 T}{2N_o} \tag{3.21}$$

the SNR per symbol period after the filter can be expressed as

$$\gamma_r = \gamma_o \sqrt{\frac{\ln 2}{\pi}} \frac{1}{B_r T} \exp[-\frac{\ln 2}{4B_r^2 T^2}] \tag{3.22}$$

A degradation factor can be defined as

$$\text{degradation} = \frac{\gamma_r}{\gamma_o} \tag{3.23}$$

Figure 3.16 shows the degradation factor as a function of the normalised 3dB bandwidth of the filter. The minimum degradation is -0.14 dB, which occurs at $B_r T = 0.59$ [4]. This result shows that the optimum filter introduces negligible degradation, and therefore if the noise source is AWGN, it is not necessary to use such an optimum filter. However, in a practical system, the dominant noise can be very strong adjacent channel interference, which must be attenuated below an acceptable level. The spurious spectral components from the frequency down converter must also be suppressed. These requirements make the optimum filter an essential part of the receiver.

The frequency response of the optimum Gaussian filter is shown in Figure 3.17.

A Gaussian filter is used in the above analysis because it is mathematically convenient to use in the theoretical optimisation process. In practice it can be approximated closely by cascading Inductor Capacitor (LC) tuned IF amplifiers.

In a TDMA system, the optimum filter also restricts the switching noise associated with the transmission bursts. The impulse response of the filter will distort the first few symbols, because of its limited bandwidth. This distortion is avoided by adopting the 'tail bit' before the information sequence, as it was mentioned section 2.5.

The bandpass filter used in this experiment is a Surface Acoustic Wave (SAW) filter, manufactured by Siemens Ltd. Figure 3.18 (a) and (b) shows the frequency response and passband phase characteristics of this filter. This filter is a close approximation to the optimum Gaussian filter discussed above, and it can be assumed to introduce no additional degradation.

The bandpassed IF signal is then passed through an amplitude limiter. This is because the amplitude of the received signal plus noise in a practical mobile radio system can vary over several orders of magnitude, and in order to not exceed the dynamic range of the balanced mixers in the circuits that follow, it is necessary to limit the amplitude of the signal. For an ideal amplitude limiter, only the SNR at its output is affected. Let the input signal to the limiter be

$$s(t) = A\cos(\omega t + \rho(t)) + n(t) \tag{3.24}$$

where $n(t)$ is the Gaussian noise after the optimum filter discussed previously. The noise power is N_r. It was shown in [5] that the SNR at the output of the limiter can be approximately given by

$$\gamma_{out} = \eta \frac{A^2}{N_r} \tag{3.25}$$

where $\pi/4 < \eta \leq 2$ is a constant dependent upon the SNR at the input of the limiter. The lower bound is reached for very low input SNR and the upper bound for very high ratios. Theoretically a 3 dB increase in SNR at the

output of the limiter can be obtained if the received SNR is high and the corresponding average BER will be reduced. On the other hand, if the SNR is low at the input of the limiter, the SNR will be worsened at the output, which leads to an increased BER. In practice the average SNR at the output of the limiter can be regarded as the same as that at the input.

This limiter was constructed using a multi-stage amplifier configuration, the output of the last stage was clamped by diodes connected back to back. The output will be saturated when the input signal level exceeds a threshold of -60dBm. Figure 3.18 (c) shows the input output amplitude response of the amplitude limiter.

3.4.5 THE CARRIER RECOVERY CIRCUIT

The block diagram of this circuit is shown in Figure 3.19 (a). Its basic structure is a a Costas loop [5-9]. The purpose of this circuit is to track the average carrier phase. Between two adjacent data transmission bursts, the transmitter sends out an unmodulated carrier to assist the carrier recovery circuit to acquire phase synchronisation. The bandpass limited signal from the bandpass limiter circuit is split into two equal phase portions and multiplied by the in-phase and quadrature components of a locally generated sine wave from a VCO. The received IF signal between the bursts can be written as

$$s(t) = A\cos(\omega t + \psi(t)) \tag{3.26}$$

where $\psi(t)$ is the phase of the IF carrier. $s(t)$ is then multiplied by the quadrature waveforms from the VCO, which differ from $s(t)$ by a phase angle $\phi(t)$. The outputs from the multipliers are

$$\begin{aligned} v(t) &= A\cos(\omega t + \psi(t))\cos(\omega t + \phi(t)) \\ &= \frac{A}{2}\cos(\phi(t) - \psi(t)) + \frac{A}{2}\cos(2\omega t + \phi(t) + \psi(t)) \end{aligned} \tag{3.27}$$

$$
\begin{aligned}
w(t) &= A\sin(\omega t + \psi(t))\cos(\omega t + \phi(t)) \\
&= -\frac{A}{2}\sin(\phi(t) - \psi(t)) + \frac{A}{2}\sin(2\omega t + \phi(t) + \psi(t))
\end{aligned}
\tag{3.28}
$$

The terms with double frequency 2ω in $v(t)$ and $w(t)$ are removed by lowpass filters and the terms containing the phase difference $(\phi(t) - \psi(t))$ are multiplied together to give an error signal $e(t)$, which is

$$
\begin{aligned}
e(t) &= -\frac{A^2}{4}\cos(\phi(t) - \psi(t))\sin(\phi(t) - \psi(t)) \\
&= -\frac{A^2}{8}\sin 2(\phi(t) - \psi(t)) \\
&= -\frac{A^2}{8}\sin 2\Delta\phi(t)
\end{aligned}
\tag{3.29}
$$

where $\Delta\phi(t)$ is the phase error. $e(t)$ has negative gradients in the region

$$
(n - \frac{1}{4})\pi < \Delta\phi(t) < (n + \frac{1}{4})\pi
$$

where $n = 0, \pm 1, \pm 2, \pm 3, \ldots$. The negative gradient is used to provide a negative feedback control to the VCO so that it will cophase with the input signal $s(t)$ when $n = 0, \pm 2, \pm 4, \pm 6, \ldots$. In other words the VCO is in phase lock with the input signal $s(t)$. However, when $n = \pm 1, \pm 3, \pm 5, \ldots$, there is a 180 degree phase difference between the two signals, which creates a phase ambiguity. In Chapter 2, section 2.3.2, the method of using differential detectors to remove such an ambiguity was discussed, which causes the average BER at the output of the differentiator to be doubled.

If the baseband quadrature waveforms are subjected to pre-detection processing (i.e. signal processing before hard decision), such as channel estimation and equalisation (which will be discussed in section 3.4.7 and Chapter 5 respectively), the phase ambiguity must be removed before the signal processor, and differential detection can not be used. Hence the following method is proposed here to remove the phase ambiguity.

Assuming the transmitter sends out a training sequence and a copy of the sequence is stored in the receiver, after receiving the first 3 samples from the

lowpass filtered quadrature waveform $w(t)$, their polarities are compared individually with those stored correspondingly.[2] The results are represented by logic symbols as: '1' if it is the same, '0' otherwise. A majority voting is then performed, so that the phase ambiguity is decided to be 0 degree if at least two '1' occurred, and 180 degree otherwise. The 180 degree ambiguity, if it exists, will be removed by inverting the lowpassed quadrature waveform $w(t)$. Since the waveforms are sampled and digitised by the Analogue to Digital Converters (ADC) before they are passed to the signal processor, the inverting of the quadrature waveform is equivalent to taking the 2's compliment[3] from the output of the ADC in the quadrature branch. Let P_{amb} represent the probability of making an incorrect decision on the phase ambiguity, then according to [10]

$$P_{amb} = C_3^2 P_e^2 (1 - P_e) \tag{3.30}$$

where C_3^2 is the combination of taking 2 samples out of 3, and P_e is the average BER. This probability can be reduced if more bits are included, at the expense of loosing information content during the transmission.

The consequences of making an incorrect decision on the phase ambiguity depends upon the structure and algorithm used by the signal processor which follows the decision circuit. In the case of a correlation estimator (which will be discussed in section 3.4.7), a wrong decision in phase ambiguity will cause the correlator output to become random noise, which could then cause the Viterbi equaliser (which will be discussed in Chapter 5) that follows to produce a large number of errors. Nevertheless, since P_e is generally small, e.g. $P_e < 0.05$, P_e^2 will be much less. In cases where P_e is large, e.g. $P_e = 0.2$, the training sequence will be severely distorted, therefore, any estimation derived from such a sequence will become less reliable.

---

[2] $w(t)$ is used here because it is sensitive to the 180 degree phase ambiguity.

[3] The 2's compliment of a binary number is obtained by inverting each bit to form a new number and then adding (binary addition) 1.

Other design considerations include the loop filter after the baseband multiplier, which has a very narrow lowpass bandwidth so that the VCO can only respond to slow phase variations. This filter is designed to be a second order type to eliminate the steady state error [5]. The overall time constant of the closed loop circuit is about 10 ms to allow a maximum Doppler frequency of 100Hz, caused by the movement of the receiver, to be cancelled. During the burst data transmission, the rapid phase variations are eliminated by this filter so that only the average phase of the modulated carrier will be used to control the VCO. The lowpass filters in the quadrature branches are active types, and were designed to have 3dB bandwidth of 100 kHz. This 100 kHz bandwidth is used to compromise between the capture range of the phase lock loop and reduces the total noise power admitted into the circuit. The VCO must be coarsely tuned by a D.C.voltage to within $\pm$ 100 kHz from 70 MHz, in order to stay inside this capture range. Figure 3.19 (b) shows the spectrum of the VCO in phase lock with a sine wave input at frequency of 70 MHz. Figure 3.19 (c) shows the situation where the input signal power was decreased, which leads to an increase in the phase noise of the input signal. It can be seen that the phase noise power in the VCO output was substantially reduced within the closed loop bandwidth. The circuit layout was also carefully planned in order to minimise the phase noise. The VCO has the same low-noise design as the one used in the modulator.

3.4.6 THE QUADRATURE DEMODULATOR AND THE BASEBAND CLOCK RECOVERY CIRCUIT

This circuit returns the baseband quadrature signalling waveforms and extracts the timing pulses, or clock, used for transmission of the information symbols. The block diagram of this circuit is shown in Figure 3.20. The 70 MHz IF signal from the bandpass filter-limiter is divided into two parts and multiplied by the inphase and quadrature components of the recovered IF carrier. The outputs are represented as

$$v(t) = A \cos\ (\omega t + \rho(t)) \cos \omega t$$
$$= \frac{A}{2} \cos\ \rho(t) + \frac{A}{2} \cos(2\omega t + \rho(t)) \qquad (3.31)$$

$$w(t) = A \cos\ (\omega t + \rho(t)) \sin \omega t$$
$$= -\frac{A}{2} \sin\ \rho(t) + \frac{A}{2} \sin(2\omega t + \rho(t)) \qquad (3.32)$$

where $\rho(t)$ is the modulated carrier phase. The output signals are lowpass filtered in order to remove the double-frequency terms. The demodulated baseband quadrature signalling waveforms are $\frac{A}{2} \cos\ \rho(t)$ and $-\frac{A}{2} \sin\ \rho(t)$ respectively. The data transmission timing sequence is recovered by multiplying the baseband quadrature waveforms together. The lowpass filtered version of this product contains a frequency component at the data transmission rate; in the experiment it is 500 kHz. The direct clock extraction method was used because it is much simpler than a digital phase-locked loop. In order to reduce the effect of the additive noise on the recovered clock phase, the baseband quadrature waveforms in the transmitter were carefully selected to have maximum fluctuations, in amplitude, at the beginning of each burst transmission. The output of the multiplier is lowpass filtered and the first 3 cycles are used to find the average phase in a logic circuit in order to reduce the phase noise. This circuit then generates a control pulse to synchronise a crystal oscillator, from where the 500 kHz sampling clock is derived. The initial three cycles accumulated by the logic circuit are also used to sample the output from the logarithmic monitor, so that the signal strength at the beginning of the burst transmission can be recorded. The demodulated quadrature waveforms are sampled simultaneously by the recovered clock and digitised into 6-bit binary words.

3.4.7 THE CHANNEL IMPULSE RESPONSE ESTIMATOR

The baseband quadrature waveforms at the outputs of the coherent demodulator can be regarded as baseband quadrature signalling waveforms passing through a linear mobile radio channel with amplitude and phase distortions

and additive random noise. The amplitude and phase distortion of the channel can be represented by a baseband complex impulse response defined as

$$c(t) = c_c(t) + jc_s(t) \tag{3.33}$$

where $c_c(t)$ and $c_s(t)$ are the baseband in-phase and quadrature components of the channel. The baseband signalling waveforms can be represented in complex form as

$$s(t) = s_c(t) + js_s(t) \tag{3.34}$$

where $s_c(t)$ and $s_s(t)$ are the in-phase and quadrature components of $s(t)$. In the absence of the additive noise, the received complex baseband waveform is given by

$$r(t) = c(t) \otimes s(t) \tag{3.35}$$

where $\otimes$ represents a convolution. If $s(t)$ is chosen to have an auto-correlation function in the form of a Delta function, i.e.

$$s(t) \otimes s^*(-t) = \delta(t) \tag{3.36}$$

where $s^*(t)$ is the complex conjugate of $s(t)$, and $\delta(t)$ is the Delta function defined as

$$\delta(t) = \begin{cases} 1, & \text{for } t = 0 \\ 0, & \text{otherwise} \end{cases} \tag{3.37}$$

then by convolving the received complex waveform with $s^*(t)$, the channel impulse response can be estimated, i.e.

$$\begin{aligned} r(t) \otimes s^*(-t) &= c(t) \otimes s(t) \otimes s^*(-t) \\ &= c(t) \otimes \delta(t) \\ &= c(t) \end{aligned}$$

Maximum Length Pseudo Random Binary Sequences (PRBS), generated by shift registers with internal feedback, satisfy equation (3.36) approximately[4] and they can be adapted for $s(t)$. The baseband signaling waveform $s(t)$, in complex notation, is

$$s(t) = A\cos\rho(t) + jA\sin\rho(t) \tag{3.38}$$

where $\rho(t)$ is the modulated phase. If $\rho(t)$ changes by exactly $\pm\frac{\pi}{2}$ each time, as it does in MSK or QPSK modulation, the sample values of s_c or $s_s(t)$ at nT time intervals will be either $\pm A$ or $\pm jA$. When the baseband shaping filter in the modulator introduces ISI to the information symbols, as in GMSK modulation, the $\rho(t)$ no longer changes by exactly $\frac{\pi}{2}$, hence the absolute sample values of $s_c(t)$ and $s_s(t)$ at nT intervals will be less than $|A|$. In a practical implementation, the ISI in $\rho(t)$ is caused by a truncated, therefore finite, shaping filter. The small deviations from the maximum magnitude A, in the real and imaginary parts of $s(t)$, can be regarded, approximately, as a sequence with phase transition exactly equal to $\pm\frac{\pi}{2}$ passing through a linear complex filter which has an impulse response of $h'(t)$. The approximation arises because the deviations are caused by $\sin\rho(t)$ and $\cos\rho(t)$, and only when the ISI in $\rho(t)$ is small can the values of $\sin\rho(t)$ and $\cos\rho(t)$ at the sampling moment be approximated by the following equations.

$$\sin\rho(t)\simeq\begin{cases}\pm 1, & \text{for } \rho(t)\simeq\pm\frac{\pi}{2}\\ \rho(t), & \text{for } \rho(t)\simeq 0 \text{ or } \pi\end{cases} \tag{3.39}$$

$$\cos\rho(t)\simeq\begin{cases}\pm 1, & \text{for } \rho(t)\simeq 0 \text{ or } \pi\\ \rho(t), & \text{for } \rho(t)\simeq\pm\frac{\pi}{2}\end{cases} \tag{3.40}$$

This approximation becomes less accurate as the BT of the baseband shaping filter is reduced, which causes larger ISI. As an example, for GMSK with $BT = 0.3$, the maximum ISI causes $\rho(t)$ to deviate less than $\pm\frac{\pi}{6}$ from

---

[4] A Maximum Length PRBS has a trangular autocorrelation function.

$\frac{n\pi}{2}$ $(n = 0, \pm 1, \pm 2, \ldots,)$ therefore the maximum approximation error is 10 percent.

Adopting the approximation described above, the signal $s(t)$ from GMSK modulation with $BT = 0.3$ is represented by a convolution process between a complex filter $h'(t)$ and an ideal data sequence $d(t)$, which is expressed as

$$s(t) = h'(t) \otimes d(t) \tag{3.41}$$

where

$$h'(t) = h'_c(t) + jh'_s(t) \tag{3.42}$$

$$d(t) = \sum_{i=0}^{M} a_i U(t - 2iT) + \sum_{i=0}^{M} b_i U(t - (2i - 1)T) \tag{3.43}$$

and a_i and b_i take values from ± 1.

A PRBS can be mapped onto $d(t)$ by matching the even and odd position digits in the PRBS with the a_i and b_i of $d(t)$ respectively.

Finally, the $h'(t)$ is included in a total distortion denoted by $h(t)$, which is used to represent multiple delays and the attenuation of the signal in the physical environment, i.e. $c(t)$, as well as the ISI introduced by the radio system itself, i.e. $h'(t)$. This total distortion is expressed as:

$$h(t) = c(t) \otimes h'(t) \tag{3.44}$$

which can be regarded as an overall system impulse response.

Up to this point in the discussion, only the design of the quadrature signalling waveforms have been considered. In order to generate these waveforms, an information symbol sequence $b(t)$ must be derived to generate the corresponding phase shifts. This process is carried out by evaluating the direction of rotation of $d(t)$ in the complex coordinate. Since an information symbol produces approximately $\pm \frac{\pi}{2}$ phase change when it leaves the shaping filter, a logical equation can be defined to relate $b(t)$ and $d(t)$ at the sampling mo-

ment nT.[5] For simplicity, b_n and d_n are used to represent the sampled values of $b(t)$ and $d(t)$ at the nT instant. This equation is expressed as

$$b_n = d_n \oplus d_{n-1} \quad \text{for} \quad n = 0, 2, 4, \ldots \tag{3.45}$$

$$b_n = \overline{d_n \oplus d_{n-1}} \quad \text{for} \quad n = 1, 3, 5, \ldots \tag{3.46}$$

where $\oplus$ and $\overline{(\bullet)}$ denote a exclusive-or and an inverse logical operation respectively.

Computer programs were written to generate the required sequence of d_n, and then to convert it into a sequence of b_n, which is then stored in an EPROM to be used as information symbols in the modulator. The sequence of d_n is stored in a separate EPROM, which was used by the correlator as the stored sequence.

A channel impulse response estimator was implemented based upon the principle described above. In order to avoid multiplications of digits, which are either time consuming or costly in the hardware, a weighted binary approach was used and this is described as follows. The quadrature waveforms from the demodulator outputs are simultaneously sampled at nT intervals and digitised into 6-bit words. A binary correlator is attached to each bit position. The binary correlators are the integrated circuits L1023 from Logic Devices Ltd. Figure 3.21 (a) shows the internal structure. Each binary correlator has two 64-bit binary delay lines, it correlates the contents of two delay lines by counting how many bits are identical in the same delayed position. This number is coded into a 6-bit binary word as the binary correlation output.

Six of these binary correlators are connected in parallel to correlate the 6-bit words from the demodulator with the stored base sequence. The output from each correlator is weighted according to its bit position in the 6-bit input. The

---

[5] Note that $b(t)$ is binary and $d(t)$ is bipolar, in the logical equation a binary 1 or a positive value of $d(t)$ is defined as logical 1, and a binary 0 or a negative value of $d(t)$ is defined as logical 0 . The anti-clock rotation of $d(t)$ in the complex coordinate is defined as logical 1.

weighted outputs are summed to give a 6-bit correlation output. Figure 3.21 (b) shows the block diagram of a 6-bit output correlator constructed from 6 binary correlators. Finally, four such correlators are connected as shown in Figure 3.21 (c) to form a complex correlator.

The complex outputs from the correlator, however, are not all required for the data processing [11]. An initial data reduction can be made during the experiment. The reason for this is that when the receiver locks its phase to the strongest input signal and the transmission clock is recovered correctly, the complex notation of the demodulator output can be expressed as

$$\begin{aligned} r(t) &= d(t) \otimes h(t) \\ &= \sum_k d(t-2kT)h_c(t-2kT) - \sum_k d(t-(2k-1)T)h_s(t-(2k-1)T) \\ &\quad + j\sum_k d(t-2kT)h_s(t-2kT) + j\sum_k d(t-(2k-1)T)h_c(t-(2k-1)T) \end{aligned} \tag{3.47}$$

Since $d(t)$ is alternatively pure real and pure imaginary, only the real part of the $r(t)$ at $t = 0, \pm 2T, \pm 4T, \ldots$ carries information, and according to equation (3.47) these real values are affected by the $h_c(t)$ at $t = 0, \pm 2T, \pm 4T, \ldots$ as well as by the $h_s(t)$ at $t = \pm T, \pm 3T, \ldots$. Similarly, at $t = \pm T, \pm 3T, \ldots$ intervals, only the imaginary part of $r(t)$ carries information and these imaginary parts are affected by the $h_c(t)$ at $t = 0, \pm 2T, \pm 4T, \ldots$ and by the $h_s(t)$ at $t = 0, \pm T, \pm 3T, \ldots$. Therefore the output from the correlator is taken from the real part at even T intervals, and from the imaginary part at odd T intervals.

During the experiment, $d(t)$ is formed by cascading four identical 63-bit maximum length PRBS together. The PRBS was generated by a 6 stage shift register with feedback taps at the 1st and the 6th stages [12]. The normalised complex correlator output for GMSK modulation with $BT = 0.3$ was measured as:

Real	0, 0, ..., 0.25, 0.93, 0.25, 0, ..., 0
Imaginary	0, 0, ..., 0

After the interleaving, a real sequence is obtained as:

$$0,\ 0,\ \ldots,\ 0,\ 0.95,\ 0,\ \ldots,\ 0.$$

This sequence is the part of the channel impulse response, which affects the data transmission, and it is referred to as the 'estimated channel impulse response' in this thesis. Figure 3.21 (d) shows the output of this sequence from the hardware correlator.

3.4.7 THE DATA BUFFER AND THE DIGITAL TAPE RECORDER CONTROLLER

A THORN-EMI SE8800 digital tape recorder was used in the experiment, which records 8-bit binary words at 33 kbyte/s . In order to record the digitised experimental data at 500 kbyte/s , a data buffer was designed. The sampled and digitised in-phase and quadrature demodulated data , the estimated signal strength and the estimated channel impulse response during a burst of transmission are temporarily stored in this buffer, which holds up to 8192 16-bit words, which are then transferred to the digital tape recorder between consecutive transmission bursts. A controller was also designed to interface the data buffer to a BBC computer to pass control commands to both the data buffer and the tape recorder. This controller also reads the data back from the tape recorder and transfers them to a IBM Personal Computer where more sophisticated data processing is performed.

3.5 CALIBRATION OF THE SYSTEM

The calibration of the system was carried out in the laboratory with an arrangement as shown in Figure 3.22. The transmitter and the receiver were connected through a variable attenuator and a commercial Rayleigh fading simulator [13]. The carrier frequency of the system was set to 450 MHz due to the availability of the front end bandpass filters and the frequency range of the simulator. The information symbol transmission rate was set at 500

kb/s , and 256-bits, which consists of four 63-bit PRBS, were transmitted in a burst. The bursts repeated every 40 ms, and between the bursts a pure sine wave was transmitted to assist the carrier recovery circuit in the receiver. In a multi-user TDMA system, like the 7-user system described in Chapter 2, section 2.4, the unmodulated carrier is transmitted during the synchronisation burst. There is only one user in the experimental system presented here, hence the synchronisation burst can be extended. The loop bandwidth in the carrier recovery circuit can be made narrower, because a longer time is allowed for the circuit to acquire the phase synchronisation. This narrower loop bandwidth can also reduce the power of the phase noise.

The receiver noise power N_r, in dBm, is calculated by:

$$N_r = N_f + 10 \log_{10} k B_r T + 30 \tag{3.48}$$

where N_f is the noise figure of the pre-amplifier and B_r is the IF bandpass filter 3-dB bandwidth, k is the Boltzmann constant and T is the absolute temperature. The receiver used in the experiment has $N_{amp} = 5$ dB , $B_r \simeq 0.6$ MHz. For $T = 300°K$, and $k = 1.38 \times 10^{-23}$ J K^{-1}, the noise power in the receiver is calculated as $N_r = -110$dBm.

The output signal from the transmitter was attenuated to a level of C dBm The signal C to receiver noise power N_r ratio is related to E_b/N_o by

$$\frac{E_b}{N_o} = \frac{CT}{N_r/B_r} = \frac{CB_rT}{N_r} \tag{3.49}$$

The attenuated signal is fed through the fading simulator to the receiver. For each signal level, the fading frequency of the simulator was set to 0 Hz, 30 Hz and 90 Hz. The in-phase and quadrature waveforms from the demodulator were sampled and digitised by the recovered transmission clock. These samples were recorded by the digital tape recorder and later transferred to the IBM Personal Computer to be analysed.

The computer performs differential detection and compares the detected symbols with those transmitted. The average BER was calculated at various

signal to noise ratios and presented in Figure 3.23 (a) and (b). Figure 3.23 (a) shows the average BER when the fading is absent. The theoretical calculated BER of coherent QPSK is included in this figure for comparison. It was found that the measured BER is consistent with the theoretical calculation. Figure 3.23 (b) shows the average BER when the fading frequency was non-zero. In this situation, irreducible errors occurred and remained as constant when the $E_b/N_o$was increased. The irreducible errors were caused by the deep fades of the received signal, where the signal was completely lost in the background noise and the recovered carrier phase became random. Since the fading frequency is inversely proportional to the carrier wave-length, at a higher carrier frequency the fading frequency will increase, which will result more irreducible errors.

The channel estimator was tested at $E_b/N_o = 20$ dB with the fading simulator removed, the correlator output was shown in Figure 3.21 (d).

3.6 CONCLUSION

A versatile TDMA experimental system has been designed, constructed and calibrated in the laboratory. The IF modulator is capable of accommodating various types of amplitude or phase modulation by setting up a look-up table from pre-calculated quadrature signaling waveforms, for a given modulation technique. The IF can be varied from 45 MHz to 90 MHz and the maximum information transmission rate is 3 Mb/s. The transmission can be continuous or in variable short time burst. The modulated IF can be frequency up-converted to suit various experimental requirements.

The coherent receiver consists of an IF carrier, a baseband clock recovery circuit and a real-time 6-bit output complex channel impulse response estimator. The baseband quadrature signaling waveforms are sampled simultaneously by the recovered clock. Signal strength in dBm is sampled at the beginning of the data transmission burst. A digital tape recorder was interfaced to the receiver via a computer to record the quadrature sampled out-

puts with the sampled signal strength and the estimated channel impulse response.

The modulator was set to use GMSK modulation with $BT = 0.3$. The information symbol transmission rate was set at 500 Kb/s, and 256-bits, which were formed by cascading four 63-bit PRBS together, are transmitted in each burst. The burst data transmission repeated every 40 ms. The optimum bandwidth of the IF filter at the receiver was numerically evaluated based upon the worst case ISI waveform pattern. If a Gaussian filter is used in the receiver for optimum detection, its normalised bandwidth was calculated to be $BT = 0.6$. An unmodulated carrier was transmitted between the data bursts to assist the carrier recovery circuit in the receiver. The transmitter and receiver were calibrated in the laboratory by using a Rayleigh fading simulator and the results are consistent with the theoretical calculations when the fading is absent. It was observed from the system calibration that when the fading frequency increased, irreducible errors occurred and increased with the fading frequency. These irreducible errors occur because of the faded received signal falling very close or below the noise power in the receiver.

The receiver was integrated with other instruments and mounted into an experimental vehicle as shown in Figure 3.24. Figure 3.25 shows the experimental transmitter.

REFERENCES

[1] Demery, A. "Wideband Characterisation of Mobile Channel", Ph.D. Thesis, Department of Electrical Engineering and Electronics, University of Liverpool, Mar 1989

[2] Aulin, T. "Continuous Phase Modulation-Part I: Full Response Signaling", IEEE Trans. Commun., vol. COM-29, NO.3, pp. 196-209, Mar 1981.

[3] Aulin, T. "Continuous Phase Modulation-Part II: Partial Response Signaling", IEEE Trans. Commun., vol. COM-29, NO.3, pp. 210-225, Mar 1981.

[4] Ishizuka, M. Hirade, K. "Optimum Gaussian Filter and Deviated-Frequency-Locking Scheme for Coherent Detection of MSK", IEEE Trans. Commun., vol. COM-28, NO.6, pp.850-857, June 1980.

[5] Viterbi, A. J. "Principles of Coherent Communication", McGraw-Hill, New York, 1966.

[6] Costas, J. P. "Synchronous Communications", Proc. IRE, vol.44, pp.1713-1718, Dec 1956.

[7] Lindsey, W. C. "Synchronization Systems in Communications", Prentice Hall, Englewood Cliffs, New Jersey, 1972.

[8] Lindsey, W. C. Simon, M. K. "Telecommunication Systems Engineering", Prentice-Hall, Englewood, New Jersey, 1973.

[9] Proakis, J. G. "Digital Communications", Mcgraw-Hill, New York, 1983.

[10] Papoulis, A. "Probability, Random Variables, and Stochastic Processes", McGraw-Hill, New York, 1985.

[11] Rashidzadeh, L. B. et al. "Design and performance of a Viterbi equaliser for GMSK modulation", IEE Colloquim on "methods of combating multipath effects in wide band digital cellular mobile systems", Oct 1987.

[12] Davis, W. D. T. "System Identification for Self Adaptive Control", Wiley-Interscience, London, 1970.

[13] "Model NJZ-17E RAYLEIGH MODULATOR instruction manual", Japan Radio Co. Ltd.

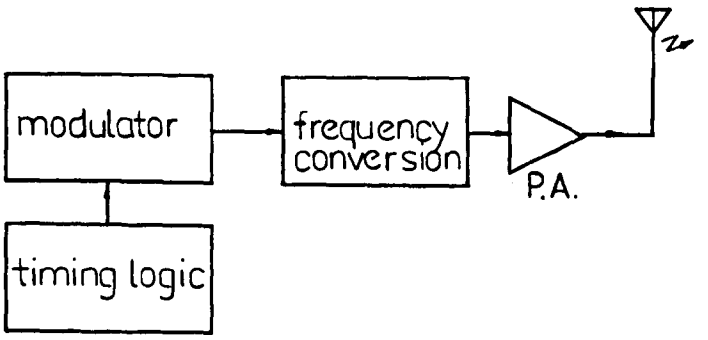

Figure 3.1 Block diagram of the transmitter.

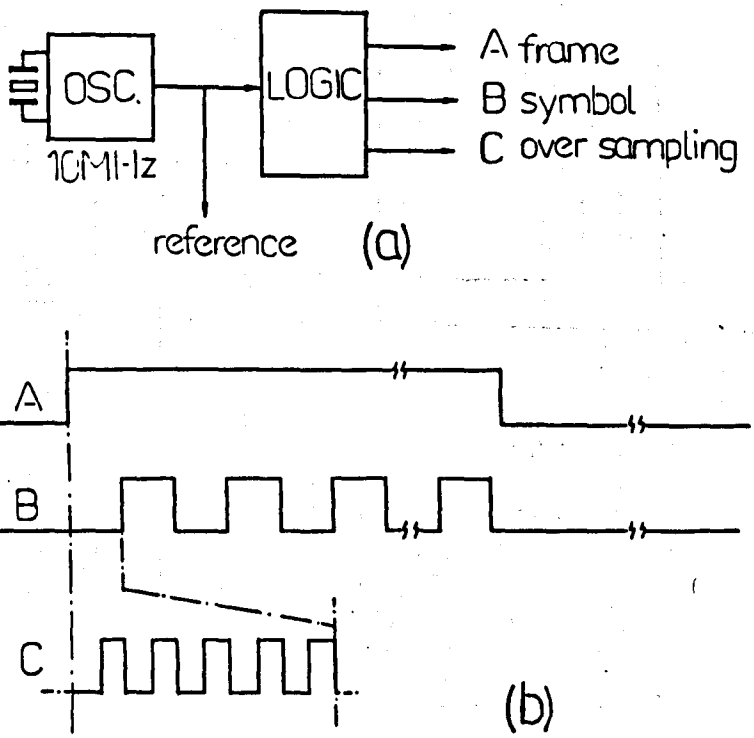

Figure 3.2 (a) Block diagram of timing control circuit, (b) the associated timing sequences.

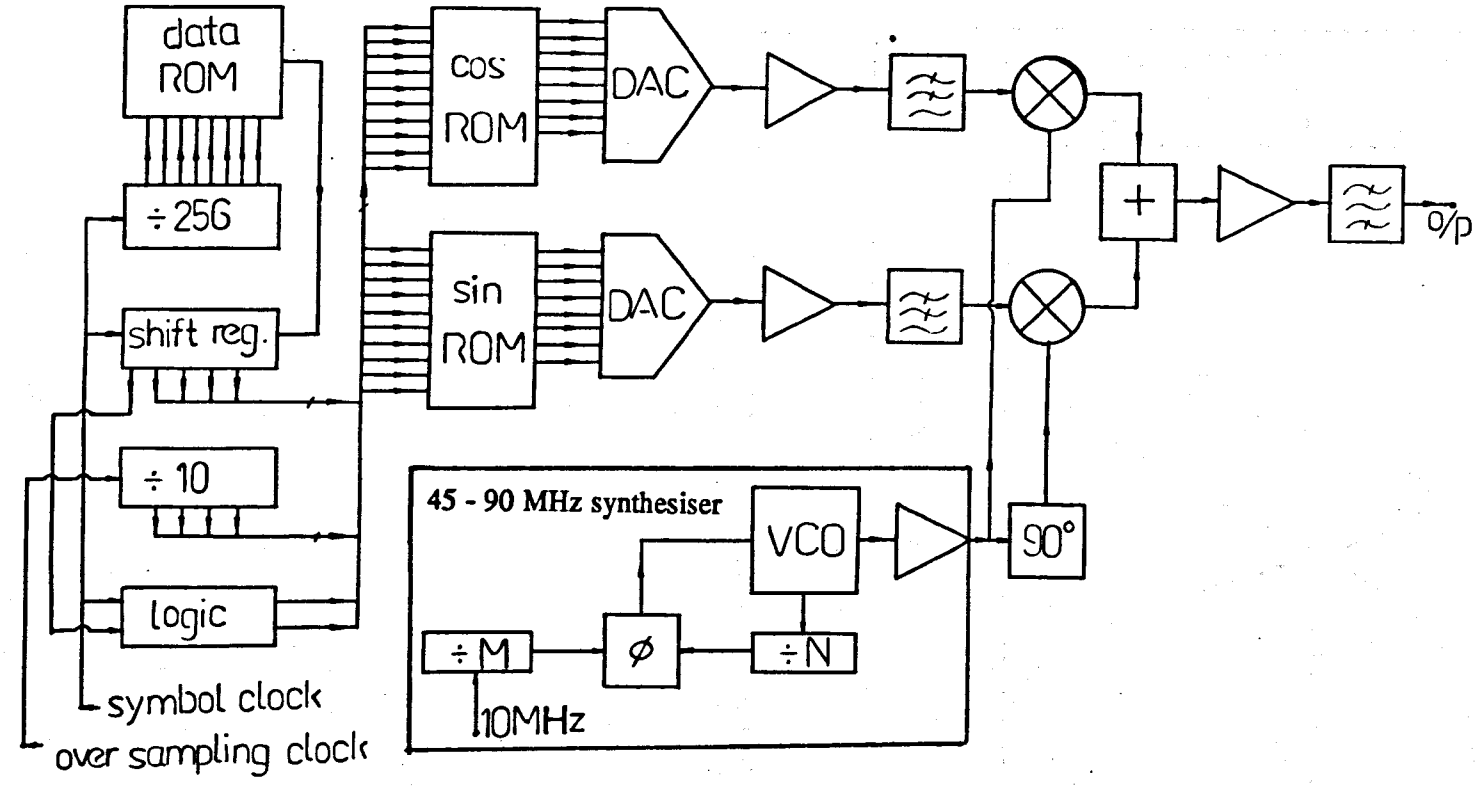

Figure 3.3 Block diagram of the quadrature modulator.

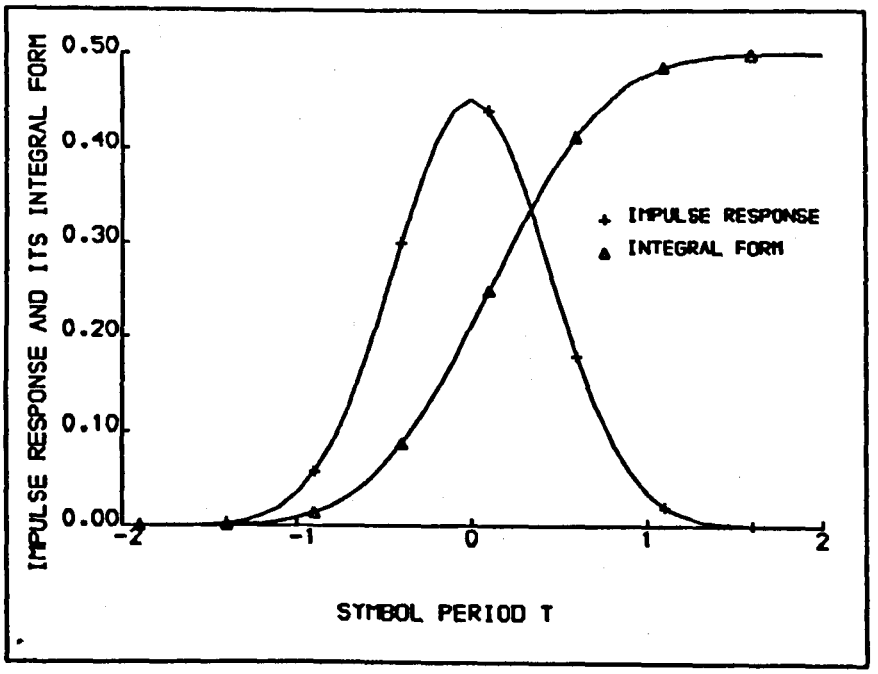

Figure 3.4 Impulse response of Gaussian filter with $BT = 0.3$, and its integral form $g(t)$.

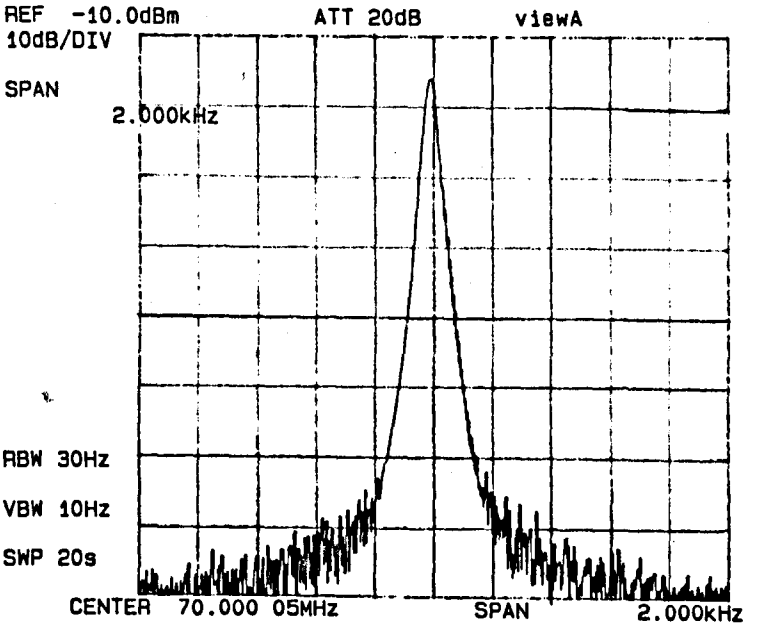

Figure 3.5 Measured power spectrum of the IF synthesiser output at 70 MHz.

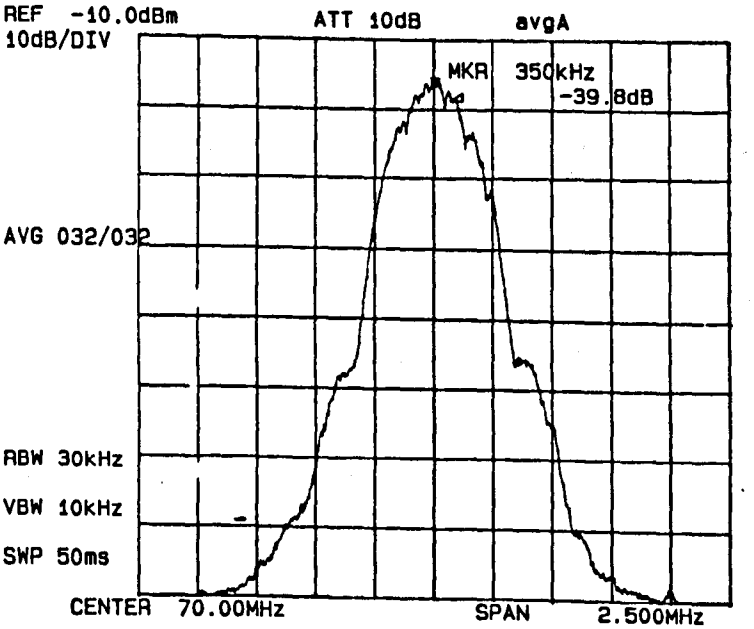

Figure 3.6 Measured power spectrum of a continuous transmission of a GMSK modulated signal, with $BT = 0.3$ at 70 MHz.

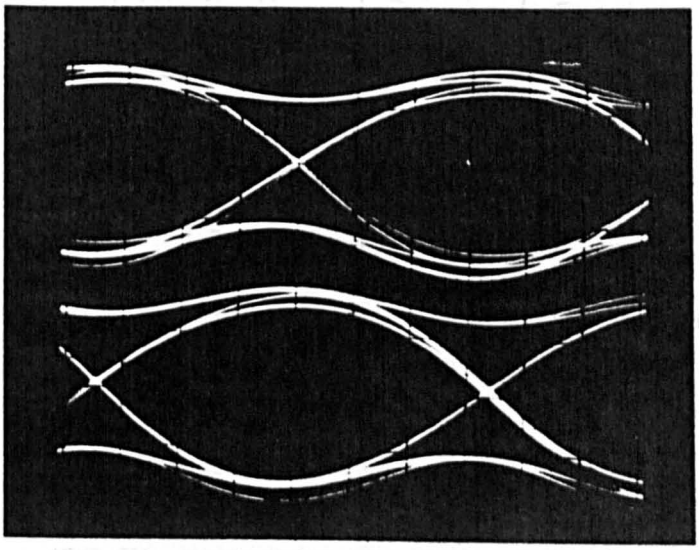

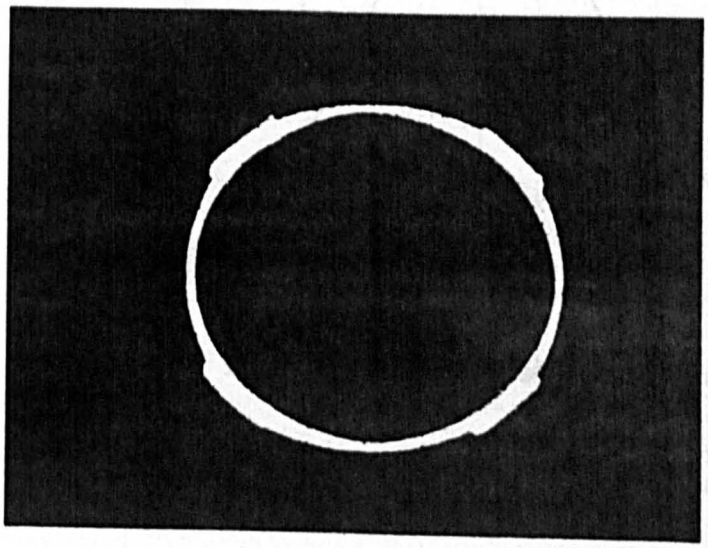

Figure 3.7 Measured waveforms of (a) quadrature baseband waveforms in GMSK modulation with $BT = 0.3$. (b) phase trajectory of the quadrature waveforms.

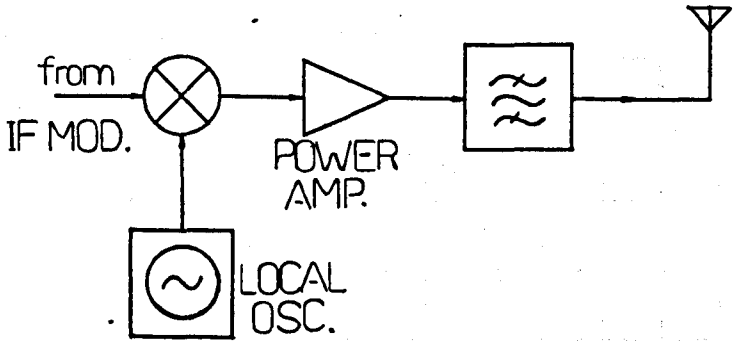

Figure 3.8 Block diagram of the frequency up conversion circuit.

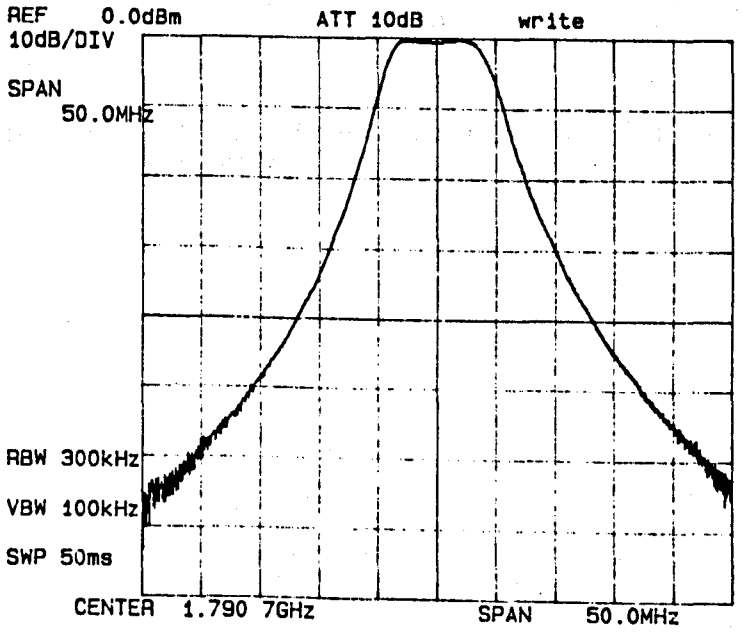

Figure 3.9 Measured frequency response of the bandpass filter at 1.8 GHz.

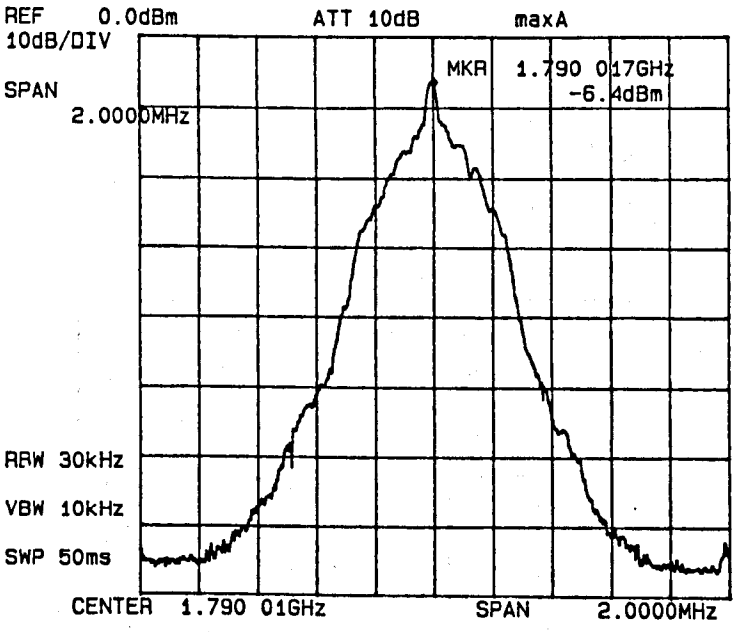

Figure 3.10 Measured power spectrum of the signal used in the experiment.

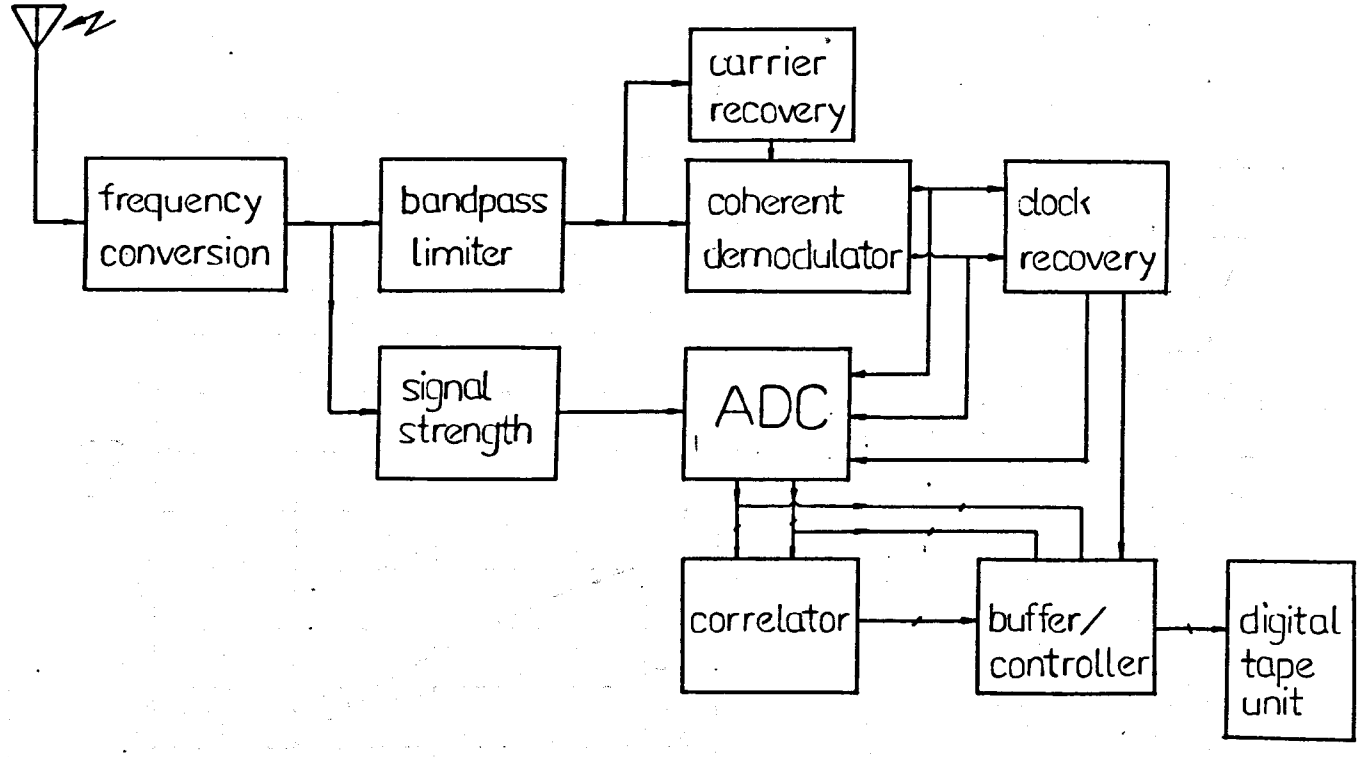

Figure 3.11 Block diagram of the receiver.

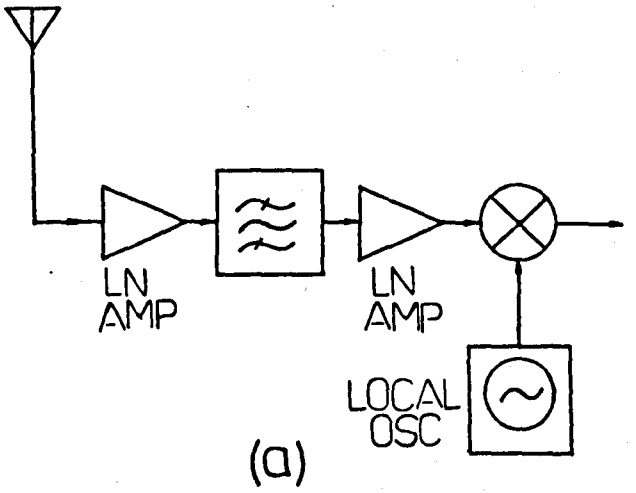

(a)

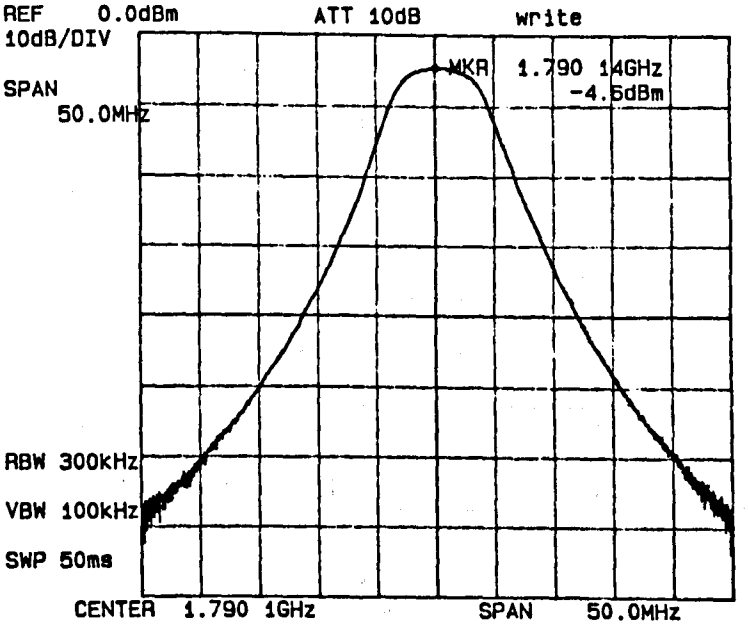

(b)

Figure 3.12 (a) Block diagram of the frequency down conversion circuit. (b) Measured frequency response of the bandpass filter at 1.8 GHz.

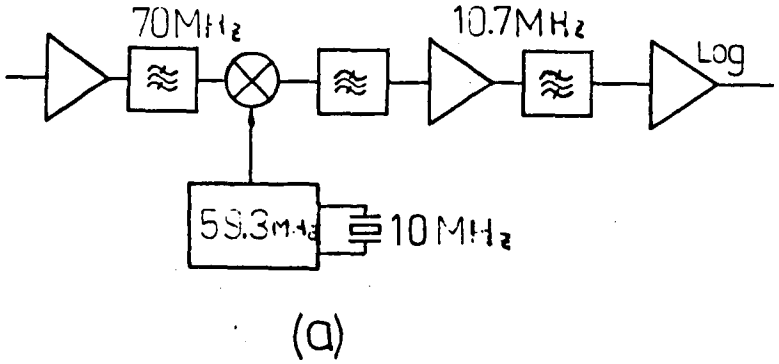

(a)

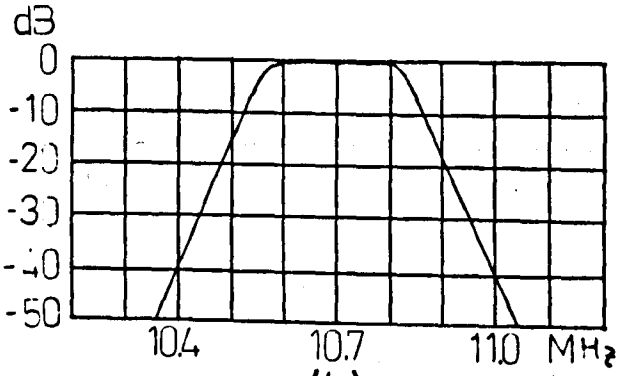

(b)

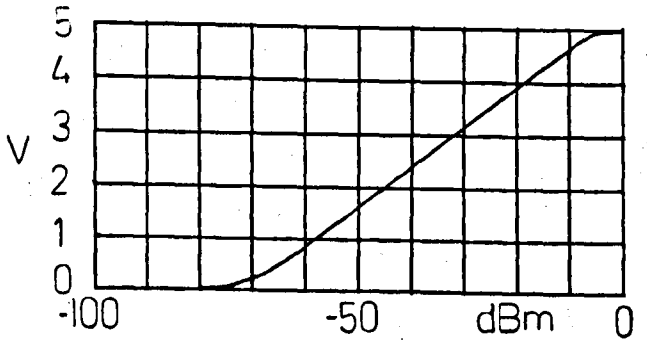

(c)

Figure 3.13 (a) Block diagram of the logarithmic signal amplitude monitor. (b) Measured frequency response of the 10.7 MIIz bandpass filter. (c) Measured input output characteristic of the monitor

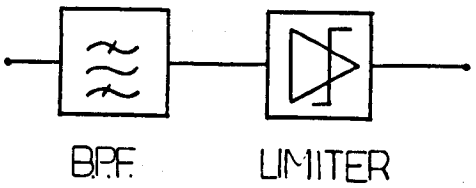

Figure 3.14 Block diagram of the IF bandpass limiter.

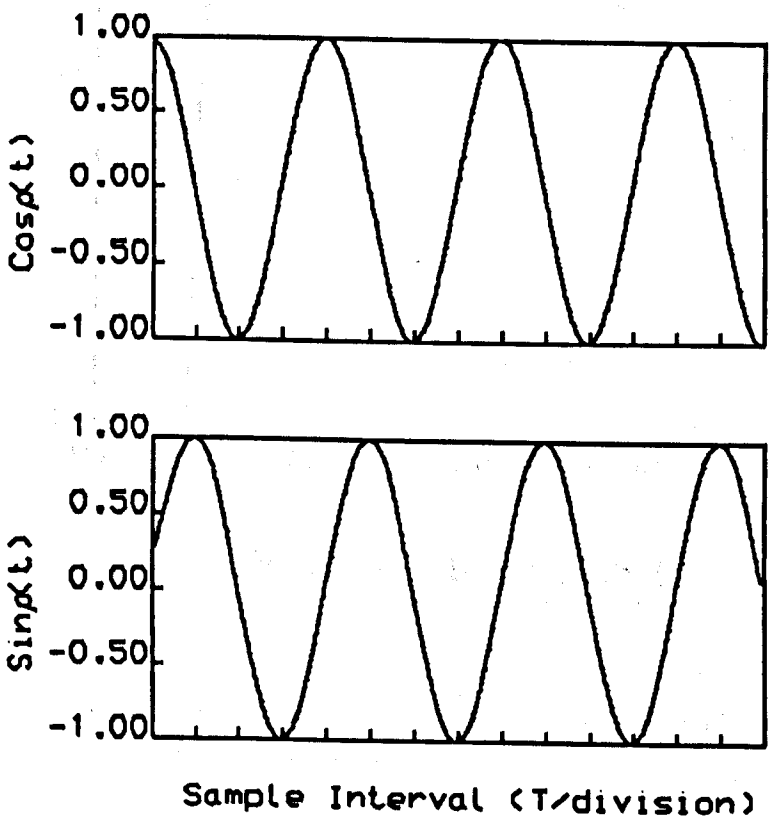

Figure 3.15 The worst case quadrature waveforms of GMSK with $BT = 0.3$ signal.

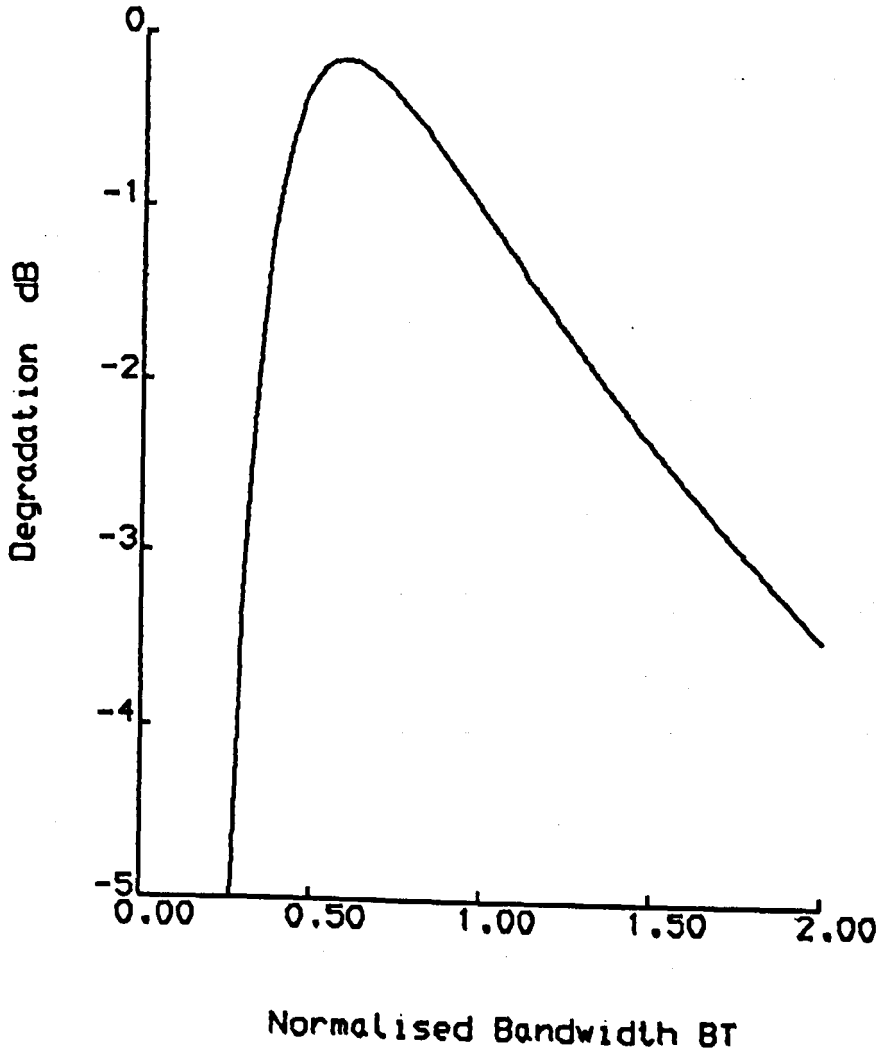

Figure 3.16 Degradation against the normalised bandwidth of a Gaussian filter.

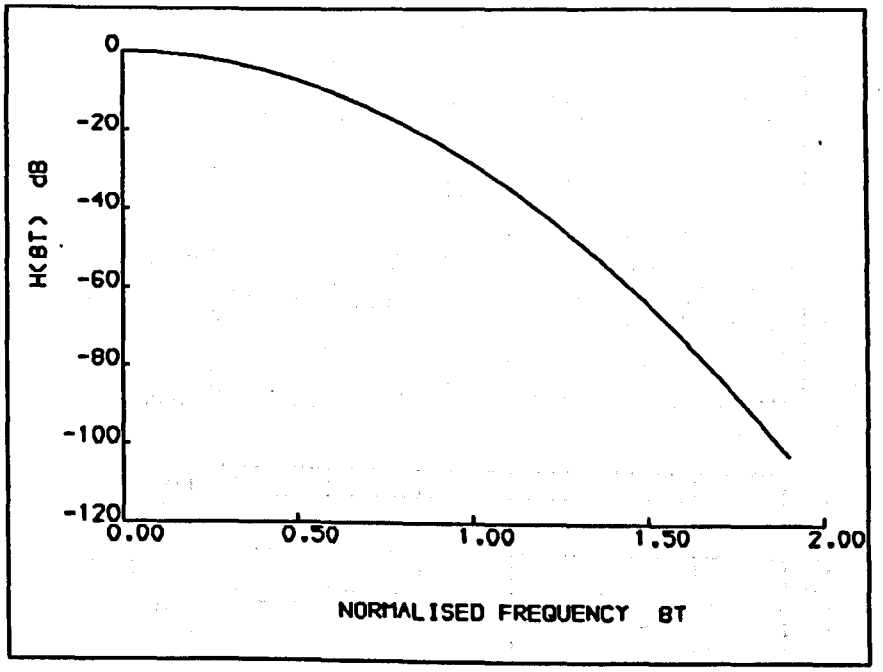

Figure 3.17 Frequency response of the optimum Gaussian filter with $B_rT = 0.59$

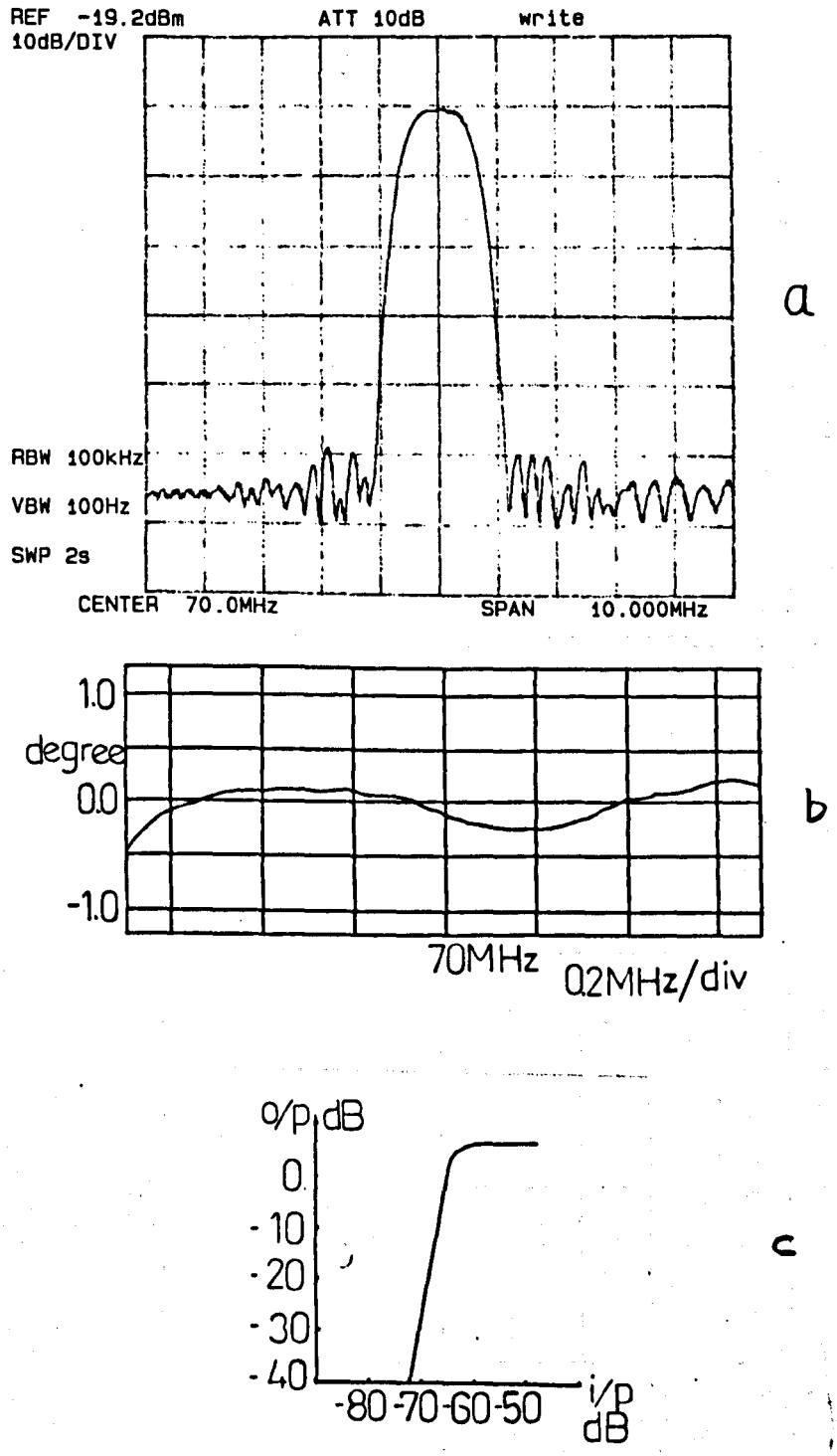

Figure 3.18 (a) Frequency response of the SAW filter used in the receiver. (b) The phase characteristics of the SAW filter. (c) The input and output amplitude characteristics of the IF bandpass limiter.

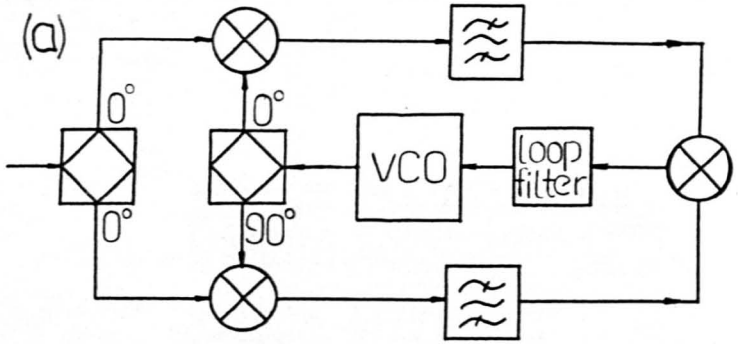

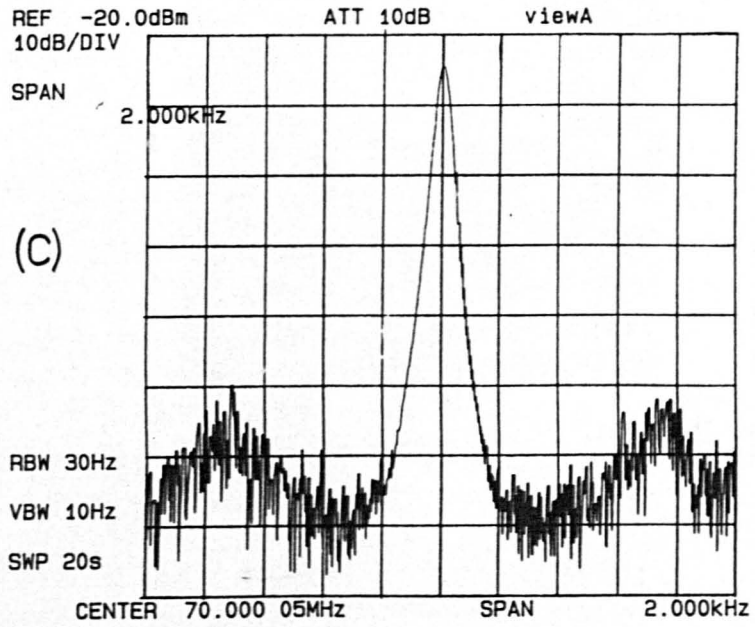

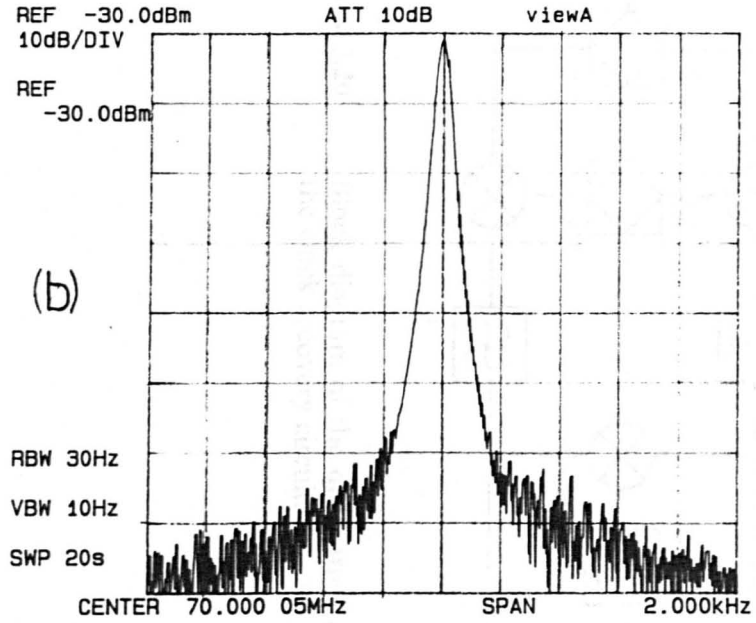

Figure 3.19 (a) Block diagram of the IF carrier recovery circuit. (b) Spectrum of the recovered IF signal when the input signal to noise ratio is 20 dB. (c) Spectrum of the recovered IF signal when the input signal to noise ratio is 10 dB.

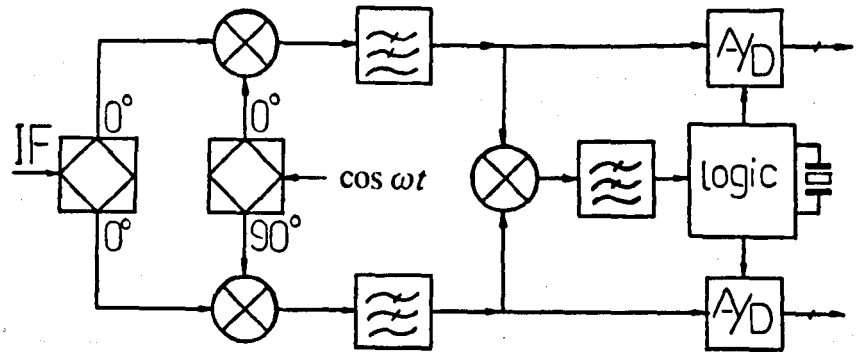

Figure 3.20 Block diagram of the quadrature demodulator and the clock recovery circuit.

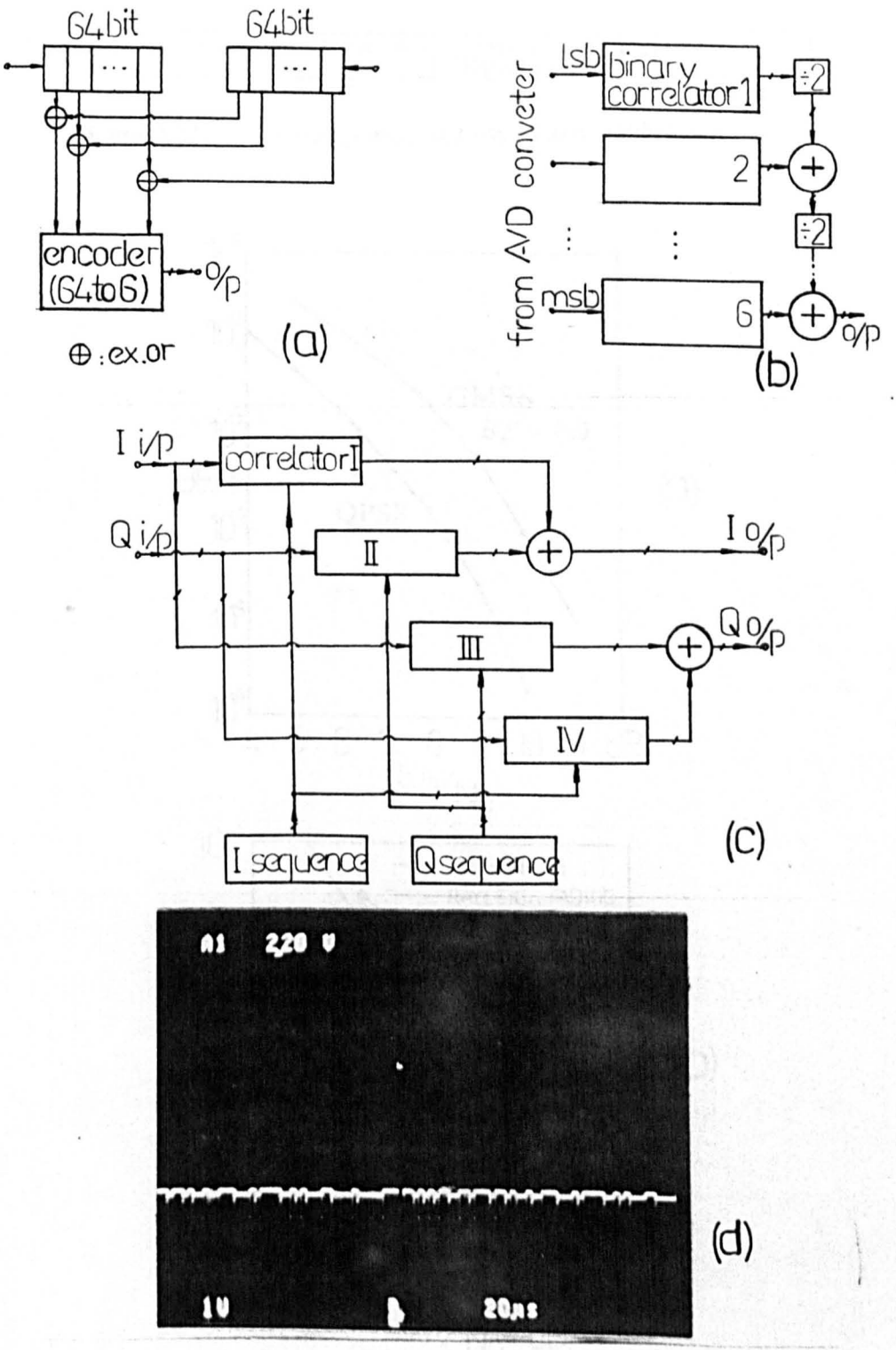

Figure 3.21 (a) The internal structure of the L1023 binary correlator. (b) Block diagram of a 6 bit input correlator. (c) Block diagram of a 6 bit input complex correlator. (d) Interleaved output from the complex correlator.

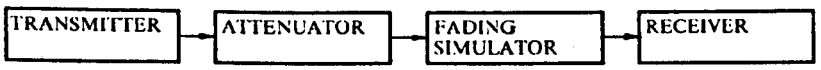

Figure 3.22 Arrangement for the system calibration.

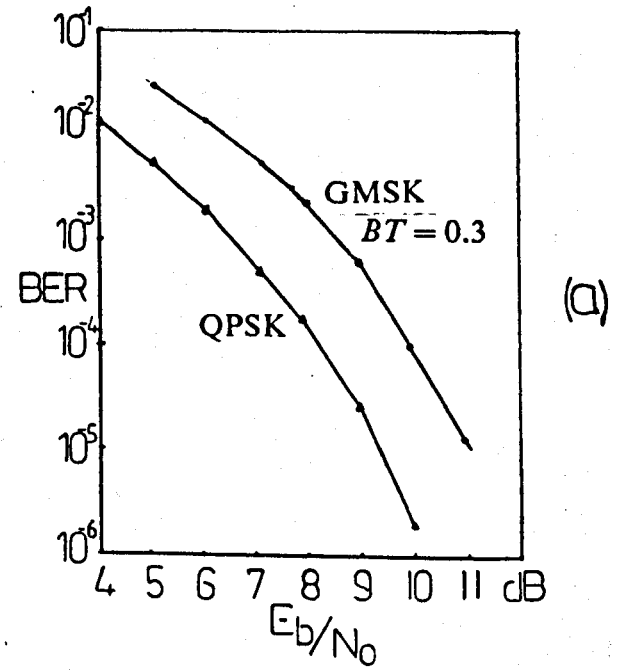

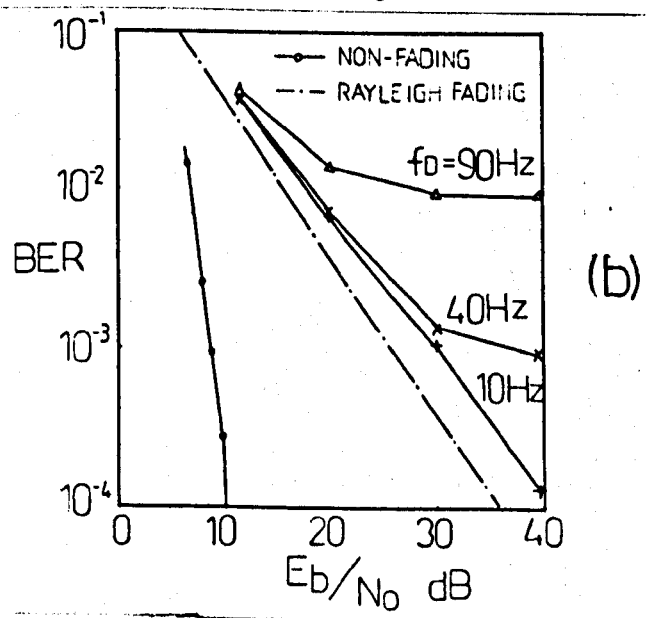

Figure 3.23 (a) Measured BER of GMSK with $BT = 0.3$ compares with the theoretical coherent QPSK in AWGN and without fading. (b) Measured BER of GMSK with $BT = 0.3$ subject to Rayleigh fading.

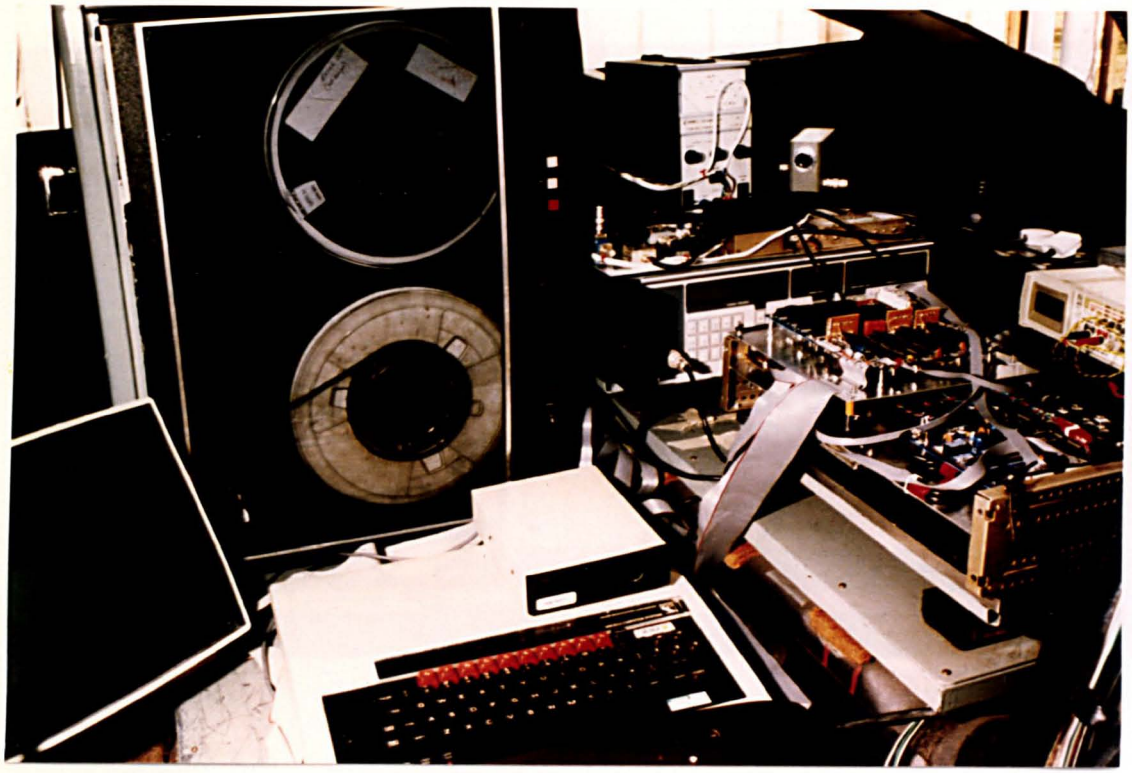

Figure 3.24 The experimental receiver mounted inside the test vehicle.

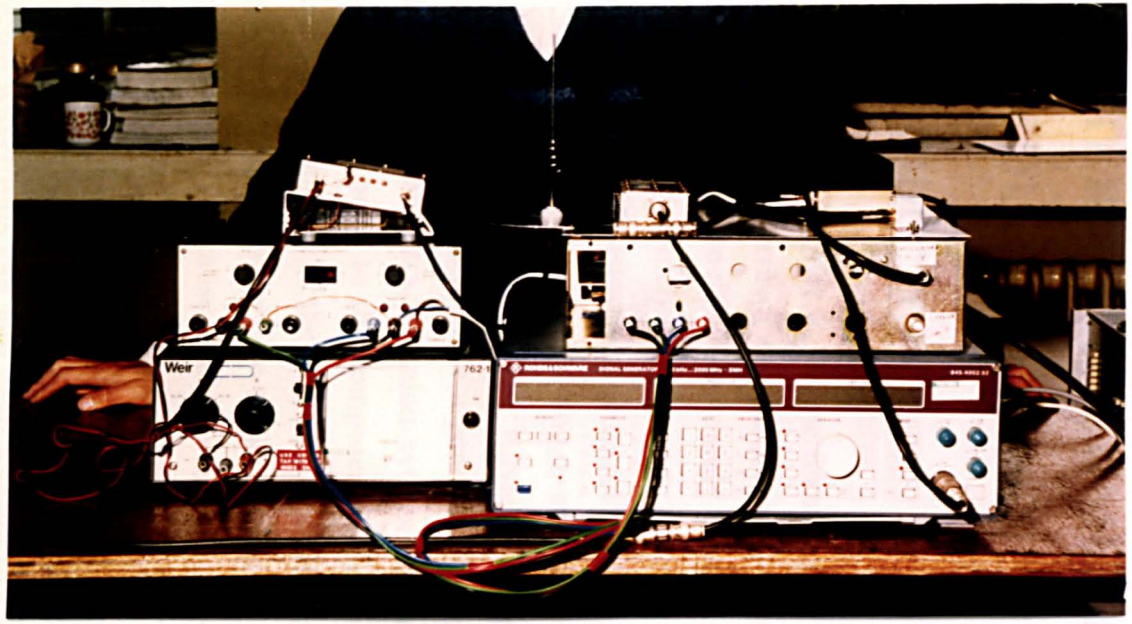

Figure 3.25 The experimental transmitter.

CHAPTER 4 EXPERIMENTAL PROCEDURE AND RESULTS

4.1 INTRODUCTION

As discussed in Chapter 2, the performance of a digital mobile radio transmission system in term of the statistics of bit errors is critically dependent upon the radio channel, which mainly introduces two types of distortion to the radio signal, namely fading and imperfect channel impulse response. These two types of distortion are directly related to the physical environment and the carrier frequency. Although computer simulations based upon statistical models (such as AWGN, Rayleigh fading and characterised channel impulse response) can provide a general assessment of the performance of a digital mobile radio transmission system, experimental measurements must be carried out, prior to the computer simulation, in order to estimate accurately the parameters of the statistical models and to characterise the channel impulse response at a specific radio frequency. The experimental measurement is necessary because at higher radio frequencies and hence shorter wave lengths (eg. the wave length is 17 cm at 1.8GHz), the radio propagation characteristics (refection, diffraction, attenuation etc.) are different from those at lower (eg.800 MHz) frequencies. As discussed in Chapter 2, multiple reflected wavefronts can add destructively to result in signal fading, whereas a large building obstructs the radio wave to create a 'shadow' (where radio signal is weak or lost in the background noise) behind it. The shorter wave length also leads to increased attenuation in the radio wave as it propagates through the physical environment. For example, when the diameters of the cross sections of the branches of the trees or the size of the leaves are of the magnitude of approximately a quarter of the wavelength (eg. a quarter

wavelength is 4.3 cm at 1.8GHz), they will act as resonators to trap the radio energy, hence larger attenuations are expected [1].

The recent release of the radio spectrum around 1.8 GHz for the PCN system has attracted a growing amount of attention and interest from both telecommunication industries and academic research institutions, and developing a practical digital radio telephone network at 1.8 GHz has become a challenging task. As discussed above, although a computer simulation at an early stage of the system development can provide a cost effective solution in assessing the performance of the PCN system subject to various design concepts and techniques, statistical parameters and impulse responses of the radio channel must be estimated by experimental measurements before any computer simulation program concerning the radio channel can be developed.

There have been experimental investigations at radio frequencies around 1.8GHz reported in the literature; they can be generally classified into two categories. Firstly they are signal strength studies such as those reported in references [2,3], where the radio signal strength was measured at various physical distances from the transmitting antennas mounted at some fixed heights above the local ground level. From such measurements mathematical models were derived, which can be used to provide a general prediction of the average signal strength at a given physical location. The second type of experimental investigation estimated the channel impulse responses inside buildings, such as reported in reference [4], where reflected and delayed radio energy was measured in the time domain in order to characterise the indoor communication channel. However, both types of experimental investigation were conducted separately in time and physical locations, hence it is difficult to justify using these results simultaneously in one computer simulation program. Furthermore, a practical mobile radio system (such as a PCN) must support users who are inside buildings as well as those who are outside, where the physical environment determines the propagation characteristics to be different from that indoors. For example, scattered signals with longer delays may exist outdoors due to larger physical separations between the buildings,

and if the strengths of such delayed signals are significant, ISI will arise in a digital transmission system.

Such concerns provide the motivation to carry out an experimental investigation outside buildings using a radio frequency of 1.8 GHz. Instead of producing generalised statistical parameters to characterise the channel, the objective of this experiment is to assess the performance of a bursty data transmission (TDMA) system which uses a specific digital modulation technique (GMSK) in term of the average BER and the cumulative error free gap length distributions (this will be discussed later in section 4.3.5).

The versatile test equipment developed in Chapter 3 has the capability of simultaneously estimating the real time radio channel impulse responses and recording the demodulated baseband signals, which can be analysed by various signal processing algorithms at a later stage of the experiment. This equipment also enables representative channel impulse responses to be selected from a large amount of measured data, and the corresponding average BER and the gap distributions can be evaluated, so that the effect of a real communication channel on a specific type of digital transmission (eg. TDMA with GMSK modulation) at a particular carrier frequency (eg. 1.8GHz) can be studied. From a system operator's point of view, with certain modifications, using such equipment in the field measurement will provide important information for planning a digital transmission system.

The experimental system described in Chapter 3 was used in a field experiment conducted in areas around The University of Liverpool precinct. This chapter describes the experimental procedure and presents some sample results derived from the statistical analysis on the measured signal level and the channel impulse response. The average BER and gap distributions are evaluated and presented with the corresponding channel impulse responses, which are representative among the measurements. Such a presentation is aimed to illustrate the relationship between the statistical bit error distributions and real time radio communication channels.

4.2 EXPERIMENTAL PROCEDURE

4.2.1 TRANSMITTER SETUP

A dipole antenna was mounted on the roof of the Department of Electrical Engineering, which is about 30 metres above the local ground level. The antenna was connected to the transmitter through a low-loss cable 7 metres long. The power level at the end of the cable was measured as 34 dBm, and the antenna had a VSWR of 1.12. The power fed to the antenna was approximately 2.5 W. The information transmission rate was set at 500 kb/s. The modulation was GMSK with $BT = 0.3$. Four cascaded 63-bit maximum length PRBS were sent out in a burst transmission. The burst repetition period was set to 40 ms, which is limited by the maximum recording speed (byte/s) of the digital tape recorder.

4.2.2 THE RECEIVER

The receiver was mounted inside an experimental vehicle (a converted family hatch-back car), together with the digital tape recorder, a BBC computer and a radio frequency signal generator. A dipole antenna identical to that used in the transmitter was mounted vertically on top of the vehicle at 1.5 m above the road level. A Hewlett Packard manually adjustable attenuator was connected between the antenna and the receiver input to protect the receiver from saturation. A digital voltmeter was used to check the DC output of the logarithmic signal level monitor to facilitate the manual selection of the attenuation. Once the measurement was started in a specific area the attenuation was kept constant.

4.2.3 THE TEST AREAS

The measurements were made within 1 km of the transmitter. The selected routes for the experiment are inside The University of Liverpool precinct,

which represents a typical urban area. Figure 4.1 shows a photograph taken at the antenna position, looking towards the area where the measurements were made. The maximum speed of the vehicle during the measurement was approximately 10 mph, and no attempt was made to keep the speed constant.

4.3 THE RESULTS

4.3.1 ORGANISATION OF THE RECORDED DATA

The recorded data were down loaded from the digital tape recorder to an IBM Personal Computer, via the buffer controller, in the laboratory. The multiplexed recorded data containing the signal amplitude, channel impulse response and sampled baseband quadrature waveforms were separated by the computer and stored in sequentially ordered files, so that the results could be cross referenced later. Figure 4.2 shows a section of the estimated signal amplitude and the channel impulse response from the experiment.

4.3.2 OBJECTIVE OF THE DATA PROCESSING

The experimental system was designed to be able to assess the instantaneous quality of data transmission. The data processing is optimised with this objective in mind, such that the statistical analysis over an excessive number of transmission bursts was avoided. The analysis was carried out within a group which contained a certain number of burst transmissions. The number of transmission bursts that should be included in the data processing can be determined approximately as follows. The maximum vehicle speed during the experiment was 10 mph (i.e. 4 m/s) and the transmission bursts repeated every 40 ms. Hence the vehicle moved 0.16 metre or one wave length at 1.8 GHz between two consecutive bursts. If the recorded data within 15 metres in distance is regarded as having independent statistical characteristics, then at least 100 consecutive transmission bursts can be grouped together. The

statistical analysis of the recorded data was carried out within such groups, with each group containing 200 to 600 burst transmissions.

Although the results obtained from the statistical analysis could be different from one group to another (because of movement of the receiver), certain types of results may be representative. Such results can provide useful information on how the quality of data transmission is affected in specific situations, which could be used to complement the computer simulations. Some representative results will be presented in the following sections.

4.3.3 CUMULATIVE DISTRIBUTION OF THE RECEIVED SIGNAL LEVEL

The first statistical analysis is to evaluate the PDF of the received signal level, which was sampled at the beginning of each transmission burst. From the discussion in section 2.5.4, it is clear that the TDMA burst is very short, and the received signal amplitude during this time interval can be regarded as constant. As the receiver moves across an area where a standing wave pattern was generated in space by the superposition of multiple delayed wavefronts, the amplitude of the received signal at each burst can be regarded as a sampled value of the standing wave. These sampled values, which were collected by moving the receiver across a local area, form a random process. The probability distribution of the random process can be analysed as follows. Since the sampling interval is equal to the transmission burst period, and the receiver travelled at irregular speed, the sampled values will not represent the precise shape of the standing wave in space. However, when a sufficient number of samples are taken within a short physical distance, and provided that the standing wave is highly periodical, the sampled values should have the same PDF as that of the continuous standing waves. Therefore if the PDF of the standing wave is Rayleigh distributed, then the PDF of the sampled values will be the same.

As discussed in section 2.4.2, if the amplitude r of the received signal is Rayleigh distributed, with a PDF given by

$$p(r) = \frac{2r}{\sigma^2} \exp(-r^2/\sigma^2) \tag{4.1}$$

where

$$\sigma^2 = < r^2 > \tag{4.2}$$

and r^2/σ^2 is the normalised signal power, or the normalised signal level.

The CDF of the Rayleigh distribution, or the probability that the received amplitude is between 0 and l, is calculated as

$$P(l) = \int_0^l p(r)\, dr \;=\; 1 - \exp(-l^2/\sigma^2) \tag{4.3}$$

Hence the Rayleigh CDF is a function of the normalised signal level.

In order to investigate whether the amplitude of the received signal is Rayleigh distributed, the CDF of the normalised received signal level was evaluated and plotted on Rayleigh-scaled graph paper, where the Rayleigh CDF appears as a straight line. Figures 4.3 to 4.5 show such plots. Figures 4.3 and 4.4 show the CDF of the measured signal levels from groups each containing 300 samples, which correspond to 300 burst transmissions. Because of the relatively small number of samples contained in each group, the CDF of the normalised signal levels appeared to be less continuous, and deviations from the Rayleigh CDF, which is shown as a straight line, are apparent at the top and bottom ends of the normalised signal level.

Figure 4.5 shows the CDF evaluated from 1000 sampled values, which is very close to the Rayleigh distribution. This result verified the assumption made in Chapter 2 that the sampled signal amplitudes, obtained during each transmission burst, form a random process which has the same statistical distribution as in a continuous transmission. The TDMA system therefore suffers from the same signal fading.

4.3.4 THE ESTIMATED CHANNEL IMPULSE RESPONSE

The real time channel impulse response was estimated at each transmission burst by discretely correlating the sampled received baseband signals with a stored PRBS. During each transmission burst, four consecutive 63-bit PRBS's were sent out, therefore at the output of the digital correlator there should be four estimated channel impulse response profiles. Each profile has 63 values(taken at $2\mu s$ intervals), which is represented by a vector as

$$\hat{h}_i = \{h_{i,-31}, h_{i,-30}, \cdots, h_{i,-1}, h_{i,0}, h_{i,1}, \cdots, h_{i,30}, h_{i,31}\} \tag{4.4}$$

where $h_{i,k}$ denotes the kth($-31 \leq k \leq 31$) sample value in the ith transmission burst. The amplitude of $h_{i,k}$ is normalised with respect to 31, which is the peak output value of the digital correlator. The measured channel impulse responses were found to be unchanged during a transmission burst by comparing the four estimated channel impulse responses corresponding to the four cascaded PRBS. The estimation from the first sequence of each burst was not accurate because 3 bits at the beginning of the burst transmission were used to check the carrier phase ambiguity (section 3.4.5) and to regenerate the sampling clock; they were excluded from the correlation process. The estimated channel impulse responses from separated burst transmissions were found to be different. The estimation according to the second PRBS at each burst was then taken to represent the channel impulse response during that burst. The statistical analysis of the estimated channel impulse response was carried out as follows. The probability density function of the amplitude of the sampled values at a fixed time delay can be evaluated over N consecutive impulse responses as

$$p_k(x) = \frac{1}{N} \sum_{i=1}^{N} \delta(h_{i,k} - x) \tag{4.5}$$

where $N \geq 100$, and $-1.0 \leq x \leq 1.0$ is the normalised amplitude. Figure 4.6 (a) shows the PDF of the main signal $h_{i,0}$, where a few isolated local average values exist, due to the distortions in the channel. Figure 4.6 (b) shows the PDF of the delayed signal $h_{i,1}$ (i.e. at 2 μs from the main signal), in this case the PDF is centred at $x = 0$. The negative values are due to the 180° phase delays with respect to the main signal. Although the PDF's in these two figures did not appear to have a recognisable shape, it is expected that they should be Rayleigh distributed, as discussed in Chapter 2.

Another type of analysis is to calculate the probability of the magnitude (absolute value) of the signal at a fixed time delay exceeding a predetermined threshold. The result from this analysis will help a system designer to decide whether the ISI is a dominant contribution towards the degradation in the system perfomance, and hence to use cost-effective techniques (eg. equalisers) to minimise its effect. From the evaluated PDF $p_k(x)$, this probability can be calculated as

$$P_k(V) = N\left(\sum_{x=-\infty}^{-V} p_k(x) + \sum_{x=V}^{\infty} p_k(x) \right) \qquad (4.6)$$

where $V > 0$, and $P_k(V)$ is the probability of the magnitude of the signal at time delay kT ($T = 0.2\mu$s) exceeding the threshold V. Figure 4.7 shows an example obtained from the experimental data recorded at the area around the junction of Oxford Street and Mount Pleasant, which is shown in the centre part of the photograph in Figure 4.1. The threshold was set to $V = 0.15$ (i.e. 15 per cent of the maximum normalised signal amplitude). Figure 4.7 shows that, in this particular instance, the delayed signals with magnitude greater than 15 per cent of the maximum normalised signal amplitude were observed at time delay of $\pm 2T = \pm 4\mu$s from the main signal.

The variation of the estimated channel impulse response can be monitored by evaluating the correlation function of the delayed signal at time kT. This function is defined as

$$R_k(n) = \frac{1}{L} \sum_{i=1}^{L} h_{i,k}\, h_{i+n,k} \qquad (4.7)$$

where $0 < L < N$. $R_k(n)$ as a measure of the similarity between the delayed signals , at time kT from the arrival of the main signal, separated by n transmission bursts.

Figure 4.8 (a) and (b) show two examples of $R_0(n)$, which are the correlations of the main signals. These figures show that strong correlation exists between the main signals over consecutive transmission bursts. This is because the coherent receiver always locks to the strongest radio signal; as a result the main signal in the estimated channel impulse response is always positive. Figure 4.8 (a) shows the signal levels were almost the same over 15 bursts. Figure 4.8 (b) shows a lower correlation, which implies the signal levels between adjacent bursts were different, due to the distortion in the channel.

Figure 4.9 (a) and (b) show two examples of $R_1(n)$, which is the correlation of the amplitudes of the delayed signal at time $T = 0.2\mu s$. Figure 4.9 (a) shows that a moderate correlation exists between the delayed signals in adjacent transmission bursts, whereas Figure 4.9 (b) shows a negative correlation, which indicates the delayed signals between adjacent transmission bursts having opposite polarities.

4.3.5 GAP DISTRIBUTION

One way to represent the quality of a digital transmission is to evaluate the error-free gap-length distribution. As discussed in Chapter 2, an error-free gap is defined to have a length which is equal to the number of consecutive none-erroneous bits (or correct bits) [6]. Before a realistic length of an error burst can be decided, the error-free gap-length must be studied, hence the cumulative error-free gap distribution is investigated. For simplicity, in the following text the error-free gap is referred to as the gap, and the cumulative error-free gap length distribution is referred to as the gap distribution. The

knowledge of the measured gap distribution will enable system designers to select efficient signal processing techniques (eg. coding and interleaving etc.) to protect the original transmitted data. For example, in a practical digital transmission system, extra bits for error protection are inserted into the original bit stream by using block encoding techniques [7]. Knowledge of the average gap length will be extremely valuable, because from it the system designer can determine the average burst error length and select a cost effective error control code. For example, a large number of extra protection bits must be inserted into the data stream if the gap length is short, or a smaller number if the gap length is long. The more protection bits that are used in a digital transmission, the less information it will carry in a given time interval. An optimum number of protection bits should therefore be selected in order to balance between error protection and the information content of the transmission.

During the data analysis, the computer performed hard decisions on the recorded data, and compared the detected data sequence with that stored. The bit error pattern was established and the gap distribution was calculated. Some sample results from the analysis are used here in order to illustrate the relationship between the estimated channel impulse response and the quality of the data transmission. Four representative channel impulse responses were selected, these are referred to as Channel (I), (II), (III) and Channel (AVE). The associated gap distributions were evaluated. The average signal-to-noise ratio E_b/N_o, which was evaluated from the recorded signal level over the receiver noise level, was also included. Figure 4.10 shows the four impulse responses, and the four corresponding gap distributions are shown in Figure 4.11. These results are tabulated in Table 4.1, and are described as follows.

Channel (I) has an average $E_b/N_o \simeq 25$ dB. This channel introduces negligible ISI, the average gap length is 48, and the average BER is 1.7 percent.

Channel (II) has an average $E_b/N_o \simeq 15$dB. The main signal is attenuated and ISI is observed. The average gap length is about 6, and the average BER is 12.5 percent.

Channel (III) has an average $E_b/N_o \simeq 5$dB, and the main signal is almost completely lost in the background noise. The average gap length is 3, and the average BER is 40 percent.

Channel (AVE), which represents an average situation, has an average $E_b/N_o \simeq 20$ dB, and the average gap length is 21. The average BER is 3.8 percent.

These sample results are representative from analysising the experimental data recorded in Liverpool University precinct, which is a typical urban area.

4.4 CONCLUSION

A field trial of TDMA data transmission using GMSK modulation with $BT = 0.3$, at a carrier frequency of 1.8 GHz was conducted in the Liverpool University precinct. The channel impulse response and the received signal amplitude were estimated and recorded, together with the simultaneously sampled in-phase and quadrature baseband signaling waveforms. The recorded data were transferred to a computer and analysed in the laboratory. It was found that the probability density distribution of the amplitude of the received signal, measured at the beginning of each transmission burst, is Rayleigh distributed over a sufficient long record of data.

Statistical analysis of the probability distribution of the amplitudes of the delayed baseband signal in the estimated channel impulse responses, which were measured at a typical urban area, has shown that significant ISI (e.g. echoes with more than 15 per cent of the maximum signal amplitude) were likely to occur between $\pm 4\mu$s from the arrival of the main signal.

By correlating the delayed signals over consecutive burst transmissions, it was found that the main signals were positively correlated, and occasionally this correlation was reduced due to the channel distortion. The correlation between the delayed signal at time T from the main signal showed that the delayed signals in adjacent burst transmissions could be loosely correlated.

The quality of the data transmission was measured by evaluating the error free gap distribution. Sample results were presentated using four gap distributions which were calculated according to four representative channel impulse responses at certain SNR. The average gap lengths were observed to range from 48, for Channel (I), which was virtually free from ISI and with $E_b/N_o \simeq 25dB$, to 3, where the main signal was almost lost completely in the noise.

REFERENCES

[1] Lee, W. C. Y. "Mobile Communication Engineering ", McGraw-Hill, New York, 1974.

[2] Okumura, Y. et al. "Field strengthand its variability in VHF and UHF land-mobile radio service", Rev. Elec. Commun. Lab., vol.16, no.9, Sept-Oct 1968.

[3] Harley, P. "Short distance attenuation measurements at 900 MHz and 1.8 GHz using low antenna height for microcells", IEEE Journal on Selected Area in Commun., vol.7, no.1, Jan 1989.

[4] Bultitude, R. J. C. et al. "A comparison of indoor radio propagation characteristics at 910 MHz and 1.75 GHz" IEEE Journal on Selected Area on Commun., vol.7, no.1, Jan 1989.

[5] Jakes, W. C. "Microwave Mobile Communications", John Wiley & Sons, New York, 1974.

[6] IEEE Dictionary of Definition of Terms.

[7] Lin, S. Costello, Jr. D. J. "Error Control Coding: Fundamentals and Applications", Prentice-Hall, New Jersey, 1983.

Figure 4.1 Part of the Liverpool University precinct, viewing from the transmitter antenna, where the experiment was carried out.

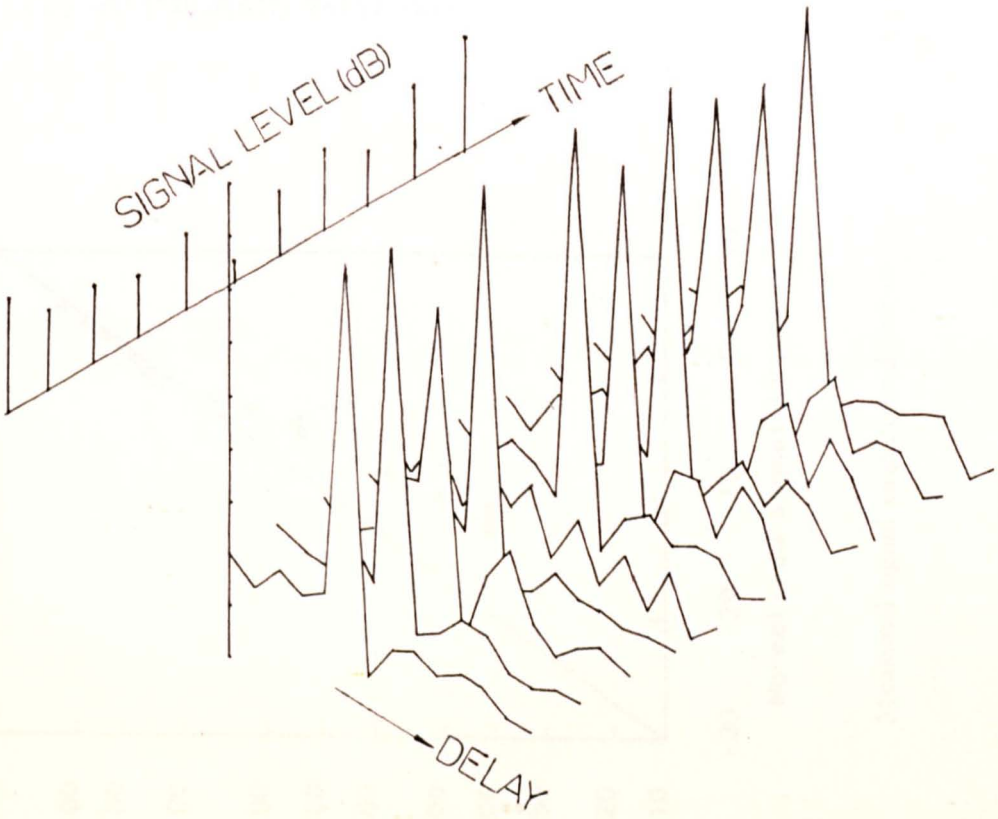

Figure 4.2 Example of the estimated signal amplitude and the channel impulse response in consecutive burst transmissions.

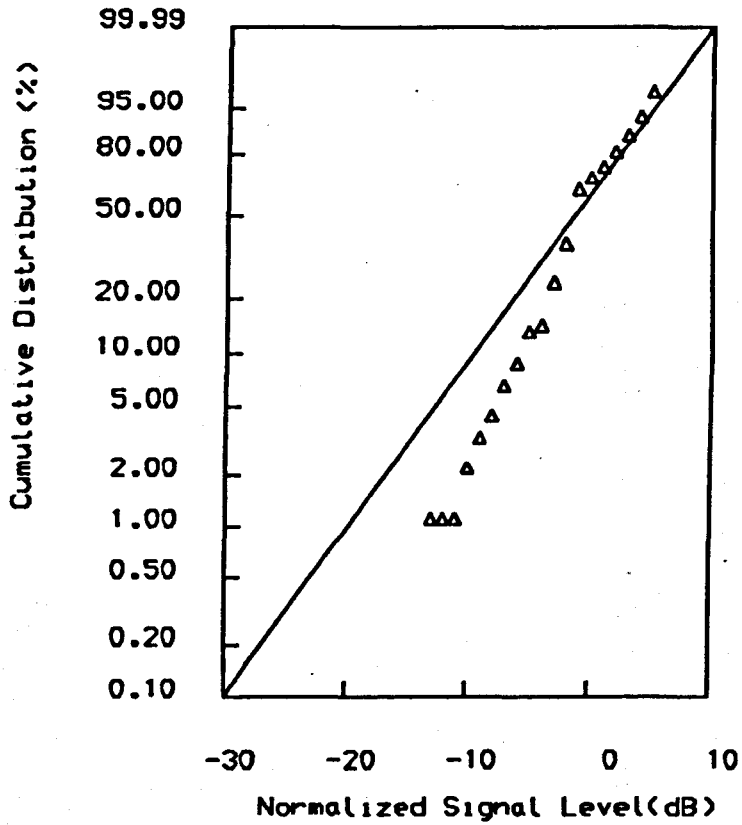

Figure 4.3 Measured signal amplitude distribution.

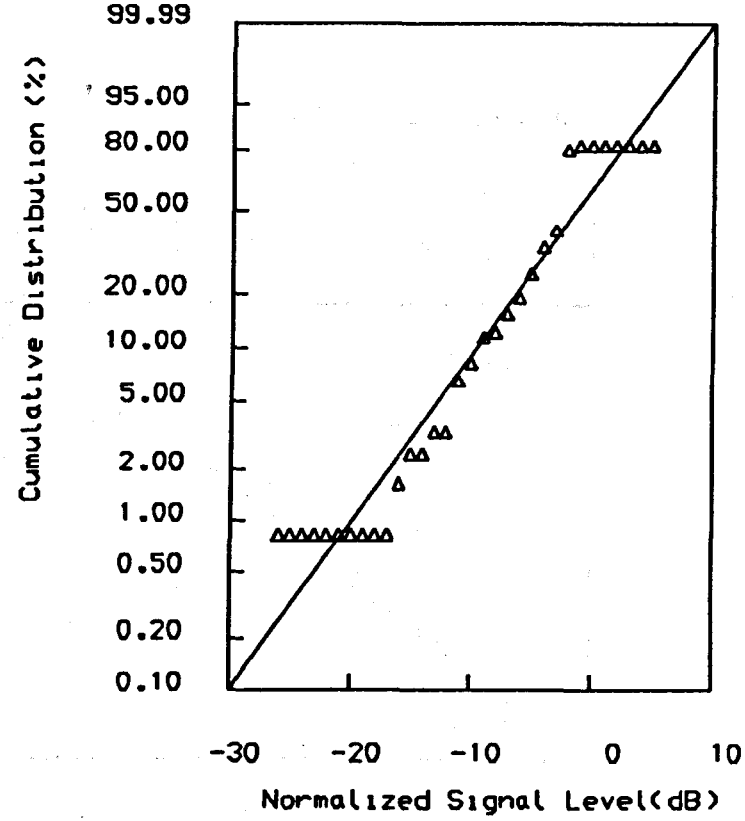

Figure 4.4 Measured signal amplitude distribution.

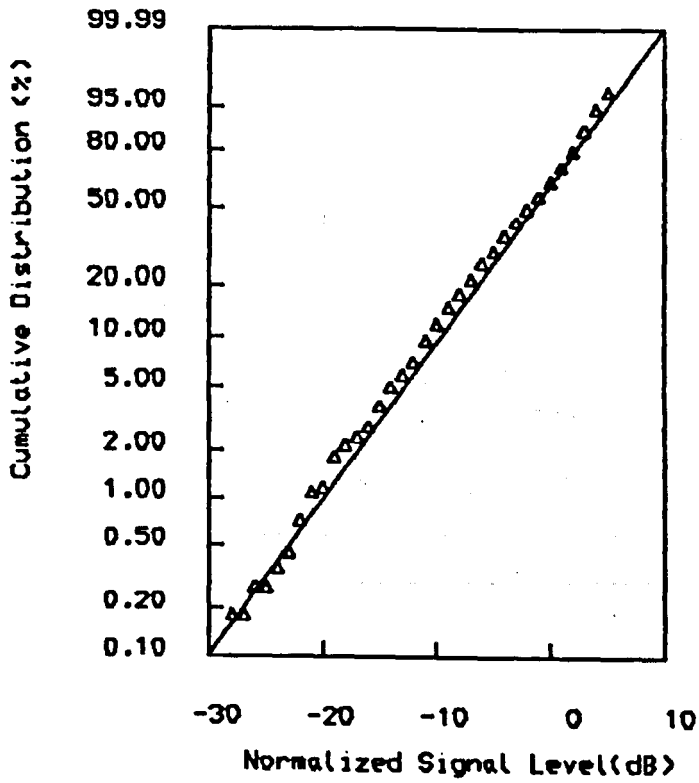

Figure 4.5 Measured signal amplitude distribution over 1000 samples.

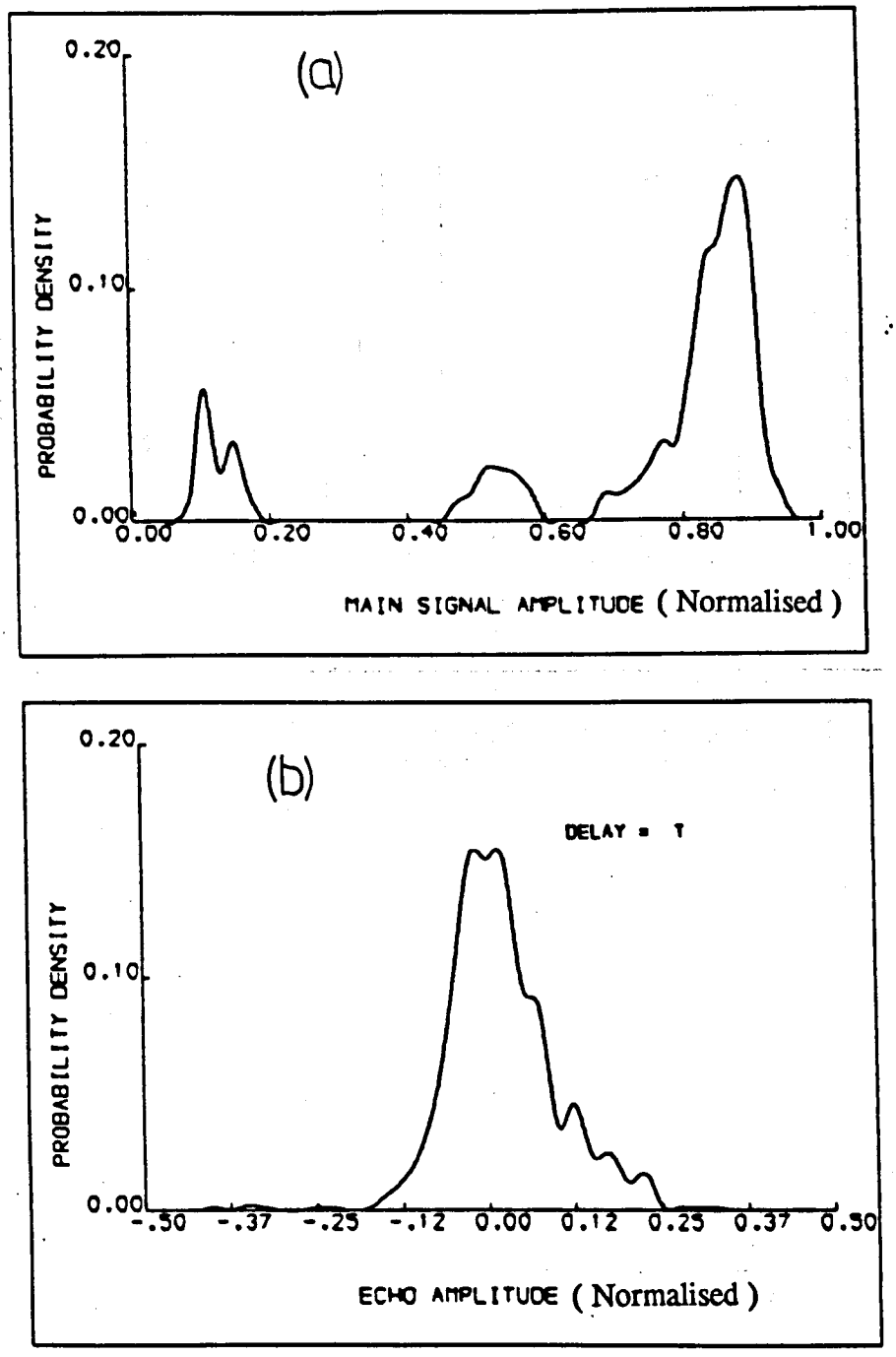

Figure 4.6 PDF of the amplitude of the delayed signal in the estimated channel impulse response. (a) main signal. (b) signal at delay T.

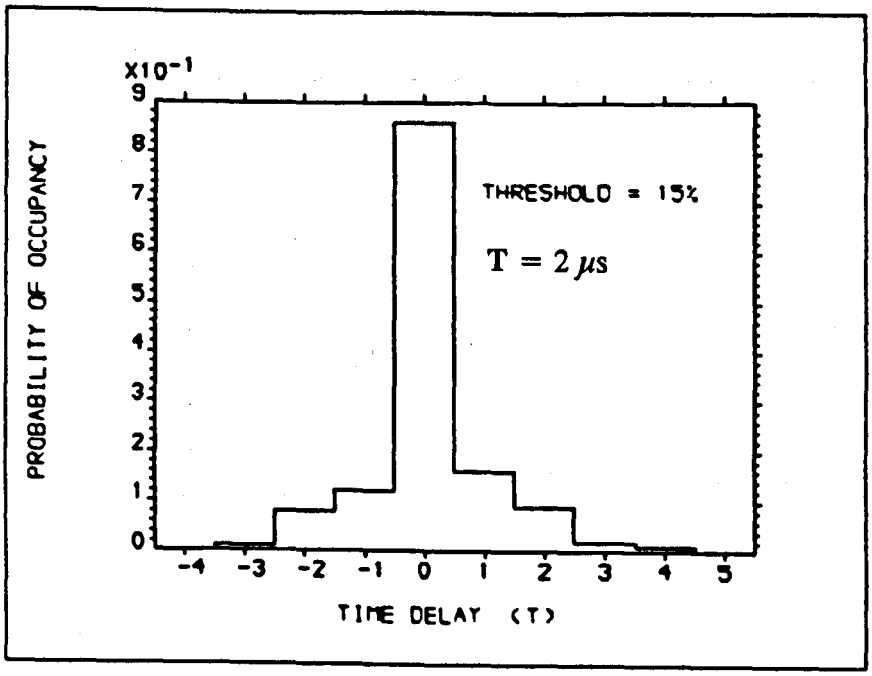

Figure 4.7 CDF of the amplitude of the delayed signal at T in the estimated channel impulse response.

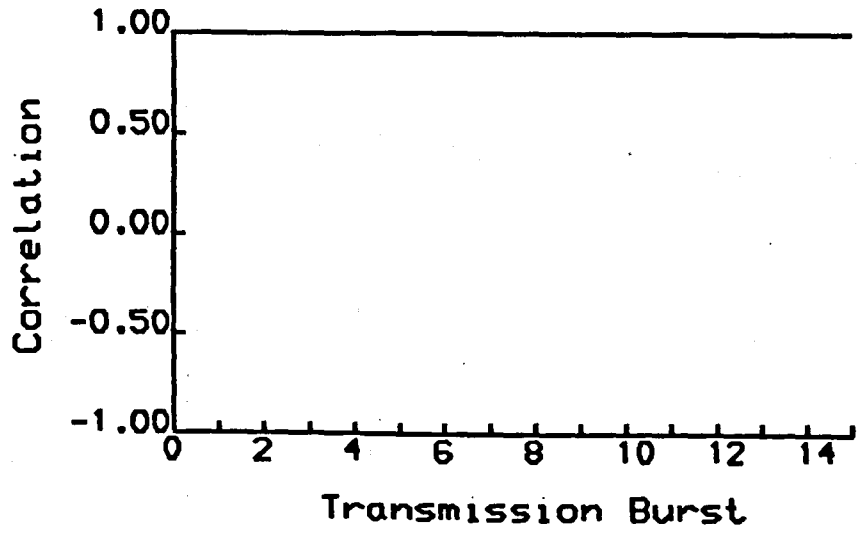

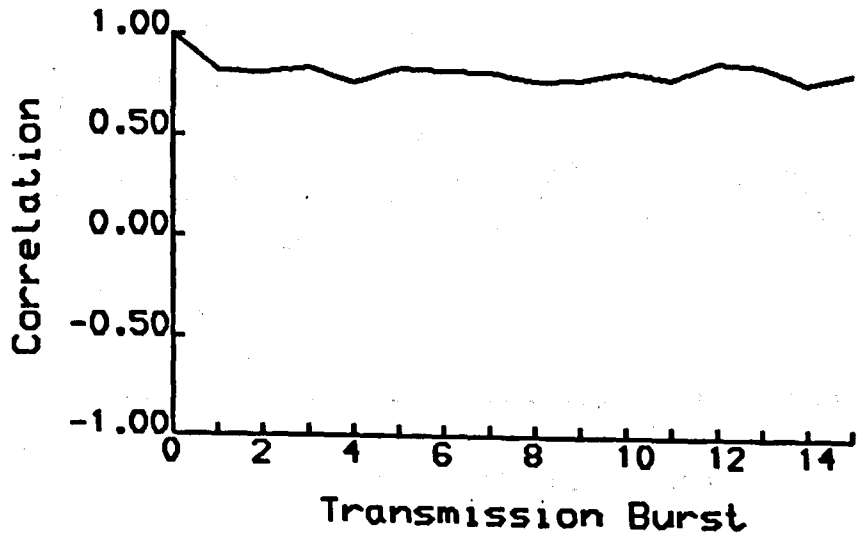

Figure 4.8 Two correlation functions of the main signal in the estimated channel impulse response.

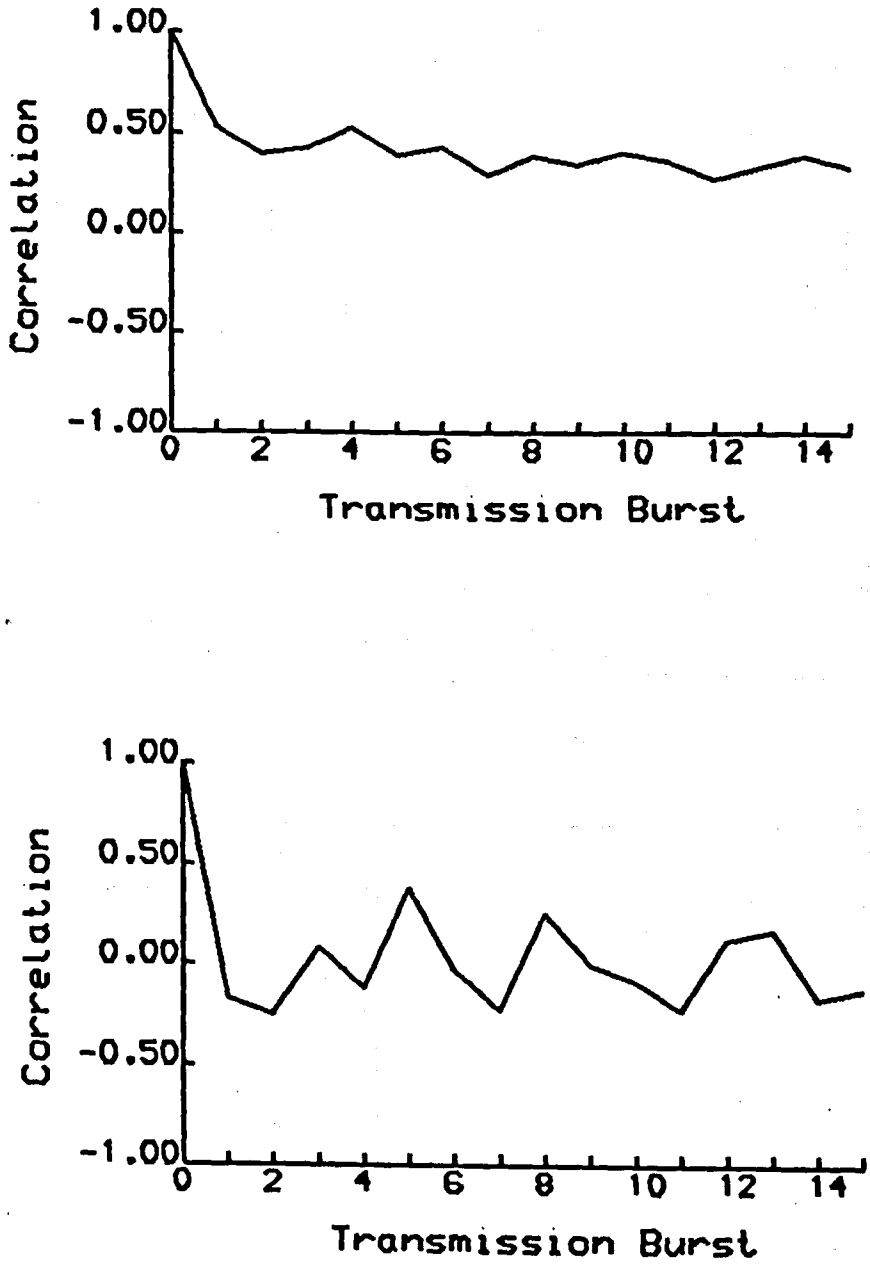

Figure 4.9 Two correlation functions of the delayed signal at T in the estimated channel impulse response.

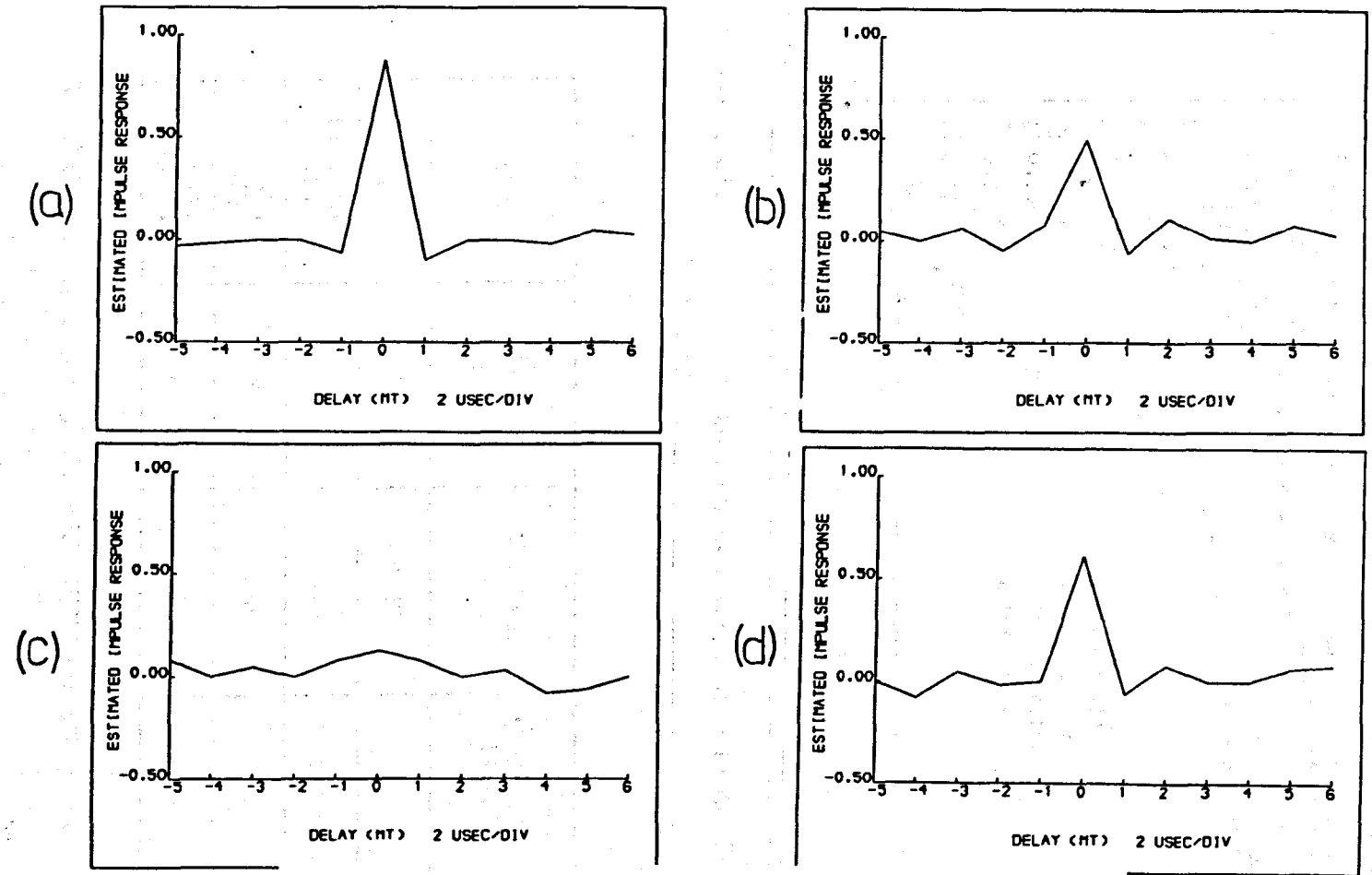

Figure 4.10 Four representative estimated channel impulse response. (a) Channel (I), (b) Channel (II), (c) Channel (III), (d) Channel (IV).

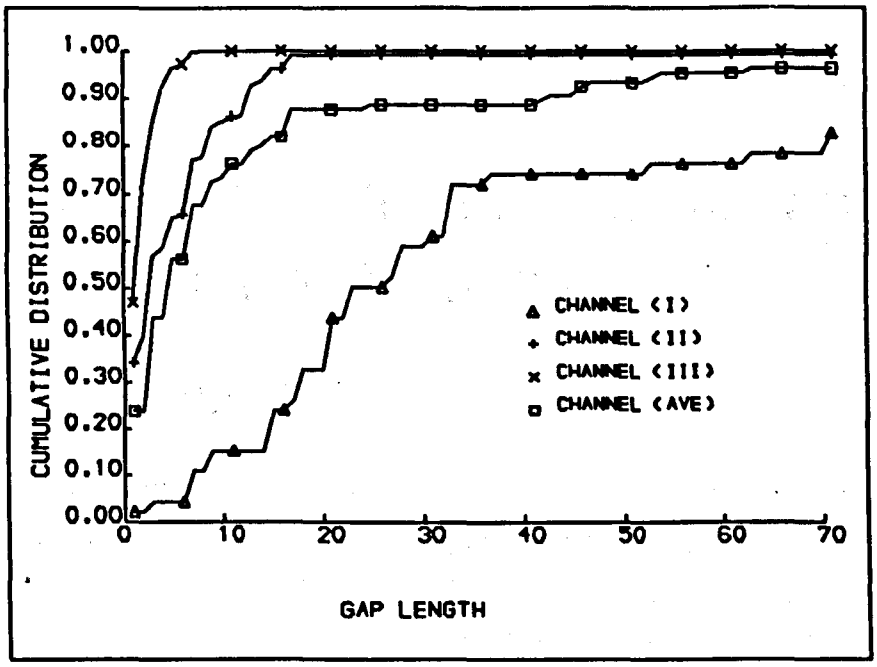

Figure 4.11 Four gap distributions corresponding to the four channels.

CHANNEL	E_b/N_o (dB)	AVERAGE BER	AVERAGE GAP LENGTH
CHANNEL (I)	25	0.017	48
CHANNEL (II)	15	0.125	6
CHANNEL (III)	5	0.40	3
CHANNEL (AVE)	20	0.038	21

TABLE 4.1 BER associated with different Channels and E_b/N_o,

CHAPTER 5 DATA PROCESSING BY CHANNEL EQUALISERS

5.1 INTRODUCTION

The results from the experimental investigation, presented in Chapter 4, have illustrated the deterioration in the quality of the data transmission caused by the distortion in the radio channel. It was observed that under such distortion the average error-free gap-length was reduced from 48 to 3, whereas the averaged BER was increased from 2 percent to 40 percent. In order to improve the quality of the data transmission, signal processing techniques should be applied to combat the radio channel distortion. There are two major techniques which can be used to achieve this purpose. The first is the channel equalisation technique, which is used to process the baseband waveforms by cancelling ISI and restricting the additive noise. The second is the error control coding technique, which is used to correct the errors made by the binary detector. This chapter investigates which channel equalisation techniques should be adopted in order to provide the most cost effective solution. Two types of equaliser, with variable configuration, were implemented in computer software in order to process the recorded data. The first type is the adaptive Decision Feedback Equaliser (DFE) utilising the Fast Kalman Algorithm (FKA), which adopts the transversal tapped delay line structure to formulate the inverse channel impulse response to cancel the ISI. The second type of equaliser performs a Maximum Likelihood Sequence Estimation (MLSE) by using the Viterbi Algorithm; these are generally referred to as Viterbi Equalisers (VE). The recorded data associated with the representative channels, which were selected in Chapter 4, were processed by these two types of equalisers, and the error-free gap-length distributions after each

of the equalisation processes were compared in order to determine the most effective equaliser structure.

5.2 APPLICATION OF ADAPTIVE DECISION FEEDBACK EQUALISERS

5.2.1 INTRODUCTION

Figure 5.1 shows the generalised tapped delay line structure of a DFE, with N_f forward delay elements and N_b backward delay elements. In the following discussion this combination will be denoted by DFE (N_f, N_b). The detector is a nonlinear device, its output d'_k is the equaliser detected symbol, which is defined as:

$$d'_k = \begin{cases} 1, & \text{if } \hat{d}_k \geq 0 \\ -1, & \text{otherwise} \end{cases} \tag{5.1}$$

where $\hat{d}_k$ is the sample value estimated by the equaliser, and k represents the kT time instant. The estimation made by the equaliser $\hat{d}_k$ is given by:

$$\hat{d}_k = \sum_{l=-Nf+1}^{0} c_l v_{k-l} - \sum_{l=1}^{Nb} c_l d'_{k-l} \tag{5.2}$$

where $v_k$is the received sample at time kT, c_l is the lth tap coefficient and d'_{k-l} is the previously detected symbol. The forward section of the equaliser adjusts the delay of the main signal, whereas the ISI after the arival of the main signal is cancelled by the feedback section, provided the detected symbols in the past are correct. The optimum tap coefficients are calculated subject to the constraint of minimising the mean square error (MSE), which is defined as :

$$\text{MSE} = < |\hat{d}_k - d'_k|^2 > \tag{5.3}$$

Since the mobile radio channel is time variant, the equaliser tap coefficients must be adjusted accordingly. In order to carry out such adjustments automatically, a training sequence, which is known by the receiver, is sent out from the transmitter before the actual data transmission. The receiver, at the kT sampling instant during the training period, will calculate the error ε_k between the estimated sample $\hat{d}_k$ and the kth stored training symbol s_k, where s_k takes values from ± 1. This error is referred to as the training error and it is expressed as

$$\varepsilon_k = |\hat{d}_k - s_k| \tag{5.4}$$

During this training period, the input to the backward delay line is disconnected from the detector output and connected to the stored training sequence, so that a detection error will not be fed back to the equaliser to cause further inaccurate decisions. The training errors are processed by an adaptive algorithm which automatically calculates the tap coefficients in order to reduce the MSE. Once the MSE is reduced below a predetermined value, the training process is stopped and the output from the detector is re-connected to the input of the backward delay line. The data transmission can now be started.

In a TDMA system, due to the variations of the impulse response from one transmission burst to another, the tap coefficients of the equaliser must be updated at each burst transmission. Since the number of information symbols in a transmission burst are limited, adopting a short training sequence is essential to enable the maximum number of information symbols to be transmitted during a burst. An efficient adaptive algorithm must accordingly be selected, so that the minimum MSE can be achieved within a small number of training steps.

Among all adaptive algorithms the Kalman Algorithm [1] uses the shortest training sequence, by recursively estimating the optimum tap coefficients. The disadvantage of this Algorithm is the increased computation complexity, which can be reduced, to a certain extent, by the Fast Kalman Algorithm (FKA) [2]. The FKA differs from the conventional Kalman Algorithm only

in the ways in which the arithmetic operations are carried out. The operation of the latter is described below to illustrate the basic operational principle.

Using matrix notation,[6] at time instant kT, the received sample values v_l in the forward delay line section and the previous detected symbol $\hat{d}_i$ in the backward delay line section of the equaliser are represented by a matrix V as

$$\mathrm{V}_k = (v_k, v_{k-1}, \cdots, v_{k-N_f+1}, \ \hat{d}_{k-1}, \hat{d}_{k-2}, \cdots, \hat{d}_{k-N_b+1})^T \tag{5.5}$$

The tap coefficients are defined as

$$\mathrm{C}_k = (c_0, c_1, \cdots, c_{N_f-1}, \ c'_0, c'_1, \cdots, c'_{N_b-1})^T \tag{5.6}$$

where $(\bullet)^T$ denotes matrix transposition, c_i represents a tap coefficient in the forward delay line, c'_l is the tap coefficient in the backward delay line. $\hat{d}_k$ is the kth estimated sample value before the detector, which is given by

$$\hat{d}_k = \mathrm{V}_k^T \mathrm{C}_k \tag{5.7}$$

Let s_k denote the kth symbol in the stored training sequence. The error covariance matrix can be expressed as

$$\mathrm{P}_k = (\mathrm{C}_{opt} - \mathrm{C}_k)(\mathrm{C}_{opt} - \mathrm{C}_k)^T \tag{5.8}$$

Where C_{opt} represents the matrix of the optimum tap coefficient. An acceptable minimum MSE, ε_{opt} is also preset before the training process. The Kalman Algorithm starts at time kT by going through the following steps.

STEP 1: Assuming C_k and P_k are known, the estimated symbol from the equaliser is calculated as

$$\hat{d}_k = \mathrm{V}_k^T \mathrm{C}_k \tag{5.9}$$

STEP 2: From the error between the estimated symbol and the stored training symbol, the tap coefficient for time $(k+1)T$ is calculated as

---

[6] In the following text, a capital letter will be used to denote a matrix

$$C_{k+1} = C_k + K_k \ (\hat{d}_k - s_k) \tag{5.10}$$

Where K_k is the Kalman gain, which is defined as

$$K_k = P_k \ V_k \ (V_k^T \ P_k \ V_k + \varepsilon_{opt}^2)^{-1} \tag{5.11}$$

STEP 3: The error covariance at time $(k+1)T$ is predicted by the algorithm as

$$P_{k+1} = P_k - K_k \ V_k^T \ P_k \tag{5.12}$$

STEP 4 : STEP 1 is repeated at time $(k+1)T$, until all the symbols in the training sequence are processed. The algorithm will then fix the tap coefficients, and the data transmission can be started.

It has been shown theoretically [3] that, in the absence of additive noise, the KA should be able to reduce the MSE to within 3dB of the final steady state error, after $2N$ steps of iteration, where N is equal to the total number of forward and backward delay sections.

$$N = N_f + N_b \tag{5.13}$$

5.2.2 APPLICATION OF DFE WITH FKA

The recorded data associated with the four representative channel impulse responses, which were selected in Chapter 4, are processed by the DFE utilising FKA. The DFE were implemented in computer software with a variable number of forward and backward delay sections. The training process is carried out at the beginning of each transmission burst by using the first PRBS in that burst as the training sequence. The initial tap coefficients were set to zero and the initial error covariance matrix was set to be an identity matrix I,

$$P_k = \begin{pmatrix} 1 & 0 & . & 0 \\ 0 & 1 & . & 0 \\ 0 & 0 & . & 0 \\ . & . & . & . \\ 0 & 0 & . & 1 \end{pmatrix} \qquad (5.14)$$

The minimum error ε_{opt} was chosen to be 0.02, as a result of the quantisation noise in the 6 bit representation in the recorded data. The tap coefficients were fixed after 63 iteration training steps, and the recorded data in a burst were passed through the equaliser. The output from the equaliser detector is used to compare with the transmitted PRBS in order to evaluate the average distribution.

The DFE used in the data processing were, using the notation defined in section 5.2.1, DFE(3,2), DFE(3,3), DFE(5,3), DFE(5,5). The results obtained from the equalisation process are presented in the next section.

5.2.3 RESULT AND CONCLUSION

The average gap length before and after applying DFE are shown in Table 5.1, and the corresponding BER are shown in Table 5.2. It was observed that for Channel (I), where the average signal to noise ratio is 25 dB and the ISI is very small, DFE (5,3) and DFE (5,5) provided a greater improvement in the average gap length than DFE (3,2) and DFE (3,3). All DFE offered limited improvement over Channel (II), where the average signal to noise ratio is 15 dB, and the ISI is large. The average gap length increased from 6 to 9 after various DFE were applied. For Channel (III), where the signal is almost completely lost in the noise, no improvement was made by any DFE. Over the average channel, Channel (AVE), DFE (3,2) DFE (3,3) performed better than DFE (5,3) and DFE (5,5), where the average gap length was doubled from 20 to 40. From these sample results, it can be concluded that DFE (3,2) and DFE (3,3) are the cost effective DFE structures in equalising the recorded data from the field experiment conducted in Liverpool Univer-

sity precinct. Because the data used in the processing were selected to represent some typical cases, this conclusion does not include the worst case. The definition of typical cases is not universal, the selection of the representative results depends on the experience and emphasis of system designers. The advantage of developing this versatile experimental system is to provide the designer with facilities which can be used to measure the radio channel, analyse the recorded data, and make decisions.

Figure 5.2 shows the MSE against the training steps when the DFE's were used in Channel (I). This figure shows that the MSE during the training period of every DFE was reduced below the preset minimum value in less than 20 training steps. Therefore a training sequence with as little as 20 bits can be used for the training process in the DFE.

5.3 APPLICATION OF THE VITERBI EQUALISER

5.3.1 INTRODUCTION

The VE is a practical approach to Maximum Likelihood Sequence Estimation (MLSE) [4], which is based upon the assumption that the received samples are corrupted by the AWGN, and the receiver is capable of estimating the finite time impulse responses of the channel. In order to avoid confusion in the following discussion, a non-italic capital letter will be used to represent a sequence of sampled values obtained at multiple T intervals. A small letter will be used to represent an individual sampled value in a sequence, with its subscript denoting the sampling time instant (e.g. v_n represents a sampled value obtained at time nT). On receiving a N sampled value sequence

$$\mathrm{V} = (v_0, v_1, \cdots, v_{N-1})$$

its likelihood function can be calculated, which is

$$M = p(\mathrm{V}\,|\,\mathrm{W}) \tag{5.15}$$

where

$$W = (w_0, w_1, \ldots, w_{N-1})$$

is the actual transmitted sequence, and $p(V|W)$ is a multi-variate Gaussian distribution, which involves matrix operations. The most likely sequence which maximises the likelihood function M will be selected as the equalised output.

Since the samples of AWGN are mutually independent, the likelihood function in equation (5.15) can be simplified to

$$M = \prod_{n=0}^{N-1} p(v_n | w_n) \tag{5.16}$$

where

$$p(v_n | w_n) = \frac{1}{\sqrt{\pi N_o}} exp\{ -(v_n - w_n)^2 / N_o \} \tag{5.17}$$

is the likelihood function of v_n, in the AWGN, which has a power spectral density of $N_o/2$. This simplification is valid only if $N_o/2$ remains the same over the entire sequence.

Maximising M is now equivalent to maximising each individual $\exp\{ -(v_n - w_n)^2 \}$, hence minimising the corresponding $(v_n - w_n)^2$. The natural logarithm value of M can be taken and a modified likelihood function can be defined as

$$M' \propto \sum_{n=0}^{N} (v_n - w_n)^2 \tag{5.18}$$

The most likely sequence will now have the minimum value of M'. The minimisation of M' is equivalent to finding the individual w_n which differs least, in magnitude, from the v_n.

The implementation of a VE is best illustrated by an example as follows.

If the discrete-time channel impulse response is assumed to have 3 non-zero sampled values and is represented by a matrix H as

$$\mathrm{H} = (h_0, h_1, h_2) \tag{5.19}$$

the sampled signalling sequence is represented by

$$\mathrm{S} = \sum_{n=0}^{N} s_n \ \delta(t - nT) \tag{5.20}$$

where s_n takes values from ± 1. The received sample value at sampling time kT, in the absence of noise, is calculated by a convolution process which is defined as

$$w_k = \sum_{n=0}^{2} s_{k-n} h_n \tag{5.21}$$

Assuming the values of s_{k-1} and s_{k-2} are determined, then two possible received samples, $w_k(-1)$ and $w_k(1)$ exist, corresponding to $s_k = -1$ and $s_k = 1$ respectively. The combination of $s_k \ s_{k-1}$ at time kT is referred to as a 'state'. Only four states exist in this example, because the the channel impulse response H has only 3 non-zero sample values and s_k takes values from ± 1.

A new signalling sample s_{k+1} will cause a transition between two states, which are $s_k s_{k-1}$ at time kT and $s_{k+1} s_k$ at time $(k+1)T$. Such a transition generates two possible received sample values $w_{k+1}(-1)$ and $w_{k+1}(1)$ which can be calculated by using equation (5.21).

Figure 5.3 shows the possible state transitions that could have taken place between time instants k and $k+1$, in the example described above. This structure is referred to as a section of a trellis. A branch is used in this figure to joint two states together to represent a transition. The calculated received sample value $w_{k+1}(s_{k+1})$ is written on top of the branch. The point where two branches merge is referred to as a 'node', and there are two variables assigned to it. The first is the accumulated difference $a_{i,k}$, and the second is the branch reminder $b_{i,k}$, where i ranges from 1 to 4 in this example to denote the order

of nodes, and k indicates the kT sampling instants. The purpose of these variables will be discussed in the description of the VE operation below. The contents of these variables are all set to zero at the beginning of the equalisation.

The VE operates through the following iterative steps in order to find the minimum M'.

STEP 1: Referring to Figure 5.3, at time $(k+1)T$ a received sample v_{k+1} is read in by the equaliser and is compared with the two possible received values on the transitional branches, which merge at the ith node at time $(k+1)T$. The two differences are defined as follows.

$$d_{i,k+1}(-1) = |v_{k+1} - w_i(-1)| \tag{5.22}$$

$$d_{i,k+1}(+1) = |v_{k+1} - w_i(+1)| \tag{5.23}$$

where (± 1) indicates the value of the signalling sample that caused the transition. These differences were added to the accumulated differences $a_{l,k}$ and $a_{m,k}$ (where l, m are integers taking values from $1, 2, 3, 4$) , from where the transition to the present node originated. The newly formed differences are :

$$d'_{i,k+1}(-1) = d_{i,k+1}(-1) + a_{l,k} \tag{5.24}$$

$$d'_{i,k+1}(+1) = d_{i,k+1}(+1) + a_{m,k} \tag{5.25}$$

The algorithm retains, at this moment, the branch with a smaller difference. The branch with a larger difference is discarded. The updated accumulated difference at the present node is

$$a_{i,k+1} = d'_{i,k+1}(x) \tag{5.26}$$

where x takes a value from ± 1, depends on which branch has survived, and it will be remembered by the branch reminder as

$$b_{i,k+1} = x \tag{5.27}$$

This 'compare and discard' process is repeated for all 4 nodes at time $(k+1)T$. At the end of the process, each node will be attached to a survived branch and updated $a_{i,k+1}$ and $b_{i,k+1}$.

STEP 2: Another received sample v_{k+2} is read in and a new trellis section is created and cascaded to the section in STEP 1, as shown in Figure 5.4, so that nodes at time $(k+2)T$ are connected by the corresponding transitional branches to the nodes at the $(k+1)T$.

STEP 1 and STEP 2 are repeated until all the N received samples within a TDMA transmission burst are processed. The algorithm then proceeds to STEP 3.

STEP 3: The 4 accumulated differences $a_{i,N}$ are compared, and the least difference is retained by the algorithm. This value corresponds to the minimum of M'. The node with the minimum accumulated difference is referred to as the 'survived node' and there is a continuous route, which consists of all the previous survived branches, attached to it, as shown in Figure 5.5. The signalling samples, which generate these survival branches, have been memorised by the corresponding $b_{i,k}$, which take values ± 1. These memorised values are retrieved sequentially by the VE as the equalised output.

The example described above has demonstrated the operation principle of a 4-state VE. The number of states in a VE will increase as the number of non zero samples in the channel impulse response increases. This is because a received sample value, which is calculated by the convolution process defined in equation (5.21), is now related to more adjacent signalling samples. In practice, the estimated channel impulse response includes noise components, therefore only the samples with values above the noise floor are used. If there are L such sample values present in an estimated channel impulse response, the number of states required by a VE is theoretically equal to 2^{L-1}, in order to achieve an accurate estimation of the received sequence.

5.3.2 APPLICATION OF VITERBI EQUALISERS

The same set of recorded data which was used in Chapter 4 and in section 5.2.2 are used here again to be processed by a VE implemented in computer software. The number of states used in the VE were 8, 16, 32 and 64, they are named as VE (8), VE (16), VE (32), and VE (64) respectively. The possible received samples were calculated by the computer at the beginning of each transmission burst as follows. First, a window of $N_w T$ intervals is slid over the estimated channel impulse response, and the total energy within this window is calculated. N_w is given by

$$N_w = \sqrt{\text{number of state in VE}} + 1 \tag{5.28}$$

and the energy within the window is calculated as

$$E_i = \sum_{l=i}^{i+N_w} h_l^2 \tag{5.29}$$

The sample sequences having the maximum E_i are selected as the truncated channel impulse response. The possible received sample values $w_i(\pm 1)$ are calculated by generating N_w bit binary sequences and convolving them with the truncated impulse response by using equation (5.21). The recorded data samples can then be processed by the VE. The results from the data processing by VE is presented in the next section.

5.3.3 RESULT AND CONCLUSION

The recorded data corresponding to the four representative channel impulse responses, which were selected in Chapter 4, were processed by VE (8), VE (16), VE (32) and VE (64). The average gap lengths were evaluated and tabulated in Table 5.3. The corresponding BER is shown in Table 5.4. The results can be summarised as follows. For Channel (I), where there is very little ISI and the E_b/N_o is 25 dB, there is no additional improvement in the average gap length by using VE with a number of states exceeding 16. For

Channel (II), where the ISI is large and the E_b/N_0 is about 15 dB, the improvement in the average gap length is limited and remains approximately the same for the various VE. The VE did not make any improvement on channel (III), where the signal is almost completely lost in the noise. VE (8) provided the largest improvement in the average gap length for Channel (AVE). The results show that VE with an increased number of states did not improve the average gap length in Channel (II) , (III), and Channel (AVE). This is probably because by implementing VE with longer states, more noise components are included in the calculation of the possible received samples by using equation (5.21), hence the 'compare and discard' process in the Viterbi algorithm becomes less accurate. Therefore it is concluded that VE(8) is a cost effective structure in processing the experimental data.

5.4 COMPARISON BETWEEN DFE AND VE

A general comparison based upon the average gap length between DFE and VE shows that the former equalisation strategy offers greater improvement, in processing the experimental data collected in areas around Liverpool University precinct. The differences are probably due to the noise in the estimated channel impulse response. The inclusion of such noise in the calculation of the possible received samples $w_i(\pm 1)$ in VE causes the 'compare and discard' operation to become less accurate. The DFE is more tolerant to the noise because of its transversal filter structure, which restricts the noise power in the consecutive sample values. The VE is also more sensitive to the isolated burst error pattern when the average channel distortion is small and the signal to noise ratio is high, where a short error burst causes an erroneous 'survived route' to be retained. Figure 5.6 shows a comparison of the cumulative gap distributions between DFE (3,3) and VE (32) in Channel (I), where an increase in the number of short gap lengths after VE is evident. When the ISI is large and the signal to noise ratio is reduced, as in Channel (II), the average gap length before the equalisers is shortened. In this situation the VE performed better than DFE in regions where the gap length is short. Figure 5.7 shows a comparison of the cumulative gap distrib-

utions between unequalised data, the data after DFE (3,3), and the data after VE (32) in Channel (AVE). In this figure, DFE (3,3) has a larger number of gaps with lengths shorter than 4, compared to VE (32). This is because the frequent detection errors have been fed back into the delay line in the DFE, and the decision process becomes even less accurate. Despite this error propagation effect, the average gap length after DFE (3,3) is still larger than that after VE (32).

The computation complexity in each equaliser structure can also be compared. For the DFE, if the total delay section is N, then there are $10N + 5$ multiplications for each symbol period T [1]. The VE on the other hand requires a complex correlator, and if a PRBS with N bits is used for channel estimation, the number of multiplications is N^2.

The other advantage of the DFE is that its transversal filter structure restricts the additive noise power in the demodulated baseband waveform. The disadvantage is that the detection error will be fed back to create further errors. However, from the experimental investigation, this error propagation effect is not dominant.

5.5 CONCLUSION

This Chapter has reviewed two types of channel equalisation techniques. The adaptive Decision Feedback Equaliser utilising the Fast Kalman Algorithm with variable forward and backward delay sections, and the Viterbi Equaliser with different numbers of states were implemented in computer software to process the experimental data. Comparisons were made, based upon the average gap length, between un-equalised data and that equalised by the two types of equalisers. The recorded data over four representative channels, which were selected in Chapter 4, were used in the data processing. From the results of processing these selected data, it was found that DFE performed, on average, better than VE. The average gap length was not improved generally by an increase in the number of delay line sections for DFE, or an in-

crease in the number of states for VE. Among the two types of equalisers used in the data processing, the DFE (3,3) and VE (8) were found to be sufficient in equalising an average channel, which was selected from the experimental data,

with DFE(3,3) providing a larger gap length. From this result it was concluded the DFE (3,3) is the most cost-effective equaliser structure. Although this conclusion is based on processing some selected data, and it may not represent a more general situation, it demonstrated how the measured data, which were recorded by the versatile experimental system, can be analysed and processed by applying various algorithms. These types of experiment can be carried out in many places in order to reach a more generalised conclusion.

REFERENCES

[1] Falconer, D. D., Ljung, L., "Application of Fast Kalman Estimation to Adaptive Equalisation", IEEE Trans. Commun. vol. COM-26, NO.10, pp.1439-1446, Oct. 1978.

[2] Lawrence, R. E., Kaufman, H., "The Kalman Filter for the Equalization of a Digital Communications Channel", IEEE Trans. Commun. Tech. vol. COM-19, pp. 1137-1141, Dec. 1971.

[3] Godard, D., "Channel Equalization Using a Kalman Filter for Fast Data Transmission", IBM J. Res. Develop. pp.267-273, May 1974

[4] Forney, G. D. Jr., "Maximum-Likelihood Sequence Estimation of Digital Sequence in the Presence of Intersymbol Interference", IEEE Trans. Inform. Theory, vol. IT-18, NO.3, pp. 363-378, May 1972.

[5] Tsang, K. Y., et al. "A Polypass Adaptive Training and Equalisation Method", IEE Fifth International Conference on Mobile Radio and Personal Communications, pp.142-146, Dec 1989.

[6] Haykin, S. "Adaptive Filter Theory", Englewood Cliffs, Prentice-Hall, 1986.

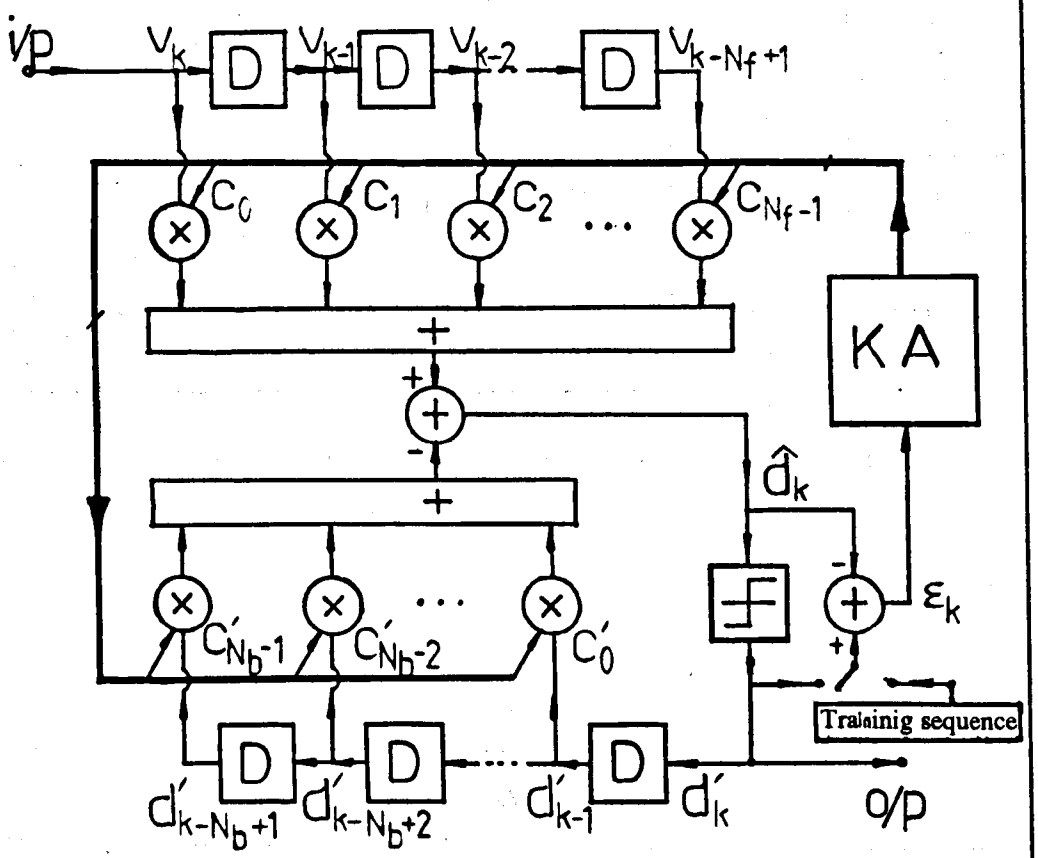

Figure 5.1 Block diagram of an adaptive Decision Feedback Equaliser (DFE) utilising Kalman Algorithm (KA).

CHANNEL	AVERAGE GAP LENGTH				
	NON EQUALISED	DFE (3,2)	DFE (3,3)	DFE (5,3)	DEF (5,5)
CHANNEL (I)	48	54	53	66	66
CHANNEL (II)	6	9	10	9	8
CHANNEL (III)	3	3	3	3	3
CHANNEL (AVE)	21	40	41	28	20

TABLE 5.1 Comparison of the average gap length before and after DFE, in different channels.

CHANNEL	AVERAGE BER				
	NON EQUALISED	DFE (3,2)	DFE (3,3)	DFE (5,3)	DFE (5,5)
CHANNEL (I)	0.017	0.015	0.015	0.013	0.013
CHANNEL (II)	0.125	0.085	0.084	0.090	0.097
CHANNEL (III)	0.40	0.39	0.39	0.39	0.37
CHANNEL (AVE)	0.038	0.021	0.020	0.030	0.042

TABLE 5.2 Comparison of the average BER before and after DFE, in different channels.

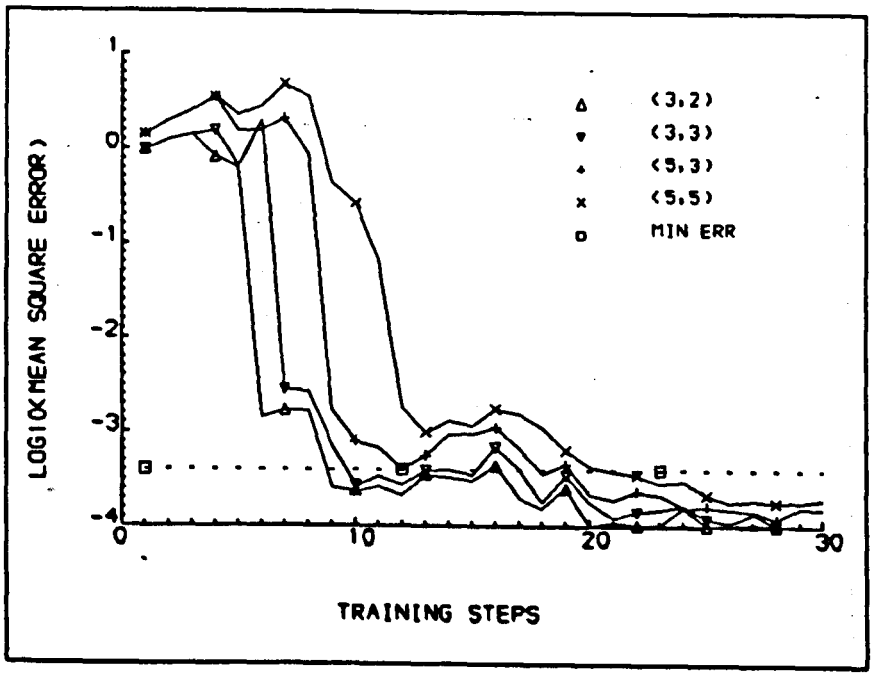

Figure 5.2 Mean Square Error (MSE) during the training process, of DFE with KA in Channel (I).

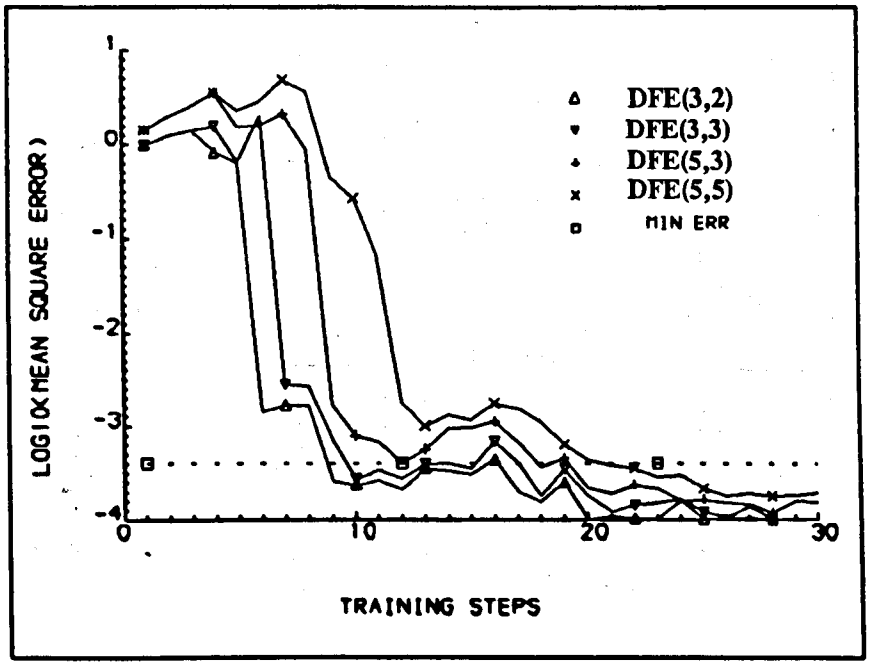

Figure 5.2[A] Mean Square Error (MSE) during the training process, of DFE with KA in Channel (I).

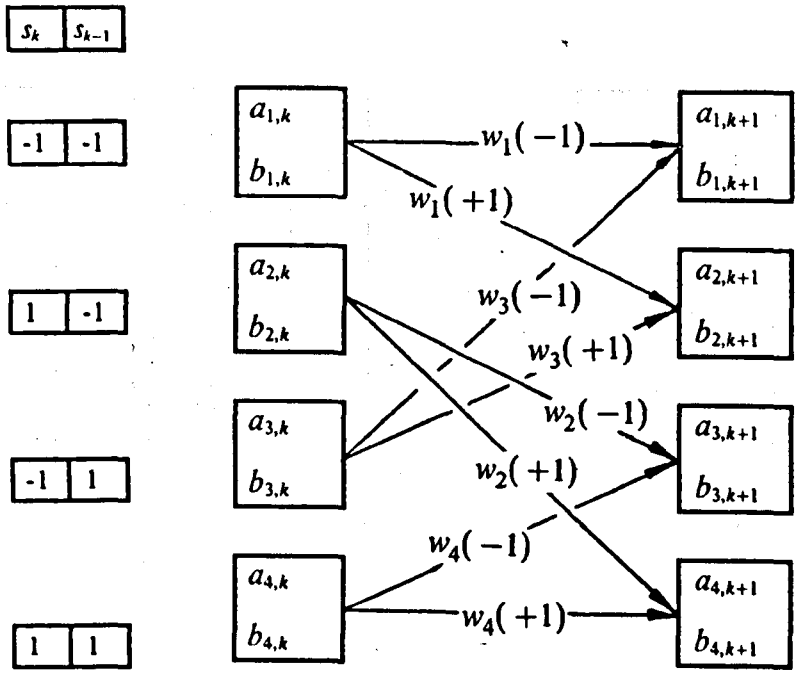

Figure 5.3 One section of trellis representing transitions in states between time kT and $(k + 1)T$

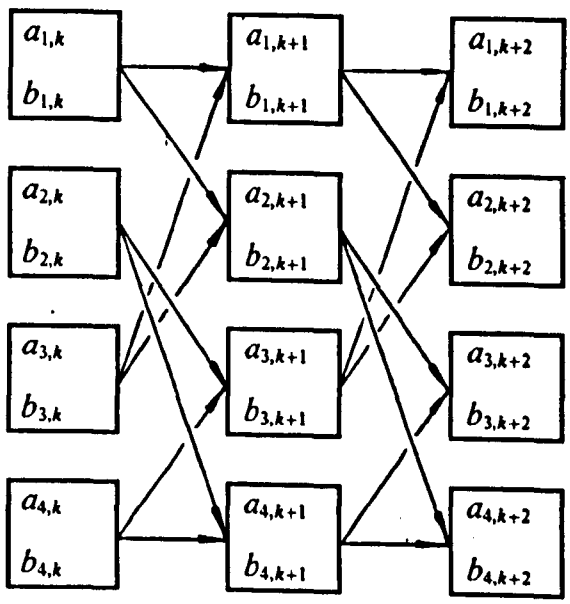

Figure 5.4 Two cascaded sections of trellis.

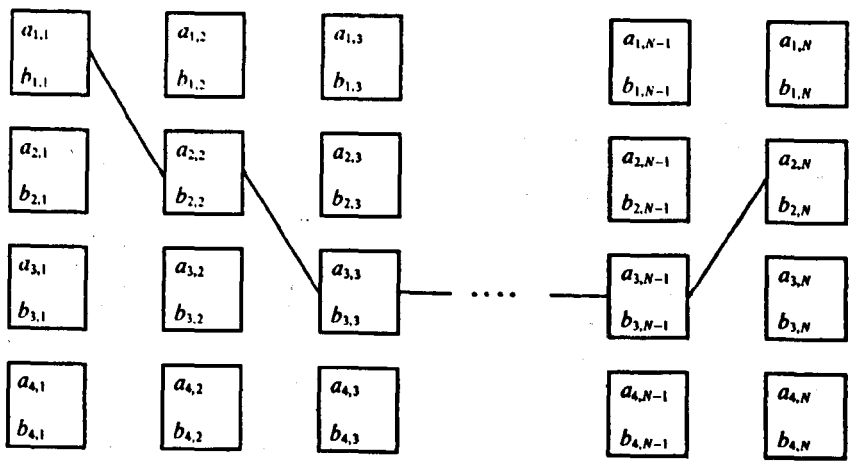

Figure 5.5 N section of trellis and a survived route.

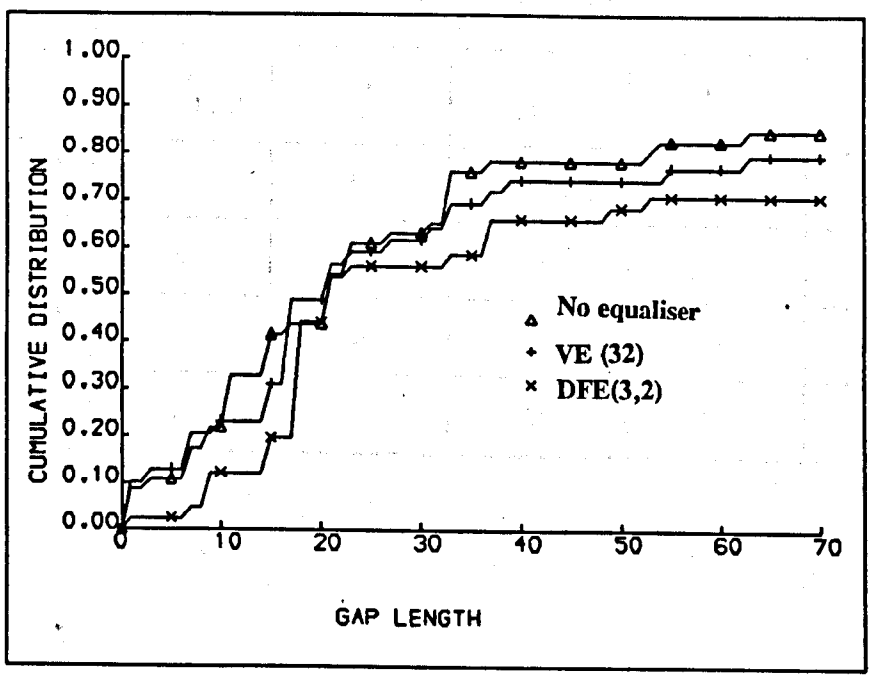

Figure 5.6 Comparison of gap distributions between un-equalised, DFE (3,3) and VE (32) in Channel (I).

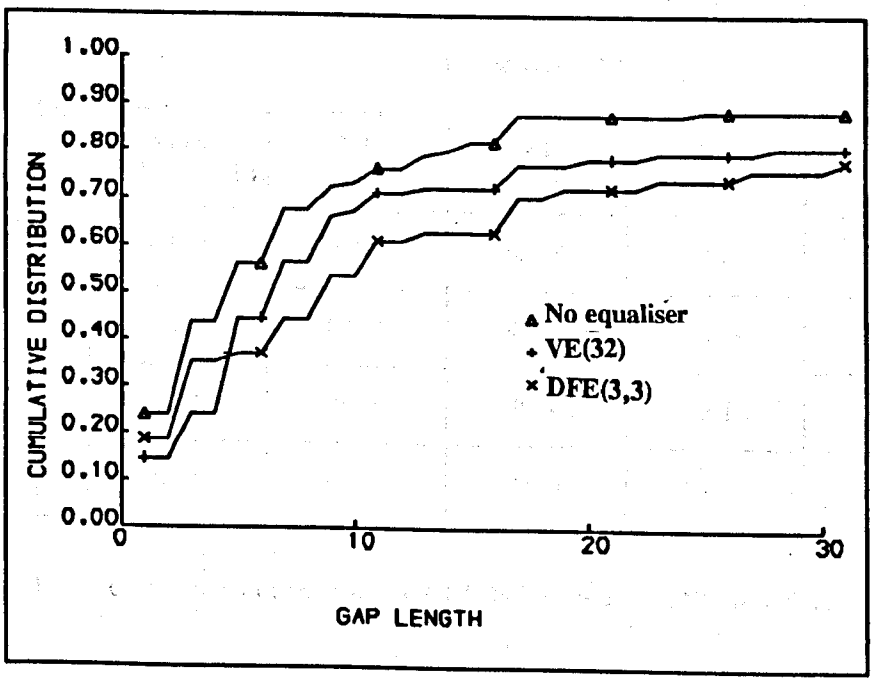

Figure 5.7 Comparison of gap distributions between un-equalised, DFE (3,3) and VE (32) in Channel (AVE)

CHANNEL	AVERAGE GAP LENGTH				
	NON EQUALISED	VT (8)	VT (16)	VT (32)	VT (64)
CHANNEL (I)	48	55	57	57	57
CHANNEL (II)	6	9	9	8	9
CHANNEL (III)	3	3	3	3	3
CHANNEL (AVE)	21	31	26	26	27

TABLE 5.3 Comparison of the average gap lengths before and after VE, in different channels.

CHANNEL	AVERAGE BER				
	NON EQUALISED	VT (8)	VT (16)	VT (32)	VT (64)
CHANNEL (I)	0.017	0.015	0.014	0.015	0.017
CHANNEL (II)	0.125	0.082	0.086	0.089	0.086
CHANNEL (III)	0.40	0.34	0.34	0.4	0.4
CHANNEL (AVE)	0.038	0.026	0.031	0.031	0.030

TABLE 5.4 Comparison of the average BER before and after VE, in different channels.

CHAPTER 6 CONCLUSIONS

This chapter concludes the work and experimental results presented in this thesis, and suggests topics for future work.

6.1 CONCLUSIONS

The design, construction and results from field experiment using a versatile TDMA digital mobile radio transmission system which operates at 1.8 GHz using GMSK modulation with $BT = 0.3$ have been presented in this thesis.

Chapter 2 contains a review of various spectrally efficient digital modulation techniques. The average BER with the coherent detection of these modulated signals in the presence of AWGN, (which was used to model the interference in a cellular radio system), were calculated in order to demonstrate that spectral efficiency in a modulation technique cannot be achieved without causing degradation in terms of increased average BER. Comparing QPSK, MSK and GMSK modulation with $BT = 0.3$, the latter was found to be much more efficient in utilising the spectrum, and theoretically it requires less than 2 dB additional signal power to achieve the same the average BER in QPSK, or 1 dB to that in MSK, subject to coherent detection.

The effect of signal fading, which is caused by multipath propagation, on the theoretical average BER was reviewed by adopting the Rayleigh and Rician distributions to statistically model the amplitude of the received signal. Special attention was paid to digital transmissions in a TDMA system, where the high data rate makes the transmission more vulnerable to the ISI introduced by the imperfect channel impulse response. A computer simulation was car-

ried out to evaluate the average BER of a TDMA transmission at 500 kb/s., over a mobile radio channel subject to AWGN and Rayleigh fading. Results from the simulation showed that the average BER remained above one percent as the signal-to-noise ratio was increased. This chapter concluded by suggesting an experimental investigation in order to acquire more detailed knowledge of the real time mobile radio channel, such as the channel impulse response, signal level, and their effect on the bit error statistics, so that cost effective signal processing techniques could be devised to reduce the average BER.

The design, construction and laboratory calibration of a coherent TDMA experimental system was described in Chapter 3. This has the versatility to accept various digital modulation techniques at variable data transmission bit rates, and is capable of estimating the real-time channel impulse response. The system was designed to include both electronic hardware and computer software, in order to provide a practical solution to testing a large number of digital signal processing techniques over a real mobile radio channel.

The coherent detection of the system was achieved at a variable IF, which is independent of the synthesised local signal sources. Such a design enables the selection of both the optimum bandpass filter in the receiver and the final transmission frequency to become flexible.

A laboratory calibration of the system was carried out by passing attenuated signal through a commercial Rayleigh-fading simulator. The result showed that, at the absence of signal fading, the measured average BER was consistent with the theoretical calculation discussed in Chapter 2. When fading was introduced, irreducible bit errors were found in the measured BER, and such errors increased with fading rate. The irreducible errors occurred because the signal was lost in the noise during deep fades, where the received signal was attenuated very close to the system noise level and the receiver could no longer track the correct phase of the signal. A real time channel impulse response estimator utilising the correlation principle was designed and implemented as an integral part of the coherent receiver. The estimator

was calibrated for a GMSK modulated signal with $BT = 0.3$. The laboratory measurements showed that the system performed according to the design specification.

The procedures and results from field trials conducted around Liverpool University precinct (which represents an average urban area), were reported in Chapter 4. The estimated channel impulse response, signal level and the sampled quadrature baseband waveforms were recorded and later transferred to an IBM Personal Computer, where statistical analysis and signal processing were carried out. The statistical analysis on a large number of sampled values of the received signal level, which were measured at the beginning of each TDMA transmission burst, showed that they were Rayleigh distributed.

The statistical analysis on the estimated channel impulse responses showed that delayed signals with significant strength (e.g. 15 per cent of the maximum main signal level) were likely to occur at $\pm 2T$ intervals from the arrival of the main signal.

The correlation function of the delayed signals over consecutive TDMA transmission bursts were also evaluated. The results showed that the correlation function of the main signals were positive and strongly correlated, although this correlation was occasionally lost because the received signal had faded close to the system noise level. The correlation function of the delayed signals at time T from the main signal showed that the correlation varies from moderate to having opposite polarity between adjacent transmission bursts.

Four representative estimated channel impulse responses were selected and the corresponding error-free gap distributions and average BER were evaluated. The average gap lengths were between 50, for a channel with small ISI and 25 dB average signal-to-noise ratio, to 5, where the main signal was lost in the noise as the result of deep fading. The corresponding average BER was between 2 per cent and 25 per cent respectively. An average situation was represented by Channel (AVE), which has an average gap length of 20 and 5 per cent in average BER.

In Chapter 5, two types of channel equalisers with various parameters were used to process some typical experimental data, in order to determine which channel equaliser is most cost effective in improving the bit error statistics. The recorded data, which were used in Chapter 4 to provided the statistical sample results, were processed by channel equalisers implemented by computer software.

The first type was the adaptive Decision Feedback Equalisers (DFE) utilising the Fast Kalman Algorithm (FKA), with a variable number of forward and backward delay taps. The gap distributions and the average BER after channel equalisation were evaluated. The results showed that all the DFE improved the average gap length when the main signal was strong against ISI, despite the error propagation caused by very occasional consecutive bit errors. DFE provided very little improvement in average gap length and BER in channels where the signal-to-noise ratio is 5 dB. The equaliser structure with 3 forward and 3 backward delay sections was found to be most cost-effective in equalising an average channel.

By calculating the MSE during the adaptation period, it was found that 20 training steps were sufficient for the FKA to reduce the MSE below the predetermined optimum level.

The second type of equalisers were Viterbi Equalisers (VE) with a variable number of states. By comparing the average gap lengths and BERs after applying various VE, it was found that there was no advantage in increasing the number of states beyond 32. This is because of the influence of noise components within the selected window on the estimated channel impulse response. The VE was also found to be sensitive to burst errors, which caused VE to select an erroneous survivor route.

A comparison between the average gap lengths after the DFE and VE showed that the DFE generally provides a larger improvement. The DFE with 3 forward and 3 backward delay sections and the 32 state VE were found to be sufficient in equalising the average channel.

In summary, the theoretical background of using spectrally efficient digital transmission systems in the mobile radio environment was reviewed and an experimental investigation was found to be necessary. A versatile experimental system was designed, constructed and calibrated in the laboratory. Field experiments were then conducted and the measured data were statistically analysed and processed by various equalisers. The advantage of using this versatile experimental system was demonstrated by presenting some sample results from various stages of the experimental investigation.

6.2 FUTURE WORK

The work carried out in this thesis is the beginning of research on quantitatively accessing the performance of a digital transmission system over a mobile radio communication channel. The experimental results obtained so far suggest that there are four main areas where work can be continued.

The first is to study how the receiver can be modified so that it will be more robust in respect of the deep signal fading, which caused most of the bit errors. Space diversity and frequency hopping techniques provide solutions to reducing the deep fades, therefore the adoption of such techniques should be investigated. Other possible improvements such as implementing a digital phase and clock recovery circuit, using 8 or 12 bit ADCs and longer PRBS in order to improve the dynamic range of the channel estimator etc., can also be considered.

The second area is to use the experimental system to conduct field experiments in different physical locations (e.g. city centres, countryside, inside buildings etc.) and to extend the statistical analysis to the bit error statistics and estimated channel impulse responses (such as those carried out in chapter 4), in order to investigate the performance of digital transmissions in those locations.

The third area is to investigate whether a more quantitative relationship between the estimated channel impulse response and the average gap distrib-

ution or the average BER can be found. (e.g. how are the mean square values of the delayed signal amplitudes related to the average gap length and BER.) This investigation can lead to the possibility of representing the mobile radio channel with a digital model.

The fourth area is to use various error control encoders and decoders, implemented in either hardware or computer software, in order to determine which is more cost effective in correcting bit errors in real time digital transmission.